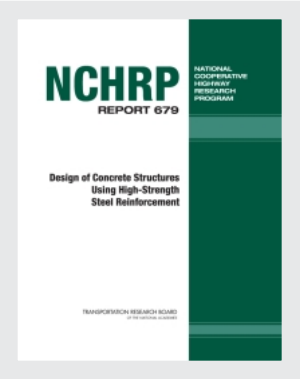

Design of Concrete Structures Using High-Strength Steel Reinforcement

ISBN 978-0-309-15541-0 | DOI 10.17226/14496

AUTHORS

Henry G Russell; Richard A Miller; Kent A Harries; Bahram M Shahrooz; Transportation Research Board

NATIONAL COOPERATIVE HIGHWAY RESEARCH PROGRAM

NCHRP REPORT 679

Design of Concrete Structures Using High-Strength Steel Reinforcement

Bahram M. Shahrooz
Richard A. Miller
University of Cincinnati
Cincinnati, OH

Kent A. Harries
University of Pittsburgh
Pittsburgh, PA

Henry G. Russell
Henry G. Russell, Inc.
Glenview, IL

Subscriber Categories
Highways • Bridges and Other Structures

Research sponsored by the American Association of State Highway and Transportation Officials
in cooperation with the Federal Highway Administration

TRANSPORTATION RESEARCH BOARD

WASHINGTON, D.C.
2011
www.TRB.org

NATIONAL COOPERATIVE HIGHWAY RESEARCH PROGRAM

Systematic, well-designed research provides the most effective approach to the solution of many problems facing highway administrators and engineers. Often, highway problems are of local interest and can best be studied by highway departments individually or in cooperation with their state universities and others. However, the accelerating growth of highway transportation develops increasingly complex problems of wide interest to highway authorities. These problems are best studied through a coordinated program of cooperative research.

In recognition of these needs, the highway administrators of the American Association of State Highway and Transportation Officials initiated in 1962 an objective national highway research program employing modern scientific techniques. This program is supported on a continuing basis by funds from participating member states of the Association and it receives the full cooperation and support of the Federal Highway Administration, United States Department of Transportation.

The Transportation Research Board of the National Academies was requested by the Association to administer the research program because of the Board's recognized objectivity and understanding of modern research practices. The Board is uniquely suited for this purpose as it maintains an extensive committee structure from which authorities on any highway transportation subject may be drawn; it possesses avenues of communications and cooperation with federal, state and local governmental agencies, universities, and industry; its relationship to the National Research Council is an insurance of objectivity; it maintains a full-time research correlation staff of specialists in highway transportation matters to bring the findings of research directly to those who are in a position to use them.

The program is developed on the basis of research needs identified by chief administrators of the highway and transportation departments and by committees of AASHTO. Each year, specific areas of research needs to be included in the program are proposed to the National Research Council and the Board by the American Association of State Highway and Transportation Officials. Research projects to fulfill these needs are defined by the Board, and qualified research agencies are selected from those that have submitted proposals. Administration and surveillance of research contracts are the responsibilities of the National Research Council and the Transportation Research Board.

The needs for highway research are many, and the National Cooperative Highway Research Program can make significant contributions to the solution of highway transportation problems of mutual concern to many responsible groups. The program, however, is intended to complement rather than to substitute for or duplicate other highway research programs.

NCHRP REPORT 679

Project 12-77
ISSN 0077-5614
ISBN 978-0-309-15541-0
Library of Congress Control Number 2011921824

COPYRIGHT INFORMATION

NOTICE

The project that is the subject of this report was a part of the National Cooperative Highway Research Program, conducted by the Transportation Research Board with the approval of the Governing Board of the National Research Council.

The members of the technical panel selected to monitor this project and to review this report were chosen for their special competencies and with regard for appropriate balance. The report was reviewed by the technical panel and accepted for publication according to procedures established and overseen by the Transportation Research Board and approved by the Governing Board of the National Research Council.

The opinions and conclusions expressed or implied in this report are those of the researchers who performed the research and are not necessarily those of the Transportation Research Board, the National Research Council, or the program sponsors.

The Transportation Research Board of the National Academies, the National Research Council, and the sponsors of the National Cooperative Highway Research Program do not endorse products or manufacturers. Trade or manufacturers' names appear herein solely because they are considered essential to the object of the report.

Published reports of the

NATIONAL COOPERATIVE HIGHWAY RESEARCH PROGRAM

are available from:

Transportation Research Board
Business Office
500 Fifth Street, NW
Washington, DC 20001

and can be ordered through the Internet at:

http://www.national-academies.org/trb/bookstore

Printed in the United States of America

THE NATIONAL ACADEMIES

Advisers to the Nation on Science, Engineering, and Medicine

The **National Academy of Sciences** is a private, nonprofit, self-perpetuating society of distinguished scholars engaged in scientific and engineering research, dedicated to the furtherance of science and technology and to their use for the general welfare. On the authority of the charter granted to it by the Congress in 1863, the Academy has a mandate that requires it to advise the federal government on scientific and technical matters. Dr. Ralph J. Cicerone is president of the National Academy of Sciences.

The **National Academy of Engineering** was established in 1964, under the charter of the National Academy of Sciences, as a parallel organization of outstanding engineers. It is autonomous in its administration and in the selection of its members, sharing with the National Academy of Sciences the responsibility for advising the federal government. The National Academy of Engineering also sponsors engineering programs aimed at meeting national needs, encourages education and research, and recognizes the superior achievements of engineers. Dr. Charles M. Vest is president of the National Academy of Engineering.

The **Institute of Medicine** was established in 1970 by the National Academy of Sciences to secure the services of eminent members of appropriate professions in the examination of policy matters pertaining to the health of the public. The Institute acts under the responsibility given to the National Academy of Sciences by its congressional charter to be an adviser to the federal government and, on its own initiative, to identify issues of medical care, research, and education. Dr. Harvey V. Fineberg is president of the Institute of Medicine.

The **National Research Council** was organized by the National Academy of Sciences in 1916 to associate the broad community of science and technology with the Academy's purposes of furthering knowledge and advising the federal government. Functioning in accordance with general policies determined by the Academy, the Council has become the principal operating agency of both the National Academy of Sciences and the National Academy of Engineering in providing services to the government, the public, and the scientific and engineering communities. The Council is administered jointly by both Academies and the Institute of Medicine. Dr. Ralph J. Cicerone and Dr. Charles M. Vest are chair and vice chair, respectively, of the National Research Council.

The **Transportation Research Board** is one of six major divisions of the National Research Council. The mission of the Transportation Research Board is to provide leadership in transportation innovation and progress through research and information exchange, conducted within a setting that is objective, interdisciplinary, and multimodal. The Board's varied activities annually engage about 7,000 engineers, scientists, and other transportation researchers and practitioners from the public and private sectors and academia, all of whom contribute their expertise in the public interest. The program is supported by state transportation departments, federal agencies including the component administrations of the U.S. Department of Transportation, and other organizations and individuals interested in the development of transportation. **www.TRB.org**

www.national-academies.org

COOPERATIVE RESEARCH PROGRAMS

CRP STAFF FOR NCHRP REPORT 679

Christopher W. Jenks, *Director, Cooperative Research Programs*
Crawford F. Jencks, *Deputy Director, Cooperative Research Programs*
Waseem Dekelbab, *Senior Program Officer*
David Beal, *Senior Program Officer* (Retired)
Danna Powell, *Senior Program Assistant*
Eileen P. Delaney, *Director of Publications*
Hilary Freer, *Senior Editor*

NCHRP PROJECT 12-77 PANEL
Field of Design—Area of Bridges

Loren Risch, *Kansas DOT, Topeka, KS* (Chair)
Marcus H. Ansley, *Florida DOT, Tallahassee, FL* (Deceased)
Theresa Ahlborn, *Michigan Technological University, Houghton, MI*
Kamal Elnahal, *US Coast Guard, Washington, DC*
Amy Eskridge, *Texas DOT, Austin, TX*
Chad E. Knavel, *Pennsylvania DOT, Harrisburg, PA*
Steven R. Maberry, *New Mexico DOT, Santa Fe, NM*
Robert J. Peterman, *Kansas State University, Manhattan, KS*
Basile Rabbat, *Portland Cement Association, Skokie, IL*
Benjamin A. Graybeal, *FHWA Liaison*
Stephen F. Maher, *TRB Liaison*

FOREWORD

By Waseem Dekelbab
Staff Officer
Transportation Research Board

This report provides an evaluation of existing *AASHTO LRFD Bridge Design Specifications* relevant to the use of high-strength reinforcing steel and other grades of reinforcing steel having no discernable yield plateau. The report also includes recommended language to the *AASHTO LRFD Bridge Design Specifications* that will permit the use of high-strength reinforcing steel with specified yield strengths not greater than 100 ksi. The material in this report will be of immediate interest to bridge engineers.

The *AASHTO LRFD Bridge Design Specifications* allow the use of reinforcing steel conforming to many different AASHTO and ASTM materials specifications, but limit the specified yield strength to 75 ksi. Reinforcement is now available that has yield strength in excess of 75 ksi. Typical steel reinforcement has well-defined yield plateaus whereas high-strength reinforcing bars generally do not. The higher strength and the lack of a well-defined yield plateau could alter structural behavior and do not satisfy some of the design assumptions in the *AASHTO LRFD Bridge Design Specifications.* Research was needed to evaluate the use of high-strength reinforcing steel in structural concrete.

The research was performed under NCHRP Project 12-77 by a team led by Dr. Bahram Shahrooz at the University of Cincinnati, Cincinnati, OH. Recommended revisions to the *AASHTO LRFD Bridge Design Specifications* to permit reinforcing bar yield strengths not exceeding 100 ksi were investigated and validated for concrete strengths up to 10 ksi and in some instances up to 15 ksi.

A number of deliverables are provided as appendices. These appendices are not published herein but are available on the TRB website (Go to http://trb.org/Publications/Public/PubsNCHRPProjectReports.aspx and look for NCHRP Report 679). These appendices are titled as follows.

- APPENDIX A—Material Properties
- APPENDIX B—Flexural Resistance of Members with Reinforcing Bars Lacking Well-Defined Yield Plateau
- APPENDIX C—Strain Limits for Tension-Controlled/Compression-Controlled and Strains to Allow Negative Moment Redistribution
- APPENDIX D—Flexure Beam Tests
- APPENDIX E—Fatigue of High-Strength Reinforcing Steel
- APPENDIX F—Shear Beam Tests
- APPENDIX G—Analytical Studies of Columns
- APPENDIX H—Beam Splice Tests
- APPENDIX I—Crack Control
- APPENDIX J—Survey Results
- APPENDIX K — Design Examples
- APPENDIX L—Proposed Changes to Section 5 of the AASHTO LRFD Specification
- APPENDIX M—2010 AASHTO Bridge Committee Agenda Item

AUTHOR ACKNOWLEDGMENTS

The research reported herein was performed under NCHRP Project 12-77 by the Department of Civil and Environmental Engineering (CEE) at the University of Cincinnati in collaboration with the University of Pittsburgh and Henry G. Russell, Inc.

The principal investigators (PIs) on this project were Bahram M. Shahrooz (PI) and Richard A. Miller (Co-PI) from the University of Cincinnati, Kent A. Harries (Co-PI) from the University of Pittsburgh, and Henry G. Russell (Co-PI) from Henry G. Russell, Inc. Graduate students Jonathan Reis and Elizabeth Ward (University of Cincinnati) and Amir Soltani and Gabriel Zeno (University of Pittsburgh) performed the research under the supervision of the PI and Co-PIs. The experimental component of the research was completed at the University of Cincinnati Large Scale Test Facility (UCLSTF) and the Watkins-Haggart Structural Engineering Laboratory (WHSEL) at the University of Pittsburgh. David Breheim at the University of Cincinnati is acknowledged for his technical assistance in various aspects of testing at UCLSTF. Daniel Kuchma of the University of Illinois at Urbana-Champaign is acknowledged for his early contributions to this project. The PIs wish to express their appreciation to Prestress Services, Melbourne, Kentucky, for fabrication of prestressed girders.

All A1035 reinforcing steel used in this study was provided by MMFX Inc. Hilltop Concrete in Cincinnati and Frank Bryan Concrete in Pittsburgh are gratefully acknowledged for their efforts in getting the concrete mixes used "just so."

Panel member Marcus H. Ansley, who passed away suddenly on June 16, 2010, is sincerely thanked for his major contributions to this project. His pioneering research on flexural and shear performance of members using A1035 reinforcement was invaluable. His insistence on examining ductility of flexural members with A1035 reinforcement helped the research team develop revised strength reduction factors. The research team would like to dedicate this report to Mr. Ansley.

CONTENTS

Note: Many of the photographs, figures, and tables in this report have been converted from color to grayscale for printing. The electronic version of the report (posted on the Web at www.trb.org) retains the color versions.

SUMMARY

Design of Concrete Structures Using High-Strength Steel Reinforcement

Recent revisions to §9.2 of the *AASHTO LRFD Bridge Construction Specifications* and to *AASHTO MP 18 Standard Specification for Uncoated, Corrosion-Resistant, Deformed and Plain Alloy, Billet-Steel Bars for Concrete Reinforcement and Dowels* permit the specification of ASTM A1035 reinforcing steel. A1035 reinforcing bars are low carbon, chromium steel bars characterized by a high tensile strength (minimum yield strength of 100 or 120 ksi determined using the 0.2% offset method) and a stress-strain relationship having no yield plateau. Because of their high chromium content, A1035 bars are reported to have superior corrosion resistance when compared to conventional reinforcing steel grades. For this reason, designers have specified A1035 as a direct, one-to-one, replacement for conventional reinforcing steel as an alternative to stainless steel or epoxy-coated bars. The specifications, however, limit the yield strength of reinforcing steel to 75 ksi for most applications. Therefore, although A1035 steel is being specified for its corrosion resistance, the benefits of its higher yield strength cannot be utilized.

A number of types and grades of steel reinforcement with yield strengths exceeding 80 ksi are commercially available in the United States. If allowed, using steel with this higher capacity could provide various benefits to the concrete construction industry by reducing member cross sections and reinforcement quantities, leading to savings in material, shipping, and placement costs. Reducing reinforcement quantities also would reduce congestion problems leading to better quality of construction. Finally, coupling high-strength steel reinforcement with high-performance concrete should result in a much more efficient use of both materials.

This report provides an evaluation of existing *AASHTO LRFD Bridge Design Specifications* relevant to the use of high-strength reinforcing steel and other grades of reinforcing steel having no discernable yield plateau. The report identifies aspects of reinforced-concrete design and of the specifications that may be affected by the use of high-strength reinforcing steel. An integrated experimental and analytical program intended to develop the data required to permit the integration of high-strength reinforcement into the LRFD specification is presented. In addition, a number of "proof tests" intended to validate existing specifications provisions applied to higher strength reinforcing steel are presented. The focus of the experimental phase of this study is the use of ASTM A1035 reinforcing steel since it captures both behavioral aspects of interest (i.e., it has a very high strength and has no discernable yield plateau). In addition, this study specifically considers the use of higher strength concrete. The experimental and analytical studies include concrete having compressive strengths of 5, 10, and 15 ksi.

The primary deliverable of NCHRP Project 12-77 was to provide recommendations for changes to the specifications necessary for the use of high-strength reinforcing steel. This report provides the background and engineering basis, in the form of experimental and ana-

lytical studies, supporting these recommendations. Although summarized in Chapter 3, the recommendations forwarded to the Project Panel, and eventually to the AASHTO Technical Committee for Concrete Design (T-10), are not presented in this document. In all cases, recommended language was proposed that specifically permits the use of high-strength reinforcing steel with specified yield strengths not greater than 100 ksi when the specific article permits it. This methodology is consistent with the manner by which the specifications handle high-strength concrete, allowing its use only when a specific article permits it. Specifications Sections 3, 5, and 9 were identified as having articles potentially requiring changes. Although considered in its entirety, no changes were identified in the *AASHTO LRFD Bridge Construction Specifications.* The 2009 revisions to §9.2 of the *Construction Specifications* permit the use of A1035 reinforcing steel.

Yield Strength

A critical objective of the present work was to identify an appropriate steel strength and/or behavior model to adequately capture the behavior of high-strength reinforcing steel while respecting the tenets of design and the needs of the designer. A value of yield strength, f_y, not exceeding 100 ksi was found to be permissible without requiring significant changes to the specifications.

Flexure

The current specifications design methodology for flexure, that is, a simple plane sections analysis using stress block factors to model concrete behavior and an elastic-perfectly plastic steel behavior (having $E_s = 29{,}000$ ksi), is shown to be appropriate for values of $f_y \leq 100$ ksi. To ensure ductility, steel strains corresponding to tension- and compression-controlled limits (defined in §5.7.2.1 of the specifications) are recommended as follows:

	Current §5.7.2.1; No Recommended Changes	Recommended Limits for High-Strength Reinforcement
	$f_y \leq 60$ ksi	$f_y = 100$ ksi
Tension-Controlled Section	$\varepsilon_t \geq 0.005$	$\varepsilon_t \geq 0.008$
Compression-Controlled Section	$\varepsilon_t \leq 0.002$	$\varepsilon_t \leq 0.004$
	Values may be interpolated between limits	

These strain limits were developed through a rigorous analytical study of 286 cases, which included seven different grades of reinforcing steel, three concrete strengths, and multiple section geometries. Six large-scale beam specimens reinforced with A1035 reinforcing steel confirmed the appropriateness of the proposed tension- and compression-controlled limits. All beam specimens met and exceeded their designed-for strength and ductility criteria and exhibited predictable behavior and performance similar to beams having conventional reinforcing steel.

Fatigue

Two large-scale proof tests conducted as part of this study and a review of available published data demonstrate that presently accepted values for the fatigue or "endurance" limit for reinforcing steel are applicable—and likely conservative—when applied to higher strength bars. Additionally, it is shown that fatigue considerations will rarely affect the design of typical reinforced-concrete members having $f_y \leq 100$ ksi.

Shear

Five large-scale reinforced-concrete beams and four AASHTO Type I prestressed girders were tested to evaluate the performance of high-strength A1035 steel as shear reinforcement in comparison to that of the commonly used A615 steel. Test specimens were designed using the specifications approach of summing concrete and steel contributions to shear resistance (i.e., $V_c + V_s$). All beams exhibited good performance with little difference noted between the behavior of spans reinforced with A1035 or A615 transverse steel. The use of current specifications procedures for calculating shear capacity were found to be acceptable for values of shear reinforcement yield $f_y \leq 100$ ksi.

Shear Friction

A series of eight push-off (direct shear) proof tests of "cold construction joint" interfaces reinforced with either A1035 or A615 bars demonstrated that current specifications requirements for such joints are adequate. Significantly, the restriction that f_y be limited to 60 ksi when calculating shear friction capacity must be maintained regardless of the reinforcing steel used. This limit is, in fact, calibrated to limit strain (and therefore interface crack opening) to ensure adequate aggregate interlock capacity across the interface and is, hence, a function of steel modulus rather than strength. It is noted that steel modulus does not vary with reinforcing bar grade.

Compression

Analytical parametric studies were performed to examine behavior of columns reinforced with A1035 longitudinal and transverse reinforcement. Results indicate the current specifications requirements for both longitudinal and transverse reinforcement design in compression members are applicable for $f_y \leq 100$ ksi.

Bond and Development

The applicability of current specifications requirements for straight bar and hooked bar development lengths was confirmed through a series of spliced-bar beam tests and pull-out tests, respectively. "Proof test" spliced-bar beam specimens, having development lengths that were shorter than those required by the present specifications equations (with all appropriate reduction factors applied), were tested. All developed bar stresses exceeding f_y and approaching the ultimate bar capacity, f_u, prior to the splice slipping, and in one case bar fracture. Tests of hooked bar anchorage resulted in bar rupture outside of the anchorage region with very little slip, clearly indicating the efficacy of the hooked bar development requirements in the specifications. Significantly, it is recommended that development, splice, and anchorage regions be provided with cover and confining reinforcement—based on current design requirements—when high-strength bars are used. Existing equations for development where no confinement is present are demonstrated to be unconservative. The presence of confining reinforcement effectively mitigates potential splitting failures and results in suitably conservative development, splice, and anchorage capacities.

Serviceability—Deflections and Crack Widths

A fundamental issue in using A1035, or any other high-strength reinforcing steel, is that the stress at service load (f_s; assumed to be on the order of $0.6f_y$) is expected to be greater than when conventional Grade 60 steel is used. Consequently, the service-load reinforcing strains

(i.e., $\varepsilon_s = f_s/E_s$) are greater than those for conventional Grade 60 steel. The large strains affect deflection and crack widths at service loads. Based on the results of the flexural tests conducted in this study, deflections and crack widths at service load levels were evaluated. Both metrics of serviceability were found to be within presently accepted limits and were predictable using current specifications provisions. A limitation on service-level stresses of $f_s \leq$ 60 ksi is recommended; this is consistent with the recommendation that $f_y \leq 100$ ksi.

Summary

The extension of present *AASHTO LRFD Bridge Design Specifications* to permit reinforcing bar yield strengths not exceeding 100 ksi was investigated and, for the most part, validated for concrete strengths up to 10 ksi, and, in some instances, 15 ksi. This study did not address seismic applications, and no such increase in permitted yield strength is addressed for Seismic Zones 2 through 4. Other limitations to the use of high-strength reinforcing steel also are identified. Recommended specifications language was proposed to the Project Panel that specifically permits the use of high-strength reinforcing steel with specified yield strengths not greater than 100 ksi when the specific article permits it. This report provides the necessary background and engineering basis, in the form of experimental and analytical studies, supporting these recommendations.

CHAPTER 1

Background

1.1 Introduction

The AASHTO *LRFD Bridge Construction Specifications* (2004) permit the use of uncoated reinforcing steel conforming to any of the specifications given in Table 1. Since all grades of reinforcing steel (bars and wires) have an ASTM designation, ASTM designations will be used throughout this report.

Recent revisions to §9.2 of the construction specifications and to *MP 18 Standard Specification for Uncoated, Corrosion-Resistant, Deformed and Plain Alloy, Billet-Steel Bars for Concrete Reinforcement and Dowels* (AASHTO 2009) permit the specification of ASTM A1035 (2009) reinforcing steel. A1035 reinforcing bars are low-carbon, chromium steel bars characterized by a high tensile strength and a stress-strain relationship having no yield plateau. Yield strength is determined using the 0.2% offset method and is specified to exceed 100 ksi or 120 ksi. Because of their high chromium content (specified to be between 8–11%; slightly less than stainless steel), A1035 bars are reported to have superior corrosion resistance when compared to conventional reinforcing steel grades. For this reason, designers have specified A1035 as a direct, one-to-one replacement for conventional reinforcing steel as an alternative to stainless steel or epoxy-coated bars. The AASHTO *LRFD Bridge Design Specifications* (2007), however, limit the yield strength of reinforcing steel to 75 ksi for most applications. Therefore, although A1035 steel is being specified for its corrosion resistance, its higher yield strength cannot be utilized.

For many years, the design of reinforced-concrete structures in the United States was dominated by the use of steel reinforcement with yield strength, f_y, equal to 40 ksi and, since about 1970, 60 ksi. Design with steel having higher yield strength values has been permitted, but since the 1971 American Concrete Institute (ACI) edition of ACI 318, yield strength values have been limited to 80 ksi. Currently, ACI 318 (2008) permits design using steel reinforcement with yield strength, defined as the stress corresponding to a strain of 0.0035, not exceeding 80 ksi. The exception is spiral transverse reinforcement in compression members where the use of yield strength up to 100 ksi is permitted. The AASHTO *LRFD Bridge Design Specifications* (2007) similarly limit the use of reinforcing steel yield strength in design to no less than 60 ksi and no greater than 75 ksi (exceptions are permitted with owner approval). Both ACI and AASHTO limits have been written and interpreted to not exclude the use of higher strength grades of steel, but only to limit the value of yield strength that may be used in design.

The limits on yield strength are primarily related to the prescribed limit on concrete compressive strain of 0.003 and to the control of crack widths at service loads. Crack width is a function of steel strain and consequently steel stress (Nawy 1968). Therefore, the stress in the steel reinforcement will always need to be limited to some extent to prevent cracking from affecting serviceability of the structure. However, with recent improvements to the properties of concrete, the ACI 318 limit of 80 ksi and AASHTO limit of 75 ksi on the steel reinforcement yield strength are believed to be unnecessarily conservative for new designs. Additionally, an argument can be made that if a higher strength reinforcing steel is used but not fully accounted for in design, there may be an inherent overstrength in the member that has not been properly taken into account. This concern is most critical in seismic applications or when considering progressive collapse states.

Steel reinforcement with yield strength exceeding 80 ksi is commercially available in the United States. If allowed, using steel with this higher capacity could provide various benefits to the concrete construction industry by reducing member cross sections and reinforcement quantities, which would lead to savings in material, shipping, and placement costs. Reducing reinforcement quantities would also reduce congestion problems leading to better quality of construction. Finally, coupling high-strength steel reinforcement with high-performance concrete should result in a much more efficient use of both materials.

Additionally, much of the interest in higher strength reinforcement stems from the fact that many of the higher strength

Table 1. Uncoated reinforcing steel permitted by 2004 AASHTO *LRFD Bridge Construction Specifications.*

Designation	Title	Note	Tested in This Study?*
AASHTO M31 ASTM A615	Deformed and Plain Carbon-Steel	standard reinforcing steel unless otherwise specified	yes
AASHTO M322 ASTM A996	Rail-Steel and Axle-Steel Plain Bars		no
ASTM A706	Low-Alloy Steel Deformed and Plain Bars	"weldable" reinforcing steel	yes
AASHTO M225 ASTM A496	Deformed Steel Wire	"cold-rolled" deformations on A82 plain wire	yes
AASHTO M55 ASTM A185	Welded Plain Wire Fabric	welded A82 wire	no
AASHTO M32 ASTM A82	Plain Steel Wire		yes
AASHTO M221 ASTM A497	Deformed Steel Welded Wire Reinforcement	welded wire fabric having wires conforming to A496	no
ASTM A955	Deformed and Plain Stainless Steel Bars	different types (allowable chemistries) of stainless steel are permitted within A955	yes

*See Appendix A.

grades are more resistant to corrosion and therefore very attractive in reinforced-concrete applications. For instance, the A1035 reinforcing steel used in this study is reported to be between 2 to 10 times more resistant to corrosion than conventional A615 "black" reinforcing steel. In some applications, A1035 reinforcing steel has replaced A615 steel on a one-to-one basis on the premise that it is more resistant to corrosion but not as costly as stainless steel grades. Clearly, if the enhanced strength of A1035 steel could be used in design calculations, less steel would be required, and this would result in a more efficient and economical structural system.

1.2 Objectives of NCHRP Project 12-77

The objective of the study presented in this report is to evaluate existing AASHTO *LRFD Bridge Design Specifications* relevant to the use of high-strength reinforcing steel and other grades of reinforcing steel having no discernable yield plateau. The focus of the experimental phase of this study is the use of ASTM A1035 (2009) reinforcing steel since it captures both behavioral aspects of interest (i.e., it has a very high strength and has no discernable yield plateau). The analytical program of this study supplements the experimental data and evaluates design issues related to other grades of reinforcing steel with no distinct yield plateau.

The project identified aspects of reinforced-concrete design and of the AASHTO *LRFD Bridge Design Specifications* that may be affected by the use of high-strength reinforcing steel. Design issues were prioritized and an integrated experimental and analytical program was designed to develop the data required to permit the integration of high-strength reinforcement into the LRFD specifications. As described in Chapter 2, this program included parametric, experimental, and analytic studies in addition to a number of "proof tests" intended to validate existing LRFD provisions when applied to higher strength reinforcing steel.

Thus, a crucial objective of the present work is to identify an appropriate steel strength and/or behavior model to adequately capture the behavior of high-strength reinforcing steel while respecting the tenets of design and the needs of the designer. As will be described throughout this report, a value of yield strength, f_y, not exceeding 100 ksi was found to be permissible without requiring significant changes to the LRFD specifications or, more critically, to the design philosophy and methodology prescribed therein. Some limitations to this increase in permissible yield strength were identified and also are discussed.

1.3 Literature Review

1.3.1 Mechanical Properties of A1035 Reinforcing Steel

A number of mechanical properties for reinforcing steel have been reported in the literature, although by far the most important are the tensile yield (f_y) and ultimate strengths (f_u); these parameters are discussed at length below. El-Hacha and Rizkalla (2002) report other mechanical properties of A1035 to be consistent with the higher tensile yield strength. Based on tests of #4, #6, and #8 bars, they report the following:

- Compressive yield strength is the same as tensile yield, f_y;
- Poisson Ratio, $\nu = 0.26$;

- Shear capacity exceeds the theoretical value of $\tau = f_y / \sqrt{3}$ by a significant margin; and
- The tensile capacity of bars is unaffected by the presence of standard 90° bends.

1.3.2 Tension Properties of A1035 Reinforcing Steel

High-strength reinforcing bars often do not have a distinct yield plateau, as shown in Figure 1. For the *representative* case of an A1035 #5 reinforcing bar shown in this figure, the yield strength is determined to be 93 ksi or 114 ksi depending on whether the value is determined as that corresponding to a strain of 0.0035 or 0.005. The yield strength is determined to be 123 ksi if the 0.2% offset method is used to determine the yield point. If a simple definition of 1% strain is used (as is commonly used for prestressing steel, another type of steel without a well-defined yield plateau), the yield stress is approximately 140 ksi. Regardless of the method used for determining yield stress, the value of 68 ksi is found for the representative A615 #5 bar shown.

A review of tensile test data from 16 previous studies of A1035 steel given in Appendix A results in the following conclusions:

- Values of yield (f_y) and ultimate (f_u) strengths and the strain corresponding to the ultimate stress are relatively consistent among different test programs.
- Values of rupture strain vary considerably although this may be an artifact of the test procedure where strain gages or extensometers typically do not capture ultimate behavior.
- The use of the ASTM A1035-prescribed 0.2% offset method for establishing yield strength results in the greatest variability (COV = 10.3%) whereas stress based on absolute strain approaches to establishing the yield strength are consistent at each strain level considered (COV ≈ 7%).
- There is little variation in material properties with bar size. Contrary to conventional wisdom, results from other studies appear to indicate that larger A1035 bars have marginally greater strengths than smaller bars. Results from the present study, however, indicate a marginal reduction in bar strength with increasing bar size.
- Regardless of the manner by which yield stress is determined, the condition that $f_u > 1.25 f_y$ is satisfied; this relationship is implicit in a number of AASHTO design articles including those relating to (1) mechanical couplers (AASHTO LRFD §5.11.5.2.2); and (2) element overstrength (AASHTO LRFD Appendix B3).

For the purposes of modeling steel behavior, some literature proposes "best fit" relationships for A1035 stress-strain behavior (Vijay et al. 2002, Rizkalla et al. 2005, Mast et al. 2008). In the present study, both Mast et al. (see Appendices C and D) and a Ramberg-Osgood (Ramberg and Osgood 1943) function are alternately adopted. Ramberg-Osgood (R-O) functions are commonly used to model prestressing strand and post-tensioning steel, and the parameters may be established directly from representative stress-strain curves. (R-O parameters for the A1035 steel tested in this study are provided in Appendix A.)

1.3.2.1 *Modulus of Elasticity, E_s*

Regardless of yield or ultimate strength, all steel reinforcing bar grades have a reported modulus of elasticity, $E_s = 29{,}000$ ksi. At stress levels below about 60 ksi, there is no evidence that the

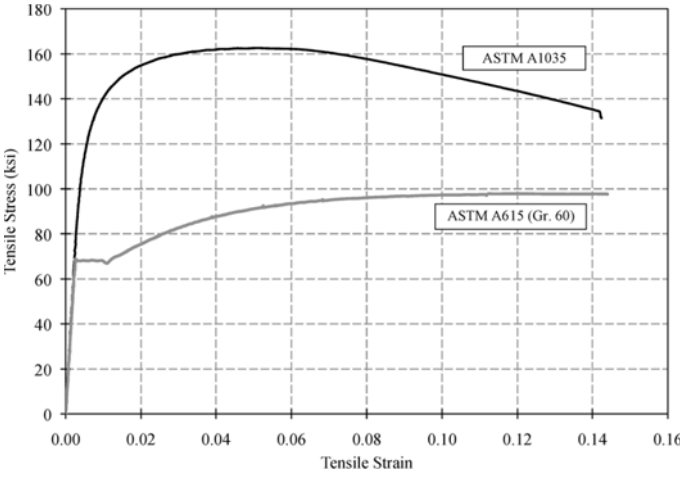

(a) Complete Stress-Strain Curves

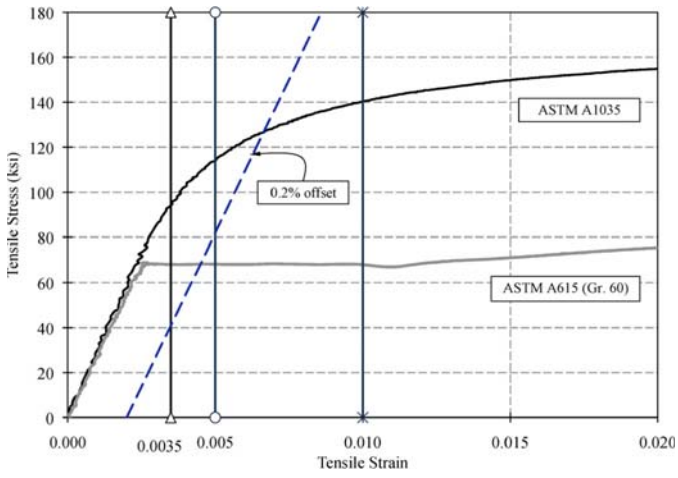

(b) Various Determinations of f_y

Figure 1. Representative Stress-Strain Curves for A1035 and A615 Reinforcing Steel.

modulus varies from steel grade to steel grade. High-strength steel does, however, exhibit a "proportional limit" where the modulus begins to decrease as is evident in Figure 1a. Although this limit is partially a function of the steel capacity, it has been observed that A1035 steel behaves in an essentially linear manner to at least 70 ksi regardless of ultimate capacity (Mast et al. 2008 and this study). It is noted that while some empirical A1035 stress-strain relationships capture the behavior at large strains reasonably well, they fail to capture the initial linear behavior accurately and therefore may not be appropriate for design. An R-O formulation or a piece-wise formulation (Mast et al. 2008) overcomes this issue.

1.3.2.2 Fatigue Performance of High-Strength Steel Reinforcement

DeJong and MacDougal (2006) and DeJong (2005) present a study of the fatigue behavior of high-strength reinforcing steel. DeJong conducted fatigue tests of ASTM A1035 steel having a reported (0.2% offset) yield value of 116 ksi and ultimate tensile strength of 176 ksi. Tests on #3, #4, and #5 bars demonstrated a fatigue strength (at $N = 1$ million cycles) of 45 ksi. Companion tests on Grade 60 reinforcing bars had a fatigue life of 24 ksi.

El-Hacha and Rizkalla (2002) report fatigue tests of #4 and #6 A1035 reinforcing bars having a nominal yield strength, $f_y = 120$ ksi. The endurance limit is not established in this study (no tests having $N > 500{,}000$ were conducted) although the behavior is reported to be generally superior to that expected for A615 bars. The tests were run with $f_{min} = 0.2f_y$ and the lowest stress range was $S = 0.45f_y = 54$ ksi at which the observed fatigue life was approximately $N = 500{,}000$ and 360,000 for the #4 and #6 bars, respectively. Projecting these *S-N* results to greater values of *N* would lead to results similar to that reported by DeJong (2005) and superior to the behavior predicted by the present AASHTO requirements (Appendix E).

No other known studies have examined the fatigue performance of high-strength reinforcing steel, although a number of studies have reported fatigue properties of reinforcing steel having $f_y < 60$ ksi. These investigations are summarized in Appendix E. Based on the data presented in Appendix E, it is seen that no studies report an endurance limit less than 24 ksi in tension-tension (i.e., f_{min} positive) tests.

1.3.3 Flexural Reinforcement

To apply the higher material resistance factor, $\phi = 0.9$ allowed by AASHTO (and ACI 318) in the design of tension-controlled reinforced-concrete flexural members, a member should exhibit a desirable ductile behavior. A desirable behavior implies that at service loads, the member should display small deflections and minimal cracking while at higher loads the member should display large deflections and sufficient cracking to provide warning before reaching its ultimate capacity. Both deflection and cracking are primarily a function of steel strain near the tension face of the member and, in general, desirable behavior of a member is related to ductility, which relates to yielding or inelastic deformation of the steel reinforcement. For lower strength reinforcing materials, the only way to obtain high strains near the tension face at nominal strength is to ensure yielding of the tension steel; however, for high-strength reinforcement, yielding is no longer necessary (Mast et al. 2008).

The objective of the work reported by Mast et al. (2008) was to assess the adequacy of a proposed 100 ksi reinforcement stress-strain relationship for A1035-compliant steel in order to establish acceptable strain limits for tension-controlled and compression-controlled sections reinforced with this high-strength steel. Mast et al. studied the behavior of concrete beams subject to flexural and axial loads at service level and nominal strength and determined the section behavior using a cracked section analysis that satisfied equilibrium and compatibility. They assumed an elastic concrete stress distribution under service load and used the ACI rectangular stress block to model concrete at nominal strength. Although they proposed a more complex empirical relationship for A1035 stress-strain behavior, Mast et al. adopted an elastic-perfectly plastic steel stress-strain relationship in their analysis. They used a steel modulus, $E_s = 29{,}000$ ksi and defined a plastic yield plateau at $f_y = 100$ ksi. This approach is equivalent to simply increasing the current code-prescribed limits on steel reinforcement yield strength to 100 ksi.

For the nominal strength, Mast et al. performed a numerical analysis considering a rectangular, singly reinforced-concrete section having a number of different reinforcement ratios. They considered a concrete compressive strength $f_c' = 6500$ psi and an ultimate compression strain $\varepsilon_{cu} = 0.003$. Mast et al. considered elastic-perfectly plastic steel behavior having yield strengths of $f_y = 60$, 80, and 100 ksi. They calculated balanced reinforcement ratios, $\rho_b = 3.95\%$, 2.60%, and 1.85% for the values of $f_y = 60$, 80, and 100 ksi, respectively. For ρ_b values greater than these limits, the section capacity was controlled by concrete compression and was therefore unaffected by the steel grade used. For sections with $\rho_b < 1.75\%$, the use of the 100 ksi elastic-plastic model typically underestimated the nominal moment capacity of the section with respect to the actual behavior. On the other hand, for $1.75\% < \rho_b < 2.7\%$, the use of the 100 ksi limitation overestimated the capacity of the section by only a marginal amount (about 2.5%), which was considered insignificant for design purposes.

Through a series of moment-curvature and deflection analyses, Mast el al. demonstrated that a simple beam designed

using 100 ksi steel at the tension-controlled strain limit of 0.0066 exhibited ductility behavior (as measured by steel strain and section curvature) similar to that exhibited by a 60 ksi design having a strain limit of 0.005. They demonstrated that the ratio of nominal to service deflections was indeed greater for the higher strength steel reinforced sections. In addition, due to the higher tension strain in the high-strength reinforcement under service loading conditions, the beams may exhibit larger crack widths than if reinforced with conventional steel. However, as shown in Mast et al. (2008), previous testing indicates that the measured crack width under service loading conditions is only slightly larger than the (so-called) acceptable crack widths for beams reinforced with conventional steel. It is proposed that since some high-strength steels have improved corrosion resistance, the increased crack widths may be acceptable as long as these are not aesthetically objectionable.

Based on this work, Mast et al. proposed variation of the flexural resistance factor, ϕ, between 0.90 and 0.65 at strain limits greater than 0.009 and less than 0.005, respectively. These limits correspond to the tension-controlled limit of 0.005 and compression-controlled limit of 0.002 presently used for 60 ksi steel in AASHTO (2007). To help prevent compression-controlled failure, they suggest providing compression reinforcement having a design yield strength, $f_y < 80$ ksi. This limit is based on the maximum stress that can be developed at a strain of 0.003, which is the ultimate concrete strain at the extreme compression face of the concrete beam.

A number of experimental studies (Seliem et al. 2006, McNally 2003, Malhas 2002, Vijay et al. 2002, Florida DOT 2002) of the flexural behavior of members reinforced with A1035 reinforcing steel support the conclusions of Mast et al. (2008). These studies all indicate that flexural members designed using the same simplified approach (i.e., elastic-perfectly plastic steel behavior at higher values of f_y) will have flexural characteristics comparable to members having conventional reinforcement grades. Where reported, cracking and deflections at service loads are only marginally greater when using A1035 steel. One study (McNally) indicates a reduction in overall ductility when using an earlier formulation (since changed) of A1035 reinforcement. Other studies (Seliem and Florida DOT) report a marked increase in ductility likely resulting from the lower reinforcement ratio that may used in conjunction with the high-strength flexural reinforcement.

1.3.3.1 Applications in Bridge Decks

Most extant applications of A1035 steel have been in bridge decks and its use is typically as a one-to-one replacement for less corrosion-resistant "black" steel. Bridge deck design is based more on serviceability criteria than on strength requirements; therefore, it is not unexpected that experimental investigations of A1035-reinforced decks exhibit no significant differences in behavior (particularly under service loads) compared to A615-reinforced counterparts (Rizkalla et al. 2005, Hill et al. 2003).

1.3.4 Shear Reinforcement

The shear behavior of reinforced-concrete beams is not well understood and calculation of the shear strength is based on semi-empirical relationships. As a result, the calculated shear strength can vary significantly (up to 250%) among different code approaches (Hassan et al. 2008). Similarly, it is unclear whether current design approaches for shear may be extended to members having high-strength steel reinforcement. One concern is whether the high stress levels induced in the reinforcement may cause excessive cracking in the concrete resulting in degradation of the concrete component of shear resistance. Sumpter (2007) sought to determine the feasibility of using high-strength steel as shear reinforcement for concrete members, particularly focusing on the member behavior under overload conditions where the steel experiences high stress levels. Sumpter reports tests of beams having shear span to depth ratios of approximately 3 alternately reinforced with A615 or A1035 longitudinal and transverse steel. Stirrup spacings used reflected the minimum and maximum permitted and an additional intermediate spacing between these limits. Due to the stiff nature of shear-critical sections, little differences between specimen behaviors were noted at service loads. As expected, observed capacity of these shear-critical members reflected the amount of shear reinforcement present. Members having A1035 shear reinforcement exhibited marginally greater capacity than those with A615 shear steel. Sumpter concludes that most observed behavior was dominated by concrete behavior and that stress in the shear reinforcement in any specimen never exceeded 80 ksi; thus, the high-strength steel ($f_y > 100$ ksi) was not fully utilized, whereas the 60 ksi steel was. A study reported by Florida DOT (2002) draws the same conclusions with respect to the stress that may be developed in shear reinforcement. Sumpter also reports that all shear crack width values at service loads were less than the ACI-implied limit for flexural cracking of 0.016 in., regardless of the reinforcement grade or details. Indeed, Sumpter reports smaller crack widths in comparable members having high-strength steel than those with conventional steel. He attributes this behavior to enhanced bond characteristics of A1035 steel resulting from differences in rib configuration. This conclusion is curious because there is typically no difference between the rib configuration of A615 and A1035 reinforcing steels, and Sumpter does not report a difference in his test program.

1.3.5 Compression Members

The concept of providing transverse reinforcement to concrete compression members is intended to improve the strength and ductility. As a concrete column is compressed axially, it expands laterally. This lateral expansion is resisted by the transverse reinforcement and a lateral confining pressure in the concrete core is developed. Concrete strength and deformability are enhanced by the resulting state of multi-axial compression (Richart et al. 1928 and countless researchers since).

Current design philosophy for compression members equates the expected loss of axial load carrying capacity due to cover spalling to the expected strength gain of the remaining core due to the presence of confining reinforcement. This approach was developed and calibrated for columns fabricated with what today may only be considered normal, or moderate strength, concrete ($f_c' < 8000$ psi) and normal strength confining steel ($f_y = 60$ ksi). There is a perceived need for greater confinement for high-strength concrete than what is required for normal strength concretes (ACI 363 1992). Strength and deformability of concrete are known to be inversely proportional; therefore, more confinement is required in order for high-strength concrete columns to reach levels of deformation expected of well-detailed normal-strength concrete columns. In general, the degree of improvement in both axial capacity and ductility due to the provision of confinement is inversely proportional to the unconfined concrete strength (Pessiki et al. 2002, Carey and Harries 2005). The use of high-strength transverse reinforcement represents one manner by which this additional confinement may be realized.

Confining pressures are generated from tensile forces in the transverse reinforcement that result from lateral expansion of the axially loaded concrete. As the lateral expansion is dependent on the mechanical properties of the concrete, the lateral strains, particularly in high-strength concrete, may be insufficient to engage the higher confining pressures made possible by the use of high-strength transverse reinforcement (Martinez et al. 1982, Pessiki and Graybeal 2000). An additional, related consideration is that the transverse strains that engage the confining reinforcement must be limited to ensure continued resistance to shear. The maximum permitted transverse strain in this regard is often reported as 0.004 (Priestley et al. 1996).

Previous research offers differing conclusions with respect to the use of high-strength transverse reinforcing steel. Ahmed and Shah (1982) demonstrated analytically that high-strength transverse reinforcement may enhance the ductility of a column while having little effect on its strength. Martinez et al. (1982) propose limiting the strength of transverse reinforcement, based on their results showing that the higher steel strength was not fully utilized. Pessiki and Graybeal (2000) also conclude that the yield capacity of high-strength transverse reinforcement cannot be developed. Polat (1992) reported that ductility and strength enhancements were less than proportional to the strength of the transverse confining steel. Muguruma et al. (1990) demonstrated very high axial ductilities using high-strength transverse reinforcement and reported yielding of transverse reinforcement having yield strengths of 198 ksi shortly after the peak axial load is achieved. Yong et al. (1988) observed two peaks on their axial load-deformation responses; the high-strength transverse reinforcement did not yield initially but had yielded at the second peak. Muguruma et al. (1991) suggest that high-strength transverse reinforcement offers better control of longitudinal bar buckling than normal strength confining steel. Cusson and Paultre (1994) report improvements in strength and ductility due to high-strength confining steel only for well-confined columns. Improvements in axial column behavior with high-strength transverse reinforcement have also been reported by Bjerkeli et al. (1990), Nagashima et al. (1992), Razvi and Saatcioglu (1994), and Nishiyama et al. (1993). Studies that have specifically used A1035 transverse reinforcement have provided similar conclusions (Restrepo et al. 2006, Stephan et al. 2003, El-Hacha and Rizkalla 2002).

1.3.6 Bond and Development

Bond characteristics of ASTM A1035 reinforcing bars should not be expected to differ significantly from those of conventional reinforcing steel grades since neither the steel modulus nor bar deformations differ (Ahlborn and Den Hartigh 2002, Florida 2002). Studies that have reported load-slip relationships for A1035 steel have not concluded that these differ in any significant manner from similar relationships established for A615 bars (Ahlborn and DenHartigh 2002, El-Hacha et al. 2002 and 2006). Limited evidence (Sumpter 2007 and Zeno 2009) suggests modestly improved bond behavior that is believed to be associated with the rib geometry resulting from the rolling of the tougher A1035 material. Nonetheless, this effect is modest and cannot be generalized across material heats.

Due to the higher bar stress to be developed, A1035 bars require a longer development length (l_{db}). However, simply increasing development length without providing confinement is an inefficient means of developing greater stresses (Seliem et al. 2006 and 2009, El-Hacha et al. 2006). With long development (or splice) lengths, the bond stress at the "front" of the development length is exhausted before the bond stress along the entire development length can be developed (Viwathanatepa et al. 1979).

Confining reinforcement around development regions or splices is required to control the splitting cracks associated with a bond failure (Seliem et al. 2009). With higher strength steel, greater bar strain and slip will occur prior to development of the bar. The associated displacement of the bar lugs drives the splitting failure beyond that where yield of conventional bars

would occur; thus, confining reinforcement is critical in developing higher strength bars.

Seliem et al. (2009) assessed the present empirical development length equations prescribed by ACI 318 (2008) and ACI 408 (2003) when applied to developing A1035 bars. ACI 318 was found to underestimate development length requirements when no confining reinforcement was present and was only marginally improved when confining reinforcement was used. The ACI 408 recommendations were found to be adequate whether confinement was present or not. Present AASHTO requirements were not assessed although these can be shown to result in comparable development lengths to the requirements of ACI 408 in cases where confinement is present. Peterfreund (2003), in a study of A1035 reinforcement for bridge decks (#4 and #5 bars only), concluded to the contrary, that is, the ACI 318 requirements for development length were adequate to develop A1035 bars with no confining reinforcement present. However, in his study, Peterfreund used the simplified ACI equation which results in development lengths almost twice as long as the more rigorous approach used by Seliem et al. and others. Seliem et al. recommended that confining reinforcement always be used when developing A1035 or other high-strength reinforcing steel.

1.3.6.1 Development of Standard Hooks

Ciancone et al. (2008) evaluated the behavior of standard hooks made using #5 and #7 A1035 steel. No confinement reinforcement was provided in the specimens. While the #5 hooks were able to develop their yield capacity of 100 ksi, the #7 hooks were not. This result suggests an effect of bar size and supports the need for confining reinforcement when developing A1035 bars.

1.3.7 Serviceability Considerations

A fundamental issue in using A1035 or any other high-strength reinforcing steel is that the stress at service load (f_s; assumed to be on the order of $0.6f_y$) may be greater than with conventional Grade 60 steel. Consequently, the service load reinforcing bar strains are greater (i.e., $\varepsilon_s = f_s/E_s$). This larger strain impacts deflection calculations and crack control parameters. Regardless of this discussion, as discussed previously, most studies of members reinforced with A1035 steel exhibit serviceability performance, as measured by both deflections and crack widths, similar to that of members reinforced with A615 bars.

1.3.7.1 Deflection Calculations

Deflection of reinforced-concrete flexural members is most typically determined using an equivalent moment of inertia in an equation for elastic deflection. Both AASHTO (2007) and ACI 318 (2008) prescribe Branson's Equation (Branson 1963) to determine an equivalent moment of inertia (I_e) of a cracked concrete section as follows:

$$I_e = \left(\frac{M_{cr}}{M_a}\right)^m I_g + \left[1 - \left(\frac{M_{cr}}{M_a}\right)^m\right] I_{cr} \le I_g \qquad \text{(Eq. 1)}$$

Where:

I_g = moment of inertia of gross concrete section;
I_{cr} = moment of inertia of fully cracked concrete section;
M_{cr} = moment to cause cracking;
M_a = applied moment at which I_e is calculated; and
m = factor as defined below.

Setting $m = 4$ accounts for tension stiffening effects at the critical section along a span, while calculations are conventionally made setting $m = 3$ to reflect the "average" stiffness across the entire span. Equation 1 is found to be generally satisfactory for beams having typical amounts of non-prestressed reinforcement; indeed this equation was originally calibrated based on beams having a reinforcement ratio of $\rho = 0.0165$ (Branson 1963). The value of I_e calculated using Equation 1 is only slightly smaller than I_g in cases where M_a is only marginally larger than M_{cr}. This case generally happens in members having a low reinforcement ratio, typically $\rho < 0.006$. For such members, the calculated value of I_e is very sensitive to changes of M_{cr} (Gilbert 1999). Thus, Equation 1 may overestimate the effective moment of inertia for lightly reinforced flexural members having an I_g/I_{cr} ratio greater than 3 (Scanlon et al. 2001, Bischoff 2005, and Gilbert 2006). As ρ decreases, I_g/I_{cr} increases exponentially and M_a/M_{cr} decreases. The result is that the effective moment of inertia, I_e, is overestimated on the order of 200% when $\rho = 0.007$ but by only about 10% at $\rho = 0.025$ (Nawy and Neuwerth 1977). Bischoff (2005) reports that Branson's Equation underestimates short-term deflection for concrete members when the reinforcing ratio is less than approximately 1% and the I_g/I_{cr} ratio is greater than 3.

Several attempts have been made by different investigators to modify Branson's Equation, aiming to improve the accuracy of the predicted deflection (Grossman 1981, Rangan 1982, Al-Zaid et al. 1991, Al-Shaikh and Al-Zaid 1993, Fikry and Thomas 1998). With the exception of Rangan (1982), none of these modifications has been adopted into building codes; Branson's Equation remains the standard calculation for computing effective moment of inertia.

The following two approaches have been proposed to modify Branson's Equation to address its efficacy when used with lower reinforcing ratios:

- Introduce a coefficient, β, into the first term of Equation 1 to modify I_g (Gao et al. 1998). β is less than unity and is calculated based on reinforcing bar modulus (for

softer reinforcing materials such as FRP) (Theriault and Benmokrane 1998, Masmoudi et al. 1998) or reinforcing ratio relative to the balanced ratio (i.e., ρ/ρ_b) (Yost et al. 2003). The latter approach is necessary when considering high-strength steel reinforcement.
- Adjust the exponent m (Dolan 1989) as a function of the reinforcing ratio (Toutanji and Saafi 2000; Al-Zaid et al. 1991) or simply increase the value of m (Brown and Bartholomew [1996] propose $m = 5$).

Other methods involving finding an effective modulus of the beam have been proposed by Murashev (1940), Rao (1966), and CEB-FIP (1993). Finally, approaches involving integrating curvature along a beam have been proposed by Ghali (1993), Toutanji and Saafi (2000), Rasheed et al. (2004), and Razaqpur et al. (2000).

Bischoff (2005), in addition to providing a thorough review of all deflection investigations briefly summarized above, proposes a method of calculating the effective moment of inertia at a section that better captures the effects of tension stiffening particularly for "soft" sections having low reinforcing ratios. This method is summarized in Equation 2.

$$I_e = \frac{I_{cr}}{1-\eta\left(\frac{M_{cr}}{M_a}\right)^2} \qquad \text{(Eq. 2)}$$

Where:

$\eta = 1 - I_{cr}/I_g$

$I_{cr} = \left[\frac{k_{cr}^3}{3} + n\rho(1-k_{cr})^2\right] bd^3$

$k_{cr} = \sqrt{(n\rho)^2 + 2n\rho} - n\rho$

n = modular ratio E_s/E_c and

ρ = reinforcing ratio.

Moment-curvature relationships may then be predicted using $M = E_c I_e \phi$. The derivation of Equation 2 is presented in Bischoff (2005) and is further shown to be essentially equivalent to the Murashev (1940) equation, of which the Branson Equation is a simplification.

1.3.7.2 Crack Control

The traditional "z-factor" or Gergely-Lutz (1968) approach of *directly* assessing cracking behavior of concrete beams was dropped by ACI 318 in 1999 and by AASHTO in 2005 in favor of a simplified version of the alternative approach proposed by Frosch (1999 and 2001) that prescribed spacing limits for longitudinal reinforcing steel thereby *indirectly* controlling crack width. The empirically tuned Gergely-Lutz approach was considered inadequate to address cases having very large concrete cover (ACI 224 2001). Additionally, Beeby (1983) showed no conclusive evidence linking reinforcement corrosion with crack width while Poursaee et al. (2010) show that a crack as small as 0.004 in. acts as a free surface with respect to water ingress. Despite the latter assertion, the simplified versions of the Frosch approach adopted by AASHTO and ACI implicitly assume a maximum crack width of 0.017 in. which was also the value assumed for exterior exposure conditions when applying the Gergely-Lutz approach prior to 1999.

The ACI 318 version of the Frosch equation for determining the maximum spacing of flexural reinforcement to affect adequate crack control is as follows:

$$s \le 15\left(\frac{40{,}000}{f_s}\right) - 2.5c_c \le 12\left(\frac{40{,}000}{f_s}\right) \qquad (f_r \text{ in psi}; c_c \text{ in inches}) \qquad \text{(Eq. 3)}$$

Where:

c_c = minimum concrete cover measured to center of reinforcing bar closest to the extreme tension face and

f_s = service load stress in reinforcing bar closest to the extreme tension face.

Equation 3 may be rewritten in terms of reinforcing bar strain (ε_s), assuming the material obeys Hooke's Law, and calibrated for any desired crack width (w) (Ospina and Bakis 2007), as follows:

$$s \le 1.15\left(\frac{w}{\varepsilon_s}\right) - 2.5c_c \le 0.92\left(\frac{w}{\varepsilon_s}\right) \qquad (w \text{ in inches}) \qquad \text{(Eq. 4)}$$

Thus, the relationship between crack width, reinforcing bar strain, and longitudinal bar spacing required to control cracking is demonstrated in a relatively simple format consistent with present design practice. The relationship is material independent, only assuming a linear behavior is present. Available data comparing the cracking behavior of steel and FRP-reinforced members confirm the implications of this approach (e.g., Creazza and Russo 2001, Bischoff and Paixao 2004). Ospina and Bakis conclude that the use of Equation 3 is valid, if not conservative, for beams having large elastic reinforcing bar strains.

AASHTO Equation 5.7.3.4-1 (AASHTO 2007) takes the same form as the ACI equation, as follows:

$$s \le \frac{700\gamma_d}{\beta_s f_s} - 2d_c \qquad (f_s \text{ in ksi}; d_c \text{ in inches}) \qquad \text{(Eq. 5)}$$

Where:

d_c = minimum concrete cover measured to center of reinforcing bar;

f_s = service load stress in reinforcing bar;

$\beta_s = 1 + \frac{d_c}{0.7(h - d_c)}$; and

h = overall depth of the concrete section.

This equation can therefore also be rearranged in a manner similar to Equation 4, resulting in the same conclusions and implications.

$$s \le 1.34\left(\frac{\gamma_d}{\beta_s}\right)\left(\frac{w}{\varepsilon_s}\right) - 2d_c \qquad \text{(Eq. 6)}$$

For Class 1 exposure, Equation 5 is calibrated, through $\gamma_d = 1$, for a crack width of 0.017 in.; for Class 2 ($\gamma_d = 0.75$) or other exposures, the de facto crack width is $\gamma_d \times 0.017$. In the commentary to §5.7.3.4, AASHTO describes the use of the γ_d term to calibrate Equation 5 for any desired crack width limitation.

It is well established that crack control is improved by using a larger number of well-distributed, smaller diameter bars to make up the required area of flexural reinforcing steel. The number of bars that can be provided, however, is restricted by minimum spacing requirements (AASHTO LRFD §5.10.3). Thus, if the area of flexural steel is provided using the greatest number of bars that may be placed in a section, such a section, theoretically, should exhibit the best control of crack widths. This relationship is manifested in Equations 4 and 6 where the crack width (w) is proportional to the flexural bar spacing (s). Ward (2009) shows that for $f_s = 36$ ksi (appropriate for bars having $f_y = 60$ ksi), Class 1 and 2 exposure crack width limits (0.017 in. and 0.0128 in., respectively) are met for all permissible designs (see Appendix I).

As seen in Equations 4 and 6, crack width (w) is also proportional to reinforcing bar stress (or strain, in this case, ε_s). Therefore, if $f_s = 60$ ksi (appropriate for bars having $f_y = 100$ ksi), crack widths are expected to increase. In this case, Ward (2009) shows that while the Class 1 exposure crack width limit (0.017 in.) is met for all practical beam design cases, the Class 2 limit (0.0128 in.) is generally only met with #5 bars and smaller (see Appendix I). The implication of this is that accepted crack width limits may not be met with higher permitted reinforcing bar stress. Ward (2009) proposes the following two alternatives to addressing crack control for beam design in the context of AASHTO LRFD (§5.7.3.4):

- Limit $f_s \le 50$ ksi in order to satisfy present Class 2 requirements; or
- Limit $f_s \le 60$ ksi and remove the Class 2 limit when considering high-strength reinforcing steel.

Indeed, AASHTO LRFD Commentary C5.7.3.4 provides the following third alternative:

> The crack width is directly proportional to the γ_d factor, therefore, if the individual Authority with jurisdiction desires an alternate crack width, the γ_d factor can be adjusted directly.

Thus a value of $\gamma_d > 1.0$ may be permitted as appropriate. This approach is additionally deemed to be appropriate for deck slabs since the value of f_s will be appreciably lower. It is also noted that deck slabs designed using the empirical approach of AASHTO LRFD §9.7.2 are not required to satisfy §5.7.3.4.

1.3.7.3 "Acceptable" Crack Widths

ACI Committee 224 (2001) suggests that crack widths exceeding 0.016 in. may be unacceptable from the standpoint of aesthetics. Similarly, Halvorsen (1987) states that a case could be made that crack widths ranging from 0.006 to 0.012 in. could be considered unacceptable for aesthetic reasons as they are visible to the naked eye; hence, generating a sense of insecurity about structural distress. Beyond this, there is little consensus as to acceptable crack widths.

1.3.7.4 Analytical Assessment of Crack Widths

Soltani (2010) conducted a detailed analytical assessment of expected crack widths. This approach accounted for nonlinear stress transfer between the bar and surrounding concrete along the development length and nonlinear bar slip relationships associated with the stress transfer. Soltani considered a range of bar sizes and reinforcement ratios and used experimentally determined R-O stress-strain relationships to model the steel reinforcement. Figure 2 provides a representative result showing anticipated average crack widths at the location of the reinforcing steel for a concrete tension zone having a reinforcing ratio of 2%. Soltani concluded that through reinforcing bar stresses of 72 ksi, average crack widths (it is only possible to consider average crack widths in an analytical context) remain below 0.016 in. for all but the largest bars considered (#10). The results were relatively insensitive to changes in reinforcing ratio. Finally, it is noted that crack widths expressed at the surface of a concrete member may be amplified from those at the reinforcing bar location due to the depth of concrete cover and/or the curvature of the member.

1.3.8 Corrosion Performance of Reinforcing Steel Grades

The quantification of corrosion resistance is beyond the scope of the present work but is summarized here in the

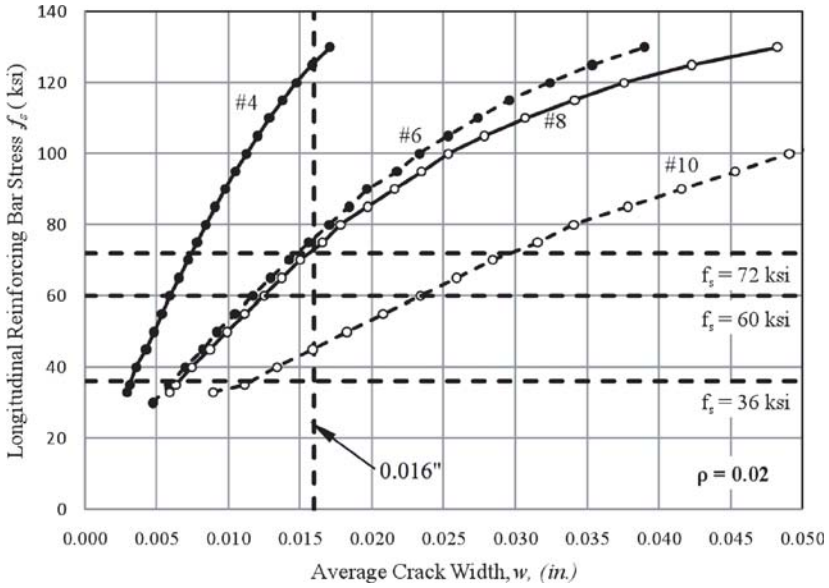

Figure 2. Theoretical average crack widths for tension zone having ρ = 0.02 (Soltani 2010).

interest of completeness and because enhanced corrosion resistance is a major factor behind the drive to adopt A1035 reinforcing steel. A1035 steel is a microcomposite Fe-C-Cr-Mn alloy that has an average chromium content of approximately 9%, which is too low to be referred to as "stainless steel" (Cr > 10.5%) but sufficiently high to impart a degree of corrosion resistance when compared to "black steel" as represented by A615 or A706. A large number of studies have compared the corrosion resistance of A1035 steel with that of A615 and A706 black steel and A955 austenitic (304 and 316), duplex (2101), and ferritic stainless steels. Generally, the relative performance of these materials in terms of their corrosion resistance is ranked from most to least susceptible to corrosion in the order indicated in Table 2. Thus, microcomposite alloys tend to be 2 to 10 times more corrosion resistant than black steel while austenitic stainless steel may be a few orders of magnitude improved. A summary of corrosion performance of reinforcing steel is presented in Appendix A and provides quantitative data available in the literature.

Table 2. Relative corrosion performance of reinforcing steel grades.

Material	Performance, where A615 = 1.0
A706 black steel	0.5 – 0.8
A615 black steel	1.0
A1035 microcomposite alloy	2 – 10
A955 2101 duplex stainless steel	2 – 10
A955 304 austenitic stainless steel	>10
A955 316 austenitic stainless steel	>20

1.4 Survey of Use of High-Strength Steel Reinforcement in Bridge Structures

A written survey intended to assess the current practice and the use of high-strength reinforcing steel was disseminated in June 2007. In all, 65 surveys were distributed to U.S. state DOTs, Canadian Ministries of Transportation (MOTs), and a few other agencies. A copy of the survey instrument and "raw" responses are provided in Appendix J.

Thirty-two surveys were returned—a response rate of 49%. Of these, 27 (84% of those returned) report no use of "steel reinforcement (not prestressing rods or tendons) with specified yield strengths greater than 60 ksi" (Question #1). The primary reason for not utilizing high-strength reinforcement (Question #1a) was not that it was not permitted per se but simply has not been used (15 of 27 respondents answering "no" to Question #1). Despite this response, some respondents went on to cite the prohibition by AASHTO on reinforcing steel having strengths greater than 60 ksi (9 of 27 respondents). Additionally, five responding jurisdictions stated their specifications specifically "prohibit yield strengths above 60 ksi." It is not clear whether the prohibition cited by these latter respondents is a specific prohibition or simply a prohibition by exclusion (such as, reinforcing steel strength *not to exceed* 60 ksi . . .). In one case, the jurisdiction specifically requires the use of ASTM A706 Grade 60 reinforcing steel. Eleven of 27 respondents identified the lack of "data on performance to satisfy our performance requirements." One such response specifically cited concerns about "strength, ductility for seismic [loading] and, to a lesser extent, weldability."

Of the five jurisdictions reporting use of high-strength reinforcing steel, three report only the use of steel up to 75 ksi, and two report use of steel having a yield strength greater than 100 ksi (Question #2). Respondents indicated that high-strength reinforcement is not excluded from use in any application and, indeed, has been applied in all applications cited in Question #3 except "spirals in piers." One jurisdiction reporting use of steel having f_y greater than 100 ksi reports its use as only "main flexural reinforcement in beams," although it is apparently "permitted" elsewhere. The second such jurisdiction reports its use as only slab reinforcement. The reasons for incorporating this steel (Question #4) are reported as being to "improve durability by enhancing corrosion resistance of reinforcement." Both jurisdictions having used f_y greater than 100 ksi in flexural applications report this use as being on an "experimental/trial" basis. Three jurisdictions report fewer than 10 structures having high-strength steel reinforcement while one reports between 10 and 50 structures (Question #5).

Design using high-strength reinforcement was facilitated by the engineer of record's best judgment (Question #6). Three of the five respondents reported simply using AASHTO design methods for 60 ksi reinforcement and replacing the steel, one-for-one, with high-strength steel bars. In one response, high-strength steel is simply used in place of 60 ksi steel for areas requiring corrosion resistance; nonetheless, increased lap lengths are prescribed in this case. A comment from this respondent follows (identifying information has been removed):

> [This jurisdiction] has mainly used [A1035] steel to aid with corrosion. We have been very conservative with its usage. Usually designing as if we are using 60 ksi rebar or in some instances more. Then we will use longer development lengths to assist with ultimate capacities. Codes [are] not fully written to use such high-strength rebar properties; therefore [this jurisdiction] hasn't generally designed for maximum strength usage in bars. However, we do look at ultimate bending capacity and increase laps if deemed prudent. We have built about five slab bridges using [A1035] entirely. We have used it in some bridge decks—three to seven. Then we use it in our P/S girders for shear reinforcing [bars] in the ends of girders and as shear reinforcement between the girders and the bridge deck—substitute it for 60 ksi rebar—assuming 60 ksi properties.

No problems or impediments to design were reported by any respondents (Questions 7 to 9). One respondent specifically stated that they were satisfied with the results versus cost of high-strength steel when compared to 60 ksi although they had concerns over crack width with higher yield strength (paraphrased by authors of this report).

> We advertised one project where high-strength bars [A1035] were allowed as an alternative to epoxy-coated rebar. The contractor elected to use epoxy-coated bars. We would only allow the rebar to be designed for up to 75 ksi, until AASHTO has specifications to account for higher strength bars.

1.4.1 Survey of Use of Stainless Steel Reinforcement in Bridge Structures

A similar, abbreviated survey (Appendix J) addressing the use of stainless steel was also conducted. In this case, 28 responses were received. Thirteen jurisdictions reported the use of stainless steel reinforcing bars; in all but one case for slab reinforcement and in most cases on an experimental basis. Design for stainless steel bars was apparently a one-for-one substitution for conventional reinforcing bars.

1.4.2 Reported Use of A1035 Reinforcing Steel in Highway Bridge Infrastructure

MMFX Inc., the only supplier of A1035 reinforcing steel, reports 25 U.S. and 4 Canadian jurisdictions that have used A1035 reinforcing steel in at least one bridge project as of December 2009. Most applications have been bridge decks. According to MMFX, most applications are simply one-to-one replacement of A615 with A1035 in order to take advantage of the improved corrosion resistance of the latter. Nonetheless, there are 17 known projects where a value greater than $f_y = 60$ ksi was used in design; these are listed in Appendix J. Design values of f_y of 75, 80, and 100 ksi are reported, although most were 75 ksi (thus, presumably taking advantage of the upper limit on f_y prescribed by AASHTO specifications).

Cross-referencing existing projects with the survey indicate that most projects were experimental "demonstration" projects. It is further noted that not all jurisdictions reported to have erected structures returned the survey. Additionally, five jurisdictions reporting in the survey no projects with high performance steel are revealed by the project list to have, in fact, one or two existing demonstration projects.

CHAPTER 2

Research Program and Findings

2.1 Research Approach

The focus of the experimental phase of this study was on the use of ASTM A1035 (2009) reinforcing steel since it captures both behavioral aspects of interest (i.e., it has a very high strength and no discernable yield plateau). The project identified aspects of reinforced-concrete design and of the AASHTO LRFD specifications that may be affected by the use of high-strength reinforcing steel. Design issues were prioritized and an integrated experimental and analytical program was designed to develop the data required to permit the integration of high-strength reinforcement into the LRFD specifications. This program included parametric, experimental, and analytical studies in addition to a number of "proof tests" intended to validate existing LRFD provisions when applied to higher strength reinforcing steel. Table 3 provides a summary of the primary aspects addressed in this study and the approach by which they were addressed. Subsequent sections of this chapter discuss each experimental and/or analytical program in turn.

2.2 Mechanical Properties of Reinforcing Steel

Table 4 provides a summary of all reinforcing bar grades and sizes tested as part of this study. Batch numbers are underlined and the specimens in which each batch was utilized are also indicated. Appendix A provides summaries of all tests conducted and axial stress-strain curves obtained from all bars tested. All tension tests were conducted in compliance with ASTM E8 and were conducted on full bar sections (not machined coupons).

As reported in Appendix A, A1035 bars and A496 and A82 wire exhibit no discernable yield plateau. A615 and A706 exhibit clearly defined yield plateaus and A955 stainless steel grades exhibit a clear "abrupt change of stiffness," but no defined plateau.

2.2.1 ASTM A1035 Reinforcing Steel

The data obtained for A1035 bars in this study are generally consistent with those reported by others as summarized in Section 1.3.2. That is

- Values of yield (f_y) and ultimate (f_u) strengths were consistent from batch to batch and bar size to bar size. The average ultimate strength was $f_u = 163$ ksi having a COV of only 3.9% across all specimens. The average rupture strain exceeded 0.10 and had a COV of 28%.
- The use of the ASTM A1035-prescribed 0.2% offset method for establishing yield strength results in an average yield strength, $f_y = 129$ ksi (COV = 4.6%). Stress corresponding to a strain of 0.007 resulted in the most consistent (COV = 4.0%) value of yield strength, $f_y = 133$ ksi.
- Yield and ultimate strength values remained essentially unaffected by bar size.
- Regardless of the manner by which yield stress was determined, the condition $f_u > 1.25f_y$ was satisfied in all cases.
- Calculated values of modulus of elasticity, E_s, determined as secant modulus at 60 ksi were very consistent, averaging 28,137 ksi (COV = 7.1%).
- All bars tested exhibited linear behavior through stress levels of at least 70 ksi.

A Ramberg-Osgood (R-O) function was established for each batch of reinforcing steel that was used in a number of subsequent analyses reported in this work. The R-O function is given in Equation 7 (Ramberg and Osgood 1943). The parameters, *A, B,* and *C,* established using a nominal value of $E_s = 29{,}000$ ksi are given in Appendix A. The general form of the resulting R-O curve is shown in Figure 3.

$$f = 29{,}000\varepsilon\left\{A + \frac{1-A}{\left[1+(B\varepsilon)^C\right]^{1/C}}\right\} \le f_{pu} \quad (\text{ksi}) \qquad \text{(Eq. 7)}$$

Table 3. Research approaches taken with respect to various aspects of this study.

Aspect of Study	Experimental		Analytical	Notes
	Parametric	Proof Tests		
Mechanical properties of reinforcing steel	X			47 batches including 8 steel grades and 13 bar sizes tested
Flexural reinforcement	X		X	6 large-scale beam tests and extensive parametric analysis
Fatigue		X		2 large-scale beam proof tests
Shear reinforcement	X			5 large-scale beam tests and 4 AASHTO Type I girders
Shear friction behavior		X		8 full-scale proof tests
Compression members			X	Extensive analytical study
Bond and development		X		18 full-scale proof tests
Deflections	Considered with flexure		X	Integration of flexural data into extensive parametric studies
Crack widths			X	

Table 4. Reinforcing steel tested in this study and its use in specimens.

ASTM Designation	Bar Size	Batch Number and Test Specimen Use				
A1035	#3	**1**: SR1 to SR5; P1035-3A	**1B**: P1035-3B	**2**: Type I-4	**3**: Type I-1 to 1-3*	
A1035	#4	**1**: all H; P1035-4A		**1B**: P1035-4B		
A1035	#5	**1**: F1; F3; D5-1; D5-2; all H; all fatigue		**2**: F4; F6; D5-3; D5-4		
A1035	#6	**1**: F2		**2**: F5		
A1035	#8	**1**: D8-1; D8-2; SR1 to SR4; all H		**2**: D8-3; D8-4; SR5		
A615	#3	**1**: D5-1; D5-2, D8-1, D8-2	**2**: D5-3; D5-4; D8-3; D8-4	**3**: all P615	**4**: all H; all fatigue	
A615	#4	**1**: F1 to F3; SR1 to SR4	**2**: F4-F6	**3**: Type I-1 to Type I-3	**4**: Type I-4	**5**: all P615
A706	#4	**1**: tension tests only		**2**: tension tests only		
A706	#6	**1**: tension tests only		**2**: tension tests only		
A706	#8	**1**: tension tests only		**2**: tension tests only		
A496	D4	**1**: tension tests only				
A496	D8	**1**: tension tests only				
A496	D12	**1**: tension tests only				
A496	D20	**1**: tension tests only				
A496	D31	**1**: tension tests only				
A82	W4	**1**: tension tests only				
A82	W8	**1**: tension tests only				
A82	W12	**1**: tension tests only				
A955 (316)	#4	**1**: tension tests only				
A955 (316)	#6	**1**: tension tests only		**2**: tension tests only		
A955 (316)	#8	**1**: tension tests only				
A955 (2205)	#4	**1**: tension tests only		**2**: tension tests only		
A955 (2205)	#6	**1**: tension tests only		**2**: tension tests only		
A955 (2205)	#8	**1**: tension tests only				
A955 (N32)	#4	**1**: tension tests only				
A955 (N32)	#6	**1**: tension tests only				
A955 (N32)	#8	**1**: tension tests only				

Notes:
*No test data are available for A1035 #3 batch 3 bars; no additional samples accompanied the bar order.
Test specimen labels:
D5-1, D5-2, D5-3, D5-4, D8-1, D8-2, D8-3, and D8-4: beam splice specimens; H: hooked specimens; F1, F2, F3, F4, F5, and F6: flexural specimens; P615, P1035-4A, P1035-4B: shear friction specimens; SR1, SR2, SR3, SR4, SR5: reinforced-concrete shear specimens; Type I-1, Type I-2, Type I-3, and Type I-4: AASHTO Type I girder shear specimens.

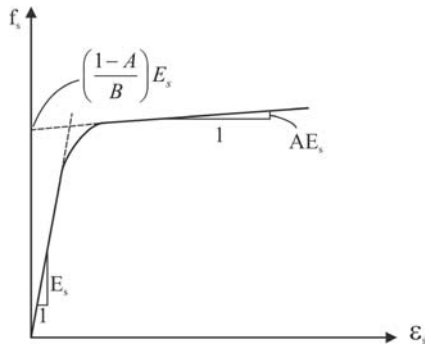

Figure 3. Ramberg-Osgood Curve and definition of parameters.

A critical objective of the present work is to identify an appropriate steel strength and/or behavior model to adequately capture the behavior of high-strength reinforcing steel while respecting the tenets of design and the needs of the designer. As will be described throughout this report, a value of yield strength, f_y, not exceeding 100 ksi was found to be permissible without requiring significant changes to the LRFD specifications or, more critically, to the design philosophy and methodology prescribed therein. Some limitations to this increase in permissible yield strength were identified and also are discussed. Based on the stress-strain diagrams obtained as part of the reported project and all previous studies, A1035 reinforcing steel easily meets a yield value of 100 ksi using the 0.2% offset method or for the 'stress at a strain' method for strains exceeding 0.004. All available test data exhibit nonlinear behavior at stresses greater than 70 ksi. Thus, it is felt that assumptions of a linear stress-strain relationship made for calculating service load displacements and crack width are likely adequate since service load stresses are traditionally taken as $f_s = 0.60f_y$. However, deflection or serviceability considerations at loads greater than this must account for the nonlinear nature of the reinforcement at high stresses.

Post-yield behavior, particularly when employing a plastic design methodology, will also be affected by both the lack of a well-defined yield plateau and the nonlinear post yield behavior. This behavior is most critical in seismic applications, which are beyond the scope of the present work.

2.3 Flexural Reinforcement

Flexural behavior and design of members reinforced with A1035 reinforcement and other grades of reinforcing bars that do not exhibit well-defined yield plateaus were examined analytically and experimentally. Different aspects of this component of the research are presented in this section.

2.3.1 Flexural Resistance

The nominal moment capacity (M_n) for non-prestressed members is commonly calculated by assuming a constant yield stress for the steel. For bars without a well-defined yield plateau, several approaches may be used to define the yield stress. In order to examine these methods, parametric studies were performed to assess the flexural resistance of members reinforced with various grades of steel reinforcement that do not have a well-defined yield plateau. The moment capacity was calculated by a number of methods ranging from simple design-oriented procedures to complex fiber analysis. In fiber analysis, a cross section is divided into layers (fibers). The cross sectional and material properties for each layer are defined, and strain compatibility between the layers is enforced. Realistic complete stress-strain relationships for concrete and steel layers are employed as opposed to simplified relationships typically used in the strain compatibility method. Therefore, complex analyses can be performed by fiber analysis technique. Comparing the results from the range of models made it possible to evaluate whether approximate methods are appropriate for members reinforced with reinforcing bars with no clear yield plateau and what material properties to use in these cases.

2.3.1.1 Members and Parameters

Sections modeled were deck slabs, rectangular beams, and T-beams with varying steel types, amounts of steel, and concrete compressive strengths. The variables considered are summarized in Table 5. A total of 286 cases were examined. Three different amounts of tensile reinforcement were incorporated in the rectangular beams. A maximum area of steel, $A_{s,max}$ was determined based on the minimum steel strain of 0.004 imposed by ACI 318-08 (ACI 2008). A minimum area of steel, $A_{s,min}$, was established to satisfy AASHTO §5.7.3.3.2 (i.e., to ensure that the flexural resistance with $A_{s,min}$ is at least $1.2M_{cr}$, where M_{cr} is the cracking moment of the section). The average of $A_{s,min}$ and $A_{s,max}$ also was considered. Rectangular beams with $A_{s,min}$ are in the tension-controlled region. Rectangular beams reinforced with $A_{s,max}$ have the lowest steel strains allowed by ACI 318-08. The average of $A_{s,min}$ and $A_{s,max}$ results in cross sections with strains between these limits. Because of the additional compression strength provided by the flanges of the T-beams, the calculated amount of steel required to provide $A_{s,max}$ (i.e., to ensure a minimum strain of 0.004) was found to be excessive and impractical. Therefore, the values of $A_{s,max}$ determined for the rectangular beams were provided in the corresponding T-beams. Nonetheless, the selected values of $A_{s,max}$ resulted in members that fell well into the tension-controlled region. Providing more steel to obtain members in the transition region was impractical; hence, only

Table 5. Variables for parametric studies.

Parameter	Deck Slab	Rectangular Beam	T-Beam
Dimensions	7 in. and 10 in. thick	12 in.×16 in., 12 in.×28 in., 12in.×36 in., 16 in.×28 in., 16 in.×36 in., and 16 in.× 40 in.	12 in.×28 in., 12 in.×36 in., 16 in.×36 in., and 16 in.× 40 in. with 96 in. effective flange width and 7 in. flange thickness
Concrete Strength, f'_c	5 ksi	5, 10, and 15 ksi	
Reinforcement Grades	A706, A496 & A82, A955 (3 grades), and A1035		
Bar Sizes	#4, #5, and #6	#6 for 12 in.-wide beams; and #8 for 16 in.-wide beams. All beams are assumed to have #4 stirrups with 2 in. of clear cover.	
Tension Reinforcement	Based on AASHTO spacing limitations	$A_{s,min}$, $A_{s,max}$, $0.5(A_{s,min}+A_{s,max})$	$A_{s,max}$ from corresponding rectangular beams

one amount of reinforcement was used for the T-beams. The amount of steel provided in the slabs was determined based on spacing limitations prescribed in AASHTO *LRFD Bridge Design Specifications,* §5.10.3.1, §5.10.3.2, and §5.10.8 (AASHTO 2004).

2.3.1.2 Capacity Calculation Procedures

The nominal moment capacity of each section was calculated both by a strain compatibility procedure using different methods for modeling the steel stress-strain relationships and a fiber analysis procedure. A commercial computer program XTRACT (2007) was used to perform the fiber analyses. The concrete was modeled using the unconfined concrete model proposed by Razvi and Saatcioglu (1999). The measured stress-strain data (refer to Appendix A) for each type of reinforcing steel were input directly into the XTRACT program. By using the experimentally obtained data, a more accurate capacity can be determined. Moment-curvature analyses were run in which the concrete strain was limited to 0.003, the level of strain used in the strain compatibility analyses. The results from fiber analyses are deemed to predict the most accurate flexural capacity.

An Excel program (Shahrooz 2010) was used to compute flexural capacities based on strain compatibility analysis. The constitutive relationship of the reinforcing bars was modeled (1) as elastic-perfectly plastic with the yield point obtained by the 0.2% offset method and the stress at both strain = 0.0035 and strain = 0.005; and (2) by the Ramberg-Osgood (1943) function determined to best fit the experimentally obtained data. The analyses utilized data from the measured stress-strain relationships of 102 samples of A706, A496 and A82, A955, and A1035 reinforcing bars. The measured relationships are presented in Appendix A. Table 6 summarizes the yield strengths obtained from each method.

An equivalent stress block for high-strength concrete, developed as part of NCHRP 12-64 (Rizkalla et al. 2007), was used to compute the concrete contribution to section behavior. Additional information is provided in Appendix B and Ward (2009).

2.3.1.3 Results

The moment capacity for each section computed based on the aforementioned methods was normalized with the corresponding capacity calculated from the fiber analyses. Table 7 summarizes the results of the strain compatibility analyses conducted using the Ramberg-Osgood function for the rectangular beams, T-beams, and slabs for all of the steel types and the selected concrete strengths considered. The computed capacities are below or nearly equal to those calculated based on fiber analysis (i.e., the ratios are close to, or slightly less than, unity). The exceptional estimates of the expected capacity based on the Ramberg-Osgood function in conjunction with strain compatibility analysis should be expected since this function closely replicates the measured stress-strain curves that were used in the fiber analyses. Additionally, the good correlation suggests that well-established procedures can be used to calculate the flexural capacity of members reinforced with bars that do not have a well-defined yield plateau so long as the stress-strain relationship is modeled accurately.

In spite of its success, the use of Ramberg-Osgood functions is not appropriate for routine design. Most designers are familiar with using a single value of reinforcing bar yield, f_y. For this reason, further strain compatibility analyses were carried out using the yield strength values given in Table 6. The results are summarized in Table 8. For the beams having 5 ksi concrete, the ratios from any of the values of yield strength are less than unity (i.e., the flexural strength can be conservatively computed based on any of three methods used to establish the yield strength). The same conclusion cannot be drawn for the beams with 10 and 15 ksi concrete. For a

Table 6. Average and standard deviations of f_y (ksi).

Bar	Method for Establishing the Yield Strength					
	0.2% Offset Method		Strain @ 0.005		Strain @ 0.0035	
	Avg. (ksi)	Std. Dev. (ksi)	Avg. (ksi)	Std. Dev. (ksi)	Avg. (ksi)	Std. Dev. (ksi)
A496 & A82	93	6.02	93	5.71	88	5.95
A706	68	3.30	68	3.83	67	3.05
A995	78	5.21	78	5.21	72	3.53
A1035	127	7.25	115	4.59	93	4.01

Table 7. Ratios of flexural capacity determined from Ramberg-Osgood strain compatibility analysis to that determined from fiber model.

Section	Average	Minimum	Maximum	Standard Deviation
Rectangular	0.944	0.835	0.999	0.037
T-beam	0.962	0.925	0.999	0.017
Slab	0.875	0.668	0.955	0.107

Note: Ratio less than 1 is conservative.

Table 9. Cases where elastic-plastic analysis overestimated flexural capacity.

Steel Type	f'_c (ksi)	ρ_g	Ratio
A706	10	3.84%	1.014
	15	3.67%	1.006
	15	3.67%	1.005
	15	4.06%	1.022
	15	4.11%	1.023
	15	2.88%	1.072
	15	4.07%	1.023
A995	15	3.43%	1.020
A1035	15	2.65%	1.007

limited number of cases (given in Table 9) involving relatively large longitudinal reinforcement ratios (ρ_g), the strength ratio exceeds unity if the capacity is based on an idealized elastic-perfectly plastic stress-strain relationship with the yield strength taken as the stress at a strain of 0.005 or determined based on the 0.2% offset method. That is, the yield strengths based on these two methods may result in slightly unconservative estimates of the expected capacity in cases with large reinforcement ratios and high-strength concrete.

The aforementioned behavior can be understood with reference to Figure 4, which depicts a measured stress-strain curve for an A706 bar along with the idealized elastic-perfectly plastic model based on the yield strength taken as the value determined from the 0.2% offset method and the stress at strain equal to 0.005. Note that in this case, these two methods result in the same values of yield strength. Between points "a" and "b" (see Figure 4) the elastic-perfectly plastic model deviates from the measured stress-strain diagram. The stresses based on this model exceed the actual values. For strains below point "a" and strains above "b," the stresses from the idealized model are equal to, or less than, the measured values. As the reinforcement ratio increases (i.e., as the amount of longitudinal steel becomes larger), the strain in the reinforcing bars at any given applied moment will become less. For the cases involving the large reinforcement ratios shown in Table 9, the steel strains fall between points "a" and "b" when the extreme concrete compressive stress of 0.003 is reached. Thus, the higher yield strength from the elastic-perfectly plastic model overestimates the actual flexural capacity.

In the case of T-beams and slabs, any of the aforementioned methods for establishing the yield strength result in acceptable, conservative flexural capacities. As is evident from Table 10, the ratios of the flexural capacity based on simple elastic-perfectly plastic models to the corresponding values from fiber analysis are less than one. The trend of data is expected, as the longitudinal strain in a T-beam will be higher than that in an equivalent rectangular beam because of the additional compressive force that can be developed in the flange. The smaller depths of the slabs will also increase the strain in the longitudinal bars. In both these cases, the larger strains will correspond to cases beyond the strain at point "b" in Figure 4, where the elastic-plastic assumption underestimates the real stress developed in the steel.

2.3.1.4 Summary and Recommendations

Considering the presented results, the use of Ramberg-Osgood functions for defining the stress-strain characteristics of reinforcing bars without a well-defined yield plateau will produce the most accurate estimate of the actual flexural

Table 8. Ratios of rectangular beam flexural capacity calculated from elastic-plastic analyses to that from fiber model.

Yield Point	f'_c (ksi)	Average	Minimum	Maximum	Standard Deviation
@ Strain = 0.0035	5	0.820	0.578	0.958	0.094
	10	0.815	0.603	0.964	0.100
	15	0.825	0.596	0.991	0.108
@ Strain = 0.005	5	0.884	0.727	0.977	0.070
	10	0.880	0.652	1.014	0.084
	15	0.891	0.688	1.072	0.092
0.2% offset	5	0.909	0.789	0.966	0.057
	10	0.884	0.756	0.971	0.075
	15	0.890	0.749	1.007	0.092

Note: Ratio less than 1 is conservative.

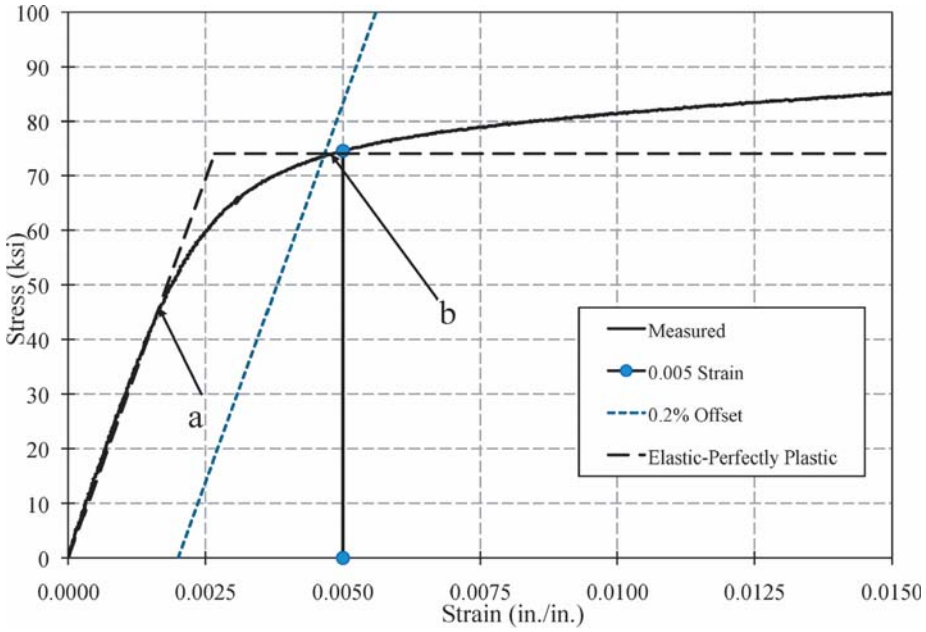

Figure 4. Typical measured stress-strain diagram and elastic-perfectly plastic model.

capacity. The use of the strain compatibility approach assuming an elastic-perfectly plastic steel stress-strain relationship having a yield stress defined at either a strain of 0.0035 or 0.005 ensures that the flexural capacity is computed conservatively and reliably for the range of reinforcement ratios and concrete compressive strengths encountered in practice. However, for beams with reinforcement ratios exceeding 2.65%, the definition of the yield stress at a strain of 0.0035 is more appropriate. The latter approach is consistent with the currently prescribed ACI 318 (ACI 2008) approach. The use of the stress at 0.0035 strain effectively ensures that the steel strain under the design condition is beyond point "b" shown in Figure 4. (Recall that this condition is enforced in the design approach through the definition of A_{smax} as the steel content that allows a steel strain of 0.004 to be achieved.)

Table 10. Ratios of T-beam and slab flexural capacity calculated from elastic-plastic analyses to that from fiber model.

T-Beams				
Yield Point	Average	Minimum	Maximum	Standard Deviation
@ Strain =0.0035	0.741	0.571	0.859	0.091
@ Strain =0.005	0.795	0.659	0.890	0.069
0.2% offset	0.748	0.718	0.764	0.019
Deck Slabs				
Yield Point	Average	Minimum	Maximum	Standard Deviation
@ Strain =0.0035	0.828	0.609	0.953	0.115
@ Strain =0.005	0.854	0.638	0.971	0.113
0.2% offset	0.909	0.839	0.951	0.043

Note: Ratio less than 1 is conservative.

2.3.2 Tension-Controlled and Compression-Controlled Strain Limits for High-Strength ASTM A1035 Reinforcing Bars

2.3.2.1 Fundamental Concepts

The current steel strain limits of 0.005 defining the lower bound of tension-controlled behavior and 0.002 or less defining compression-controlled behavior are based on having an adequate change in steel strain from service load to nominal strength. Nonetheless, the strain limits have been calibrated based on the expected performance of flexural members reinforced with Grade 60 longitudinal bars. Considering that A1035 bars could be subjected to larger service level strains and have different stress-strain relationships, the strain limits defining tension-controlled and compression-controlled behaviors need to be reevaluated.

2.3.2.2 Development

The curvature ductility of sections reinforced with A615 Grade 60 reinforcement was computed for the following cases: concrete compressive strength from 4 to 15 ksi in 1-ksi increments; tension longitudinal reinforcement (ρ) from 0.1% to 6.1% in 0.06% increments; compression longitudinal reinforcement (ρ') taken as 0, 0.5ρ, and ρ; and ratio of the effective depth of the compression longitudinal bars to the effective depth of the tensile longitudinal bars (d'/d) equal to 0 or 0.1. The stress-strain relationship of Grade 60 was modeled as elastic-perfectly plastic. For the same cases, the curvature ductility was recomputed by using A1035

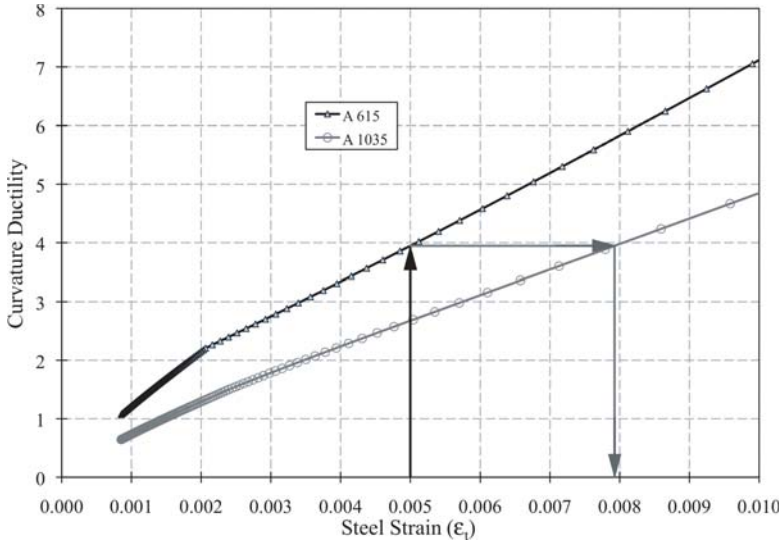

Figure 5. Example for f'_c = 4 ksi, ρ' = 0, d′/d = 0, target ε_t = 0.005 in ASTM A615.

Grade 100 reinforcement. An equation proposed by Mast (2006) was used to characterize the material properties of A1035 reinforcement. Details of the formulation are provided in Appendix C.

The relationship between the strain levels for A615 and A1035 reinforcing bars is illustrated in Figure 5 for one of the cases considered. For this example, a singly reinforced member having f'_c = 4 ksi, the strain in the A1035 bars needs to be 0.00793 in order to achieve the same implied ductility of the same tension-controlled member reinforced with A615 bars. The complete set of results is shown in Figure 6. As expected, the addition of compression bars (i.e., $\rho' > 0$) increases the strain in the tension reinforcement, which improves the ductility. As the concrete compressive strength increases, the tension reinforcement strain drops, which is an indication of reduced ductility.

2.3.2.3 Recommendations

Based on the results shown in Figure 6, the following strain limits are recommended to define tension-controlled and compression-controlled members that use reinforcement with f_y = 100 ksi in cases where the service load stresses are limited to 60 ksi. Linear interpolation may be used for f_y between

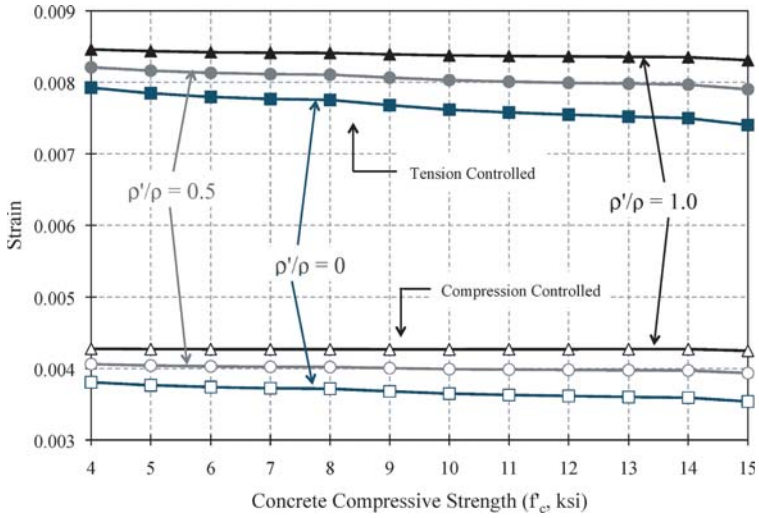

Figure 6. Equivalent strains for tension-controlled and compression-controlled members reinforced with ASTM A1035.

60 and 100 ksi for the compression-controlled limit, and 75 to 100 ksi for the tension-controlled limit.

Tension Controlled: $\varepsilon_t \geq 0.008$
Compression Controlled: $\varepsilon_t \leq 0.004$

Where ε_t is the strain in tensile strain in the extreme longitudinal reinforcement.

These limits are nearly identical to those recommended by Mast et al. (2008), that is, 0.004 and 0.009. It must be recognized that selecting a different value of f_y or f_s results in different calibrations.

2.3.3 Moment Redistribution

AASHTO §5.7.3.5 allows redistribution of negative moments at the internal supports of continuous reinforced-concrete beams. Redistribution is allowed only when the strain in the extreme longitudinal reinforcement (ε_t) is equal to, or greater than, 0.0075. This strain limit of 0.0075 is derived in Mast (1992) and can be traced to cases for which the provided area of steel is approximately one-half of that corresponding to balanced failure (see Appendix C). As derived in Appendix C, for such cases the value of ε_t is $0.003 + 2\varepsilon_y$. For Grade 60 reinforcement, the yield strain (ε_y) is 0.0021; hence, ε_t becomes 0.0072. This strain is essentially the same as 0.0075, which is the strain beyond which moment redistribution is permitted.

In the case of A1035 reinforcement, the yield strain is higher than that for Grade 60 reinforcement. As discussed in Appendix C, Mast's Equation provides a very good lower-bound estimate of A1035 stress-strain relationship. Mast's Equation is as follows:

$$if\ \varepsilon_s \leq 0.00241\ f_s = E_s\varepsilon_s$$

$$if\ \varepsilon_s > 0.00241\ f_s = 170 - \frac{0.43}{\varepsilon_s + 0.00188}$$

Based on Mast's Equation, the strain at 100 ksi is 0.0043. Using this strain as the yield strain (ε_y), the value of ε_t becomes 0.0115 ($\varepsilon_t = 0.003 + 2\varepsilon_y = 0.003 + 2(0.0043) = 0.0115$) or approximately 0.012. Therefore, 0.012 is proposed as the strain limit for which moment redistribution is allowed for members reinforced with A1035 reinforcement.

According to current AASHTO specifications, strain in the extreme tension reinforcement (ε_t) must exceed 0.0075 in order to be able to redistribute moments. This strain is 1.5 times the current strain limit of 0.005 that defines tension controlled. The proposed strain limit of 0.012 is also 1.5 times the proposed tension-controlled strain limit of 0.008.

2.3.4 Experimental Evaluation

To better understand the behavior and capacity of flexural members reinforced with A1035 bars and evaluate the aforementioned strain limits for tension-controlled and compression-controlled sections, six specimens were designed, fabricated, and tested. Appendix D provides detailed information regarding the experimental program as well as a complete record of the test data.

2.3.4.1 Test Specimens and Experimental Program

The test specimens, which were 12 in. wide by 16 in. deep flexural members with nominal 10-ksi and 15-ksi concrete and A1035 longitudinal bars, were designed, fabricated, and tested. To prevent the possibility of shear failure, #4 Grade 60 A615 stirrups were provided throughout the span. For both concrete strengths, the specimens were designed based on the following strain targets: (1) tension-controlled strain limit of 0.008; (2) 0.006, which is in the transition region between tension controlled and compression controlled, and (3) above 0.010 to examine crack widths in beams with low reinforcement ratio. The specimen details and material properties of the longitudinal bars are summarized in Tables 11 and 12, respectively.

The specimens were tested over a 20-ft simple span in a four-point loading arrangement having a constant moment region of 3.5 ft. The specimens were instrumented to capture the load, deflection, and steel and concrete strains.

2.3.4.2. Results and Discussions

Ductility. One of the concerns when using high-strength reinforcing bars such as A1035 is related to the reduced ductility resulting from the use of larger yield stresses and

Table 11. Flexural specimens.

Specimen ID	Reinforcement (A1035)		f'_c (ksi)		Target ε_t	Comment
	Layer 1	Layer 2	Design	Measured		
F1	4 #5	2 #5	10	12.9	0.0080	Tension controlled
F2	4 #6	2 #6	10	12.9	0.0060	Transition
F3	4 #5	----	10	12.9	0.0115	Tension controlled, small ρ
F4	4 #5	4 #5	15	16.5	0.0080	Tension controlled
F5	4 #6	4 #6	15	16.3	0.0060	Transition
F6	4 #5	2 #5	15	16.9	0.0103	Tension controlled, small ρ

Table 12. Measured properties of A1035 longitudinal reinforcement.

Bar Size	Specimens	Rupture Strain	Calculated Modulus of Elasticity (ksi)	Ultimate Strength (ksi)	Yield Strength (ksi)		
					@ Strain = 0.0035	@ Strain = 0.0050	0.2% Offset
#5	F1, F2, F3	0.103	26074	164.1	89.2	112.5	130.2
#5	F4, F5, F6	0.137	27280	164.9	92.9	115.0	129.2
#6	F1, F2, F3	0.103	29001	161.3	91.1	111.7	121.8
#6	F4, F5, F5	0.145	27711	165.3	94.1	117.9	134.4

the subsequent greater utilization of the concrete capacity. The midspan deflection (expressed in terms of span length, L = 20 ft) corresponding to the maximum is tabulated in Table 13. The deflections at ultimate are clearly large. All of the specimens exhibited a well-distributed crack pattern. Well before failure, noticeable crack opening and curvature of the beams were noticed (Figure 7). Prior to failure, the beams exhibited visual warning signs of distress (see Figure 8). The large deflections and visual warning signs of distress before failure attest to the ductility of the specimens.

Overall Response and Capacity. The measured load-deflection relationships are plotted in Figure 9. As discussed above, the specimens exhibit large deflections prior to failure. The expected capacities were computed based on standard strain compatibility analyses in which the stress-strain relationship of A1035 longitudinal bars was modeled (1) as being elastic-perfectly plastic having a yield strength (f_y) equal to 100 ksi, which approximately corresponds to the stress at strain of 0.004; (2) by an equation proposed by Mast (1992); and (3) by the Ramberg-Osgood function describing the measured stress-strain behavior. The ratios of observed-to-predicted behavior are given in Table 14. All of the specimens reached and exceeded their predicted capacities. Reflective of the previously described analytical work, the predictions made using the Ramberg-Osgood representation of the steel behavior are remarkably close to the experimentally observed behavior while those made using the f_y = 100 ksi assumption are quite conservative. The capacities based on Mast's Equation are reasonably close to the measured values.

In addition to being able to accurately predict the capacity of members reinforced with high-strength A1035 reinforcing bars, it is equally important to examine whether established modeling procedures can capture the stiffness at various limit states, which can conveniently be accomplished by evaluating the load-deflection response. The analytical load-deflections were obtained by using a computer program called Response 2000 (Bentz 2000). Modeling of the specimens is discussed in Appendix D. The measured and predicted load-deflection responses for specimens F1 and F4, which are deemed to represent members that will likely be encountered in practice, are compared in Figure 10. For specimen F1, which was cast with nominal 10-ksi concrete, the analytical load-deflection response is remarkably close to its experimental counterpart. In contrast, the computed load-deflection for the specimen cast with nominal 15-ksi concrete (i.e., specimen F4) exhibits a higher stiffness than the experimental data. This difference is attributed to overestimation of aggregate interlock in the matrix of 15-ksi concrete. Considering the challenges of modeling high-strength concrete, the shown load-deflection response for specimen F4 is adequate. The results shown in Figure 10 suggest that well-established techniques are applicable to members reinforced with A1035 high-strength longitudinal bars, and stiffness of such members can adequately be computed.

Table 13. Maximum midspan deflection.

Specimen	Deflection
F1	L/44
F2	L/48
F3	L/39
F4	L/38
F5	L/47
F6	L/29

Strain Level. The average strain from strain gages bonded to the longitudinal bars at midspan is plotted versus the applied load in Figure 11. For each specimen, the target design strain (ε_t in Table 11) is also plotted. The measured strains

Figure 7. Cracking patterns in Specimen F4 prior to failure.

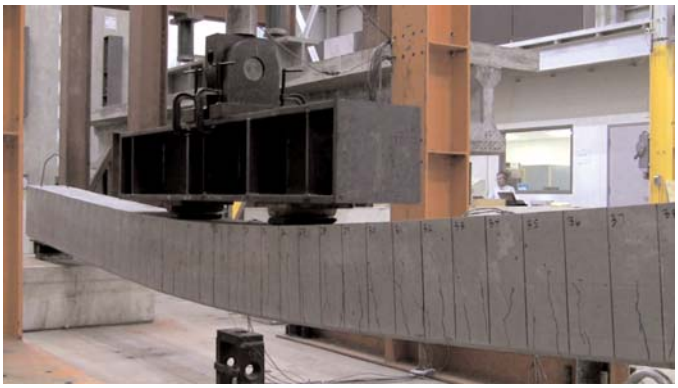

Figure 8. Crack patterns and curvature in Specimen F4 immediately prior to failure.

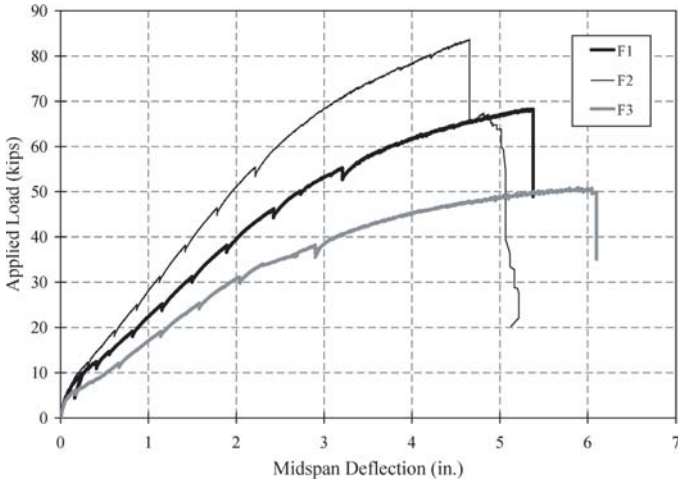

(a) Specimens F1, F2, F3

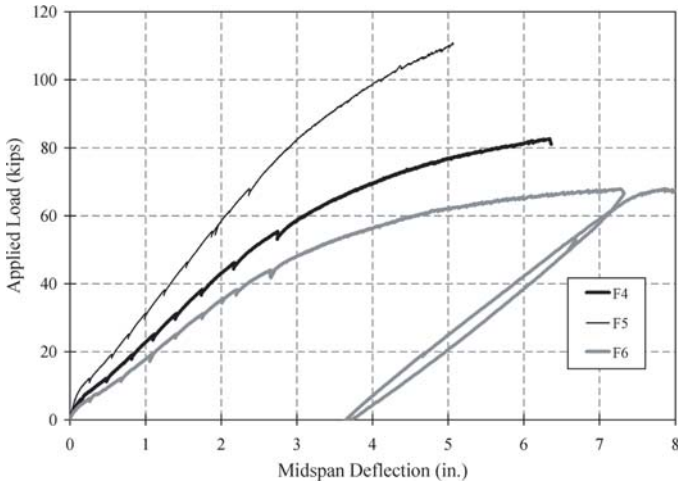

(b) Specimens F4, F5, and F6

Figure 9. Load—midspan deflection.

Table 14. Ratio of measured to computed capacities.

Specimen	Method		
	f_y = 100 ksi	Mast Eq.	Ramberg-Osgood
F1	1.47	1.12	1.07
F2	1.31	1.11	1.08
F3	1.54	1.08	1.01
F4	1.37	1.08	1.02
F5	1.35	1.19	1.14
F6	1.44	1.06	0.991

clearly demonstrate that the specimens reached and exceeded the target strains.

Two strain gages were bonded to the concrete surface at the midspan (i.e., in the constant moment region) to measure the compressive strain. The average strain was used to assess the performance of the specimens. The ratio of the peak strain to the target design strain is summarized in Table 15. The specimens developed a strain of at least 1.9 times larger than their target values prior to failure. At failure, the concrete strain (tabulated in Table 15) ranged from 0.0025 to 0.0039 with an average value of 0.0033. The selection of a maximum concrete strain of 0.003 in a compatibility analysis of members reinforced with high-strength A1035 is rational.

2.3.5 Summary and Recommendations

Considering the magnitudes of the strains in the longitudinal bars and concrete, the specimens performed adequately and met the design objective. The proposed strain limits of $\varepsilon_t = 0.008$ or higher for tension-controlled behavior and $\varepsilon_t = 0.004$ for compression-controlled are appropriate. Moreover, well-established strain compatibility analysis techniques can

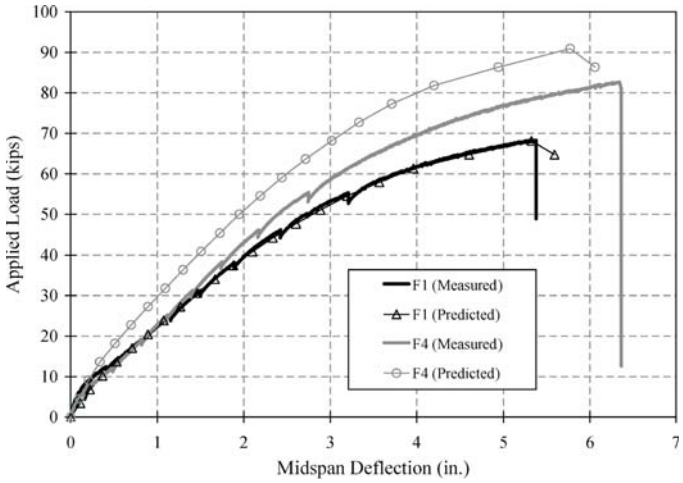

Figure 10. Measured and computed load-deflection relationships.

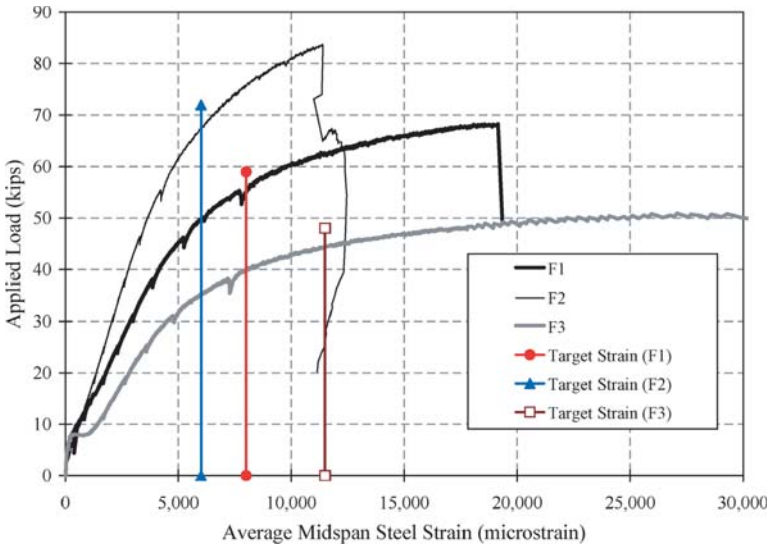

(a) Specimens F1, F2, F3

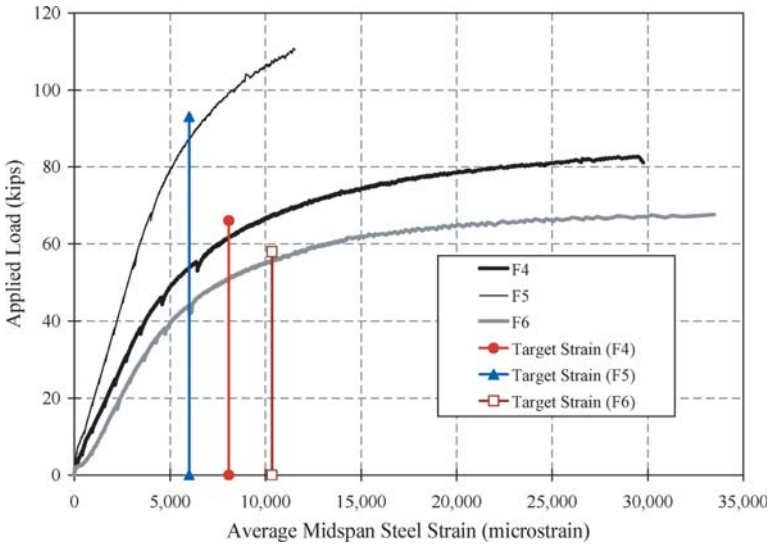

(b) Specimens F4, F5, F6

Figure 11. Load-midspan steel strain.

Table 15. Ratio of peak strain to target strain and maximum concrete strain.

Specimen	Peak Strain/ Target Strain	Peak Concrete Strain
F1	2.46	0.0025
F2	2.07	0.0027
F3	3.14	0.0034
F4	3.68	0.0038
F5	1.92	0.0039
F6	3.24	0.0033

effectively and reliably be used to determine flexural capacity of members with A1035 longitudinal reinforcement. Members reinforced with high-strength ASTM A1035 bars exhibit adequate ductility and do not suggest any unexpected response characteristics.

2.4 Fatigue Performance of High-Strength Reinforcing Steel

Fatigue is a process of progressive structural change in a material subjected to transient loads, stresses or strains. Fatigue strength is defined as the maximum transient stress range (S) that may be repeated without causing failure for a specified

number of loading cycles (N). The stress range is defined as the algebraic difference between the maximum and the minimum stress in a stress cycle: $S = f_{max} - f_{min}$ (i.e., the transient stress). Most ferrous materials exhibit an "endurance limit" or "fatigue limit" below which failure does not occur for an unlimited number of cycles, N. In general, the concrete material fatigue performance exceeds that of the steel and is not considered in design (Neville 1975).

The AASHTO (2007) limit for fatigue-induced stress in mild steel reinforcement is based on the outcome of NCHRP Project 4-7 as reported by Helgason et al. (1976). The maximum permitted stress range (f_f) in straight reinforcement resulting from the fatigue load combination is given in AASHTO LRFD (2007) §5.5.3.2 as follows:

$$f_f \le 21 - 0.33 f_{min} + 8(r/h) \qquad (\text{ksi units}) \qquad \text{(Eq. 8)}$$

Where:

f_{min} = algebraic minimum stress level (compression is negative) and

r/h = ratio of base radius to height of rolled-on transverse deformations; 0.3 may be used in the absence of actual values.

Recent revisions to AASHTO LRFD §5.5.3.2 simply incorporate the default r/h ratio as follows:

$$f_f \le 24 - 0.33 f_{min} \qquad (\text{ksi units}) \qquad \text{(Eq. 9)}$$

The AASHTO-prescribed relationship is shown (see Appendix E) to represent the lower-bound results of many fatigue studies considering a range of bar sizes and is reported applicable for Grades 40, 60, and 75 ASTM A615 reinforcing bars (Corley et al. 1978). Corley et al. report that "A No. 11 Grade 60 bar fractured in fatigue after 1,250,000 cycles when subjected to a stress range of 21.3 ksi and a minimum stress of 17.5 ksi tension. *This is the lowest stress range at which a fatigue fracture has been obtained in an undisturbed North American produced reinforcing bar*" [emphasis added]. The f_{min} term is appropriate where f_{min} is positive (i.e., tension, the usual case) but appears to be "calibrated" to result in the same stress values as were used for working stress design using Grade 40 steel. Finally, bar size is not considered in the AASHTO-prescribed limit, although it is well established that larger bar sizes typically have lower fatigue limits (Tilly and Moss 1982).

2.4.1 AASHTO Fatigue Equation and Design with High-Strength Steel

The use of high-strength reinforcement may permit a reduction of the total area of steel required for flexural resistance. The resulting larger transient stresses in the steel may adversely affect fatigue performance of the member. Specifically, if designed efficiently, both the minimum and maximum stresses will increase coincident with the value of f_y used in design. However, the maximum stress may be increased to a greater degree, resulting in a larger stress range under transient loads. For example, the value of f_{min} will generally be on the order of $0.20f_y$. For Grade 60 A615 steel, the present AASHTO requirement (Equation 9) results in a fatigue limit of 20 ksi. Applying the same equation to steel having a yield strength of 120 ksi, for instance, results in the unnecessary (and unwarranted) reduction of the permitted fatigue stress to 16 ksi. The lower fatigue limit implies that the higher strength material has reduced fatigue performance, which is contrary to all available data (Appendix E). The counterintuitive outcome, in terms of design, is that more of the higher strength steel is required to carry the same transient loads.

Although some data suggest an improved fatigue limit for higher strength bars (DeJong et al. 2006) may be permissible, there are insufficient data at this time to make any recommendation in the direction of changing the AASHTO fatigue limit (Equation 9) and/or making the fatigue limit a function of yield (or tensile) capacity. Nonetheless, the impact of applying Equation 9 to higher strength reinforcing steel is that f_{min} may be increased by taking advantage of the higher strength steel, but the increase results in an unwarranted reduction in the fatigue limit. It is, therefore, proposed to normalize f_{min} by the yield stress, f_y. Calibrating this equation so that there is no effect for Grade 60 reinforcement, one arrives at the following:

$$f_f \le 24 - 0.20(f_{min}/f_y) \qquad (\text{ksi units}) \qquad \text{(Eq. 10)}$$

While still conservative, this equation recognizes that fatigue behavior of ferrous metals is largely unaffected by the yield strength of the material itself; thus, the baseline endurance limit of 24 ksi is unchanged.

2.4.2 Effect of High-Strength Steel on the AASHTO Fatigue Provisions

In order to understand the role of fatigue in the design of reinforced-concrete flexural members, the following approach was taken.

A simply supported beam having length L was considered. Nominal moments are determined at the midspan using the following loads:

DL = dead load (self weight). This value is determined for a range of values of DL/LL_{lane}.

LL_{lane} = specified lane load = 0.64 k/ft (AASHTO LRFD §3.6.1.2.4).

LL_{truck} = greatest effect of design tandem (§3.6.1.2.3) and design truck (§3.6.1.2.2). For truck on simple span, the minimum 32-kip axle spacing of 14 ft is used.

$LL_{fatigue}$ = effect of single design truck having 32-kip axle spacing of 30 ft (§3.6.1.4.1).

It is recognized that the maximum moment does not occur exactly at the midspan; however, the error in making this assumption is quite small and becomes proportionally smaller as the span length increases (Barker and Puckett 2007). From these moments, the STRENGTH I and FATIGUE design moments are determined (§3.4.1) as follows:

$$STRENGTH = 1.25DL + 1.75LL_{lane} + (1.75 \times 1.33)LL_{truck}$$

$$FATIGUE = (0.75 \times 1.15)LL_{fatigue}$$

Where the 1.33 and 1.15 factors are for impact loading (IM) (§3.6.2.1).

In order to normalize for distribution, multiple lanes, etc., it is assumed that the STRENGTH design is optimized; therefore, the stress in the primary reinforcing steel under STRENGTH conditions is $\phi f_y = 0.9 f_y$ regardless of bridge geometry. If this is the case, the reinforcing stress associated with the FATIGUE load is as follows:

$$f_f = 0.9 f_y \times (FATIGUE/STRENGTH)$$

Similarly, the minimum sustained load will result in a reinforcing stress of

$$f_{\min} = 0.9 f_y \times (DL/STRENGTH)$$

The stress in the reinforcing steel under FATIGUE conditions is then normalized by the allowable stress [according to AASHTO Equation 5.5.3.2-1 (Equation 9, above)] to determine the ratio of transient (FATIGUE) stress to the calculated fatigue stress limit. The results from this approach are shown in Figure 12 for simple spans L = 10 to 160 ft and DL/LL_{lane} = 0.5, 1, 2, and 4. In this plot, the vertical axis reports the ratio $f_f/[24 - 20(f_{min}/f_y)]$. Based on this approach, it is not expected that the fatigue limits of §5.5.3.2 will affect design using f_y = 60 ksi over the range considered since the ratio of stress range/fatigue limit is less than unity for all cases. The effects of using f_y = 100 ksi in this simplified scenario include an expected increase in f_{min} and f_f equal to the ratio of yield strengths = 100/60 = 1.67. As seen in Figure 12, however, the calculated stress range remains below the fatigue limit given by Equation 5.5.3.2-1 for all but spans shorter than 20 ft having f_y = 100 ksi. The effect of continuing to use the extant version of Equation 5.5.3.2-1: $f_r \leq 24 - 0.33 f_{min}$, is relatively negligible, shifting the 100 ksi curves upward by less than 5% in the scenario presented.

Thus, despite the inherent conservativeness of the AASHTO LRFD 5.5.3.2 fatigue provisions, it is not believed that these will impact most rational designs for values of f_y up to 100 ksi. It has been shown that increasing the usable yield strength of steel decreases the margin of safety against fatigue. Only in the shortest of spans, where vehicular loads dominate behavior would the "fatigue check" fail and additional steel be required.

2.4.3 Fatigue of Slabs (AASHTO LRFD Section 9)

Slabs, being shallower and having a proportionally greater LL/DL ratio, may be considered to be more fatigue sensitive than the generic conditions described above. However,

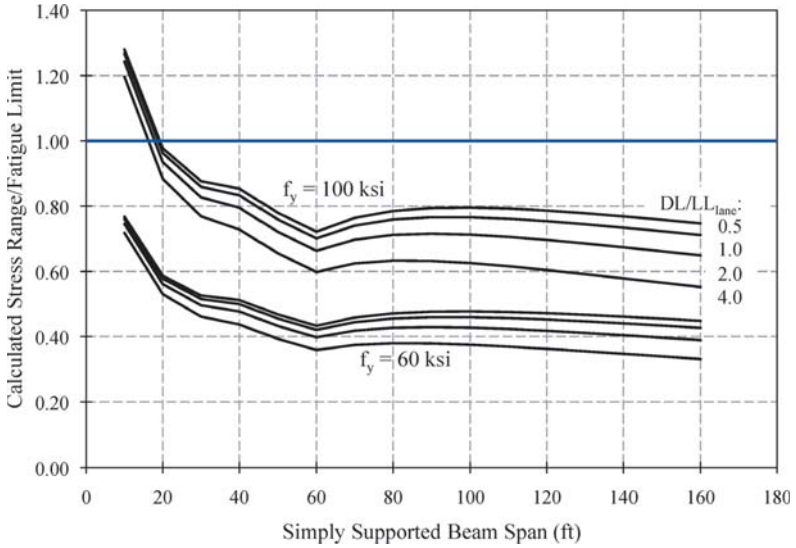

Figure 12. Transient stress-to-fatigue limit ratio for simple span bridges.

AASHTO LRFD §9.5.3 excludes concrete deck slabs from being investigated for fatigue. AASHTO justifies this exclusion based on results reported by de V Batchelor et al. (1978). It has been shown that slabs resist applied loads primarily through internal arch action (AASHTO §9.7.1) and that the nominal steel required is primarily to resist local flexural effects (punching) and to provide confinement such that the arching action may be developed (Fang 1985 and Holowka et al. 1980).

2.4.4 Fatigue Test Specimens

2.4.4.1 Fatigue Specimen Details

Specimen details were selected to correspond to the details of flexural specimen F3 (see Section 2.3.4 and Appendix D). Two beams 16 in. deep by 12 in. wide having four #5 A1035 longitudinal bars and #3 A 615 stirrups spaced at 9 in. along the entire length of the beam were cast with 10 ksi concrete. The beams were 18.5 ft long and were tested in midpoint flexure over a span of 16.5 ft. Four-inch-wide neoprene supports were used; therefore, the face-to-face dimension of the span is 16 ft-2 in. The fatigue test beams had the same shear span details as flexural specimen F3 but were not provided with a constant moment region. This difference is due to the nature of large-scale fatigue testing and the difficulties in providing accurate and safe four-point bending conditions. The measured material properties of the steel reinforcement are given in Appendix A. In summary, f_y = 130 ksi (based on 0.2% offset method), and the measured concrete compressive strength was 9.71 ksi. Cyclic testing was carried out at a frequency of 1.2 Hz. At regular intervals, the frequency was reduced to 0.003 Hz (1 cycle in 5 minutes) and a fully instrumented cycle was carried out.

2.4.4.2 Fatigue Test Protocol

Details of how the fatigue test protocol was established are provided in Appendix E. The protocol adopted involved testing the first beam at a stress range (in the primary #5 A1035 reinforcing bars) of 32 ksi. The justification being that if the beam withstands 2 million cycles at stress greater than the theoretical endurance limit (for N = 2,000,000) of 28 ksi (see Appendix E), it has de facto exceeded the current AASHTO requirements and thus represents a proof test with good confidence. Since the first beam successfully resisted 2 million cycles, the second beam was tested at a greater stress range, 46 ksi, to provide a second data point along the *S-N* curve. All test control is based on reinforcing bar stress measured using strain gages. Four strain gages were used in each specimen: one mounted on each A1035 bar. Gages on bars 1 and 3 were located 8 in. to the left of the midspan loading point and those on bars 2 and 4 were located 8 in. to the right.

2.4.4.3 Results of Fatigue Test 1

Fatigue Test 1 was conducted between 3/10/2009 and 3/31/2009. The applied load at midspan was cycled between 7 and 17 kips at a rate of 1.2 Hz for 2 million cycles. The measured stress range in the A1035 longitudinal steel was 31.1 ksi in the initial test cycles. Strain gages were lost during the first 100,000 cycles (loss of gages due to fatigue loading is expected). Due to the nature of fatigue damage, however, the stress range will increase marginally throughout the test (Neville 1975 and Harries et al. 2006). Moreover, equipment malfunction during a few initial cycles resulted in unintentional loading of Fatigue Test 1 beyond 30 kips. These higher stress range cycles had little impact on the beam behavior beyond causing additional cracks.

During fatigue cycling, no notable degradation in beam stiffness was observed. A small drift in absolute displacements was observed; the drift is attributable to degradation of the neoprene pads and "shakedown" of the test frame. Nonetheless, the differential displacement, measured between 7 and 17 kips applied load, remained essentially constant. Figure 13 shows both the deflection (left axis) and secant stiffness measured between applied loads of 7 and 17 kips (right axis) cycle histories for Fatigue Test 1. Crack width measurements both during fatigue cycling and following the fatigue test during a monotonic load cycle to 46 kips (capacity of actuator used) were remarkably consistent and confirmed the measured and analytically calculated bar stresses (Soltani 2010). Fatigue Test 1 behaved very well. The results indicate that the A1035 bars can maintain 2 million cycles at 31 ksi with little or no apparent damage.

2.4.4.4 Results of Fatigue Test 2

Fatigue Test 2 was conducted between 4/14/2009 and 4/16/2009. The applied load at midspan was cycled between 7 and 25 kips at a rate of 1.2 Hz. The measured stress range in the A1035 longitudinal steel was 45.5 ksi in the initial test cycles. One of the four reinforcing bars (a corner bar) experienced a fatigue failure at N = 155,005. The final measured cycle was N = 100,000. As shown in Figure 14, the deflections were increasing with a rising number of cycles although the differential displacement (between 7 and 25 kips) remained relatively constant. The secant stiffness (also measured between 7 and 25 kips) demonstrated some decay in the initial 100,000 cycles. The final data points at N = 155,005 in Figure 14 were obtained from a single cycle following fatigue failure and clearly indicate the effect of the loss of one of the four primary reinforcing bars. Figure 15 shows the ruptured bar following testing (and removal of cover concrete). The bar failed at the location near a stirrup which is typical of such fatigue failures because of fretting

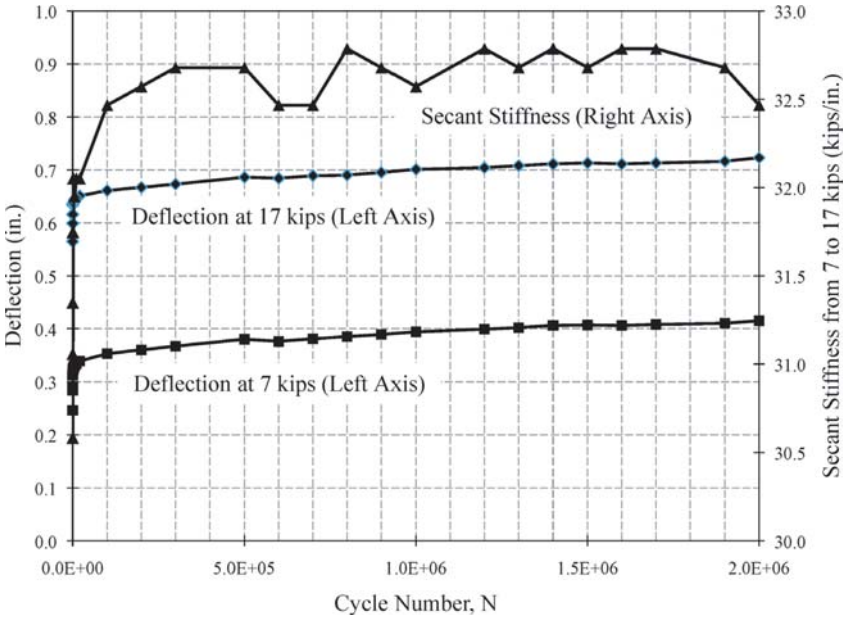

Figure 13. Cumulative damage curves for Fatigue Test 1.

effects at the transverse bar locations. Figure 15(c) shows the fracture surface of the bar, which is clearly indicative of a fatigue failure.

The failure of a bar at $N = 155{,}005$ under $S = 45.5$ ksi is very close to the prediction, which is thought to be conservative. Therefore, an investigation of the fatigue failure surface using scanning electron microscopy (SEM) was conducted (see Appendix E). The SEM revealed aluminum (Al) inclusions in the fracture surface and a significant silicon (Si) inclusion at the edge of the bar section, which is thought to have served as a crack initiator.

2.4.5 Summary of Fatigue Tests and Conclusions

The adopted *S-N* relationship described in Appendix E and the two *S-N* pairs from the tests conducted are shown in Figure 16. Since both *S-N* pairs fall to the right of the *S-N*

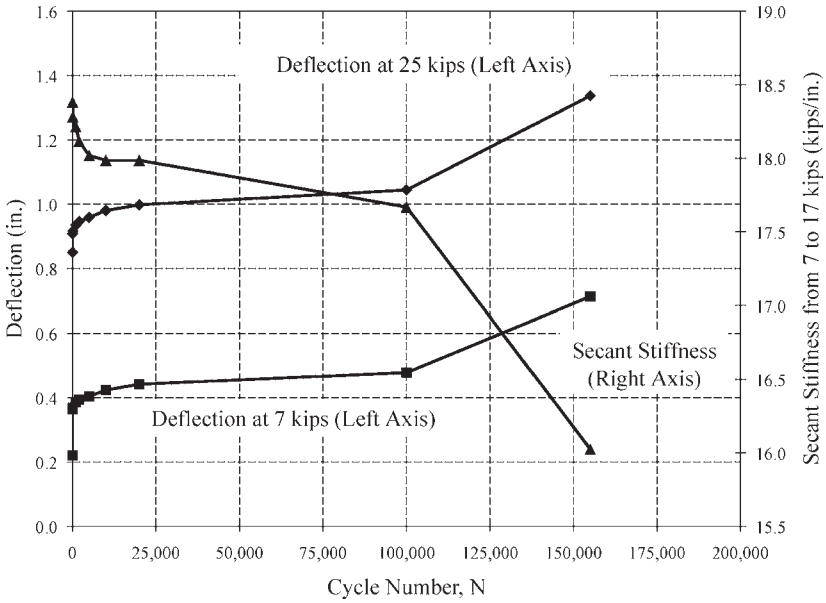

Figure 14. Cumulative damage curves for Fatigue Test 2 (fatigue failure occurred prior to obtaining the final data point).

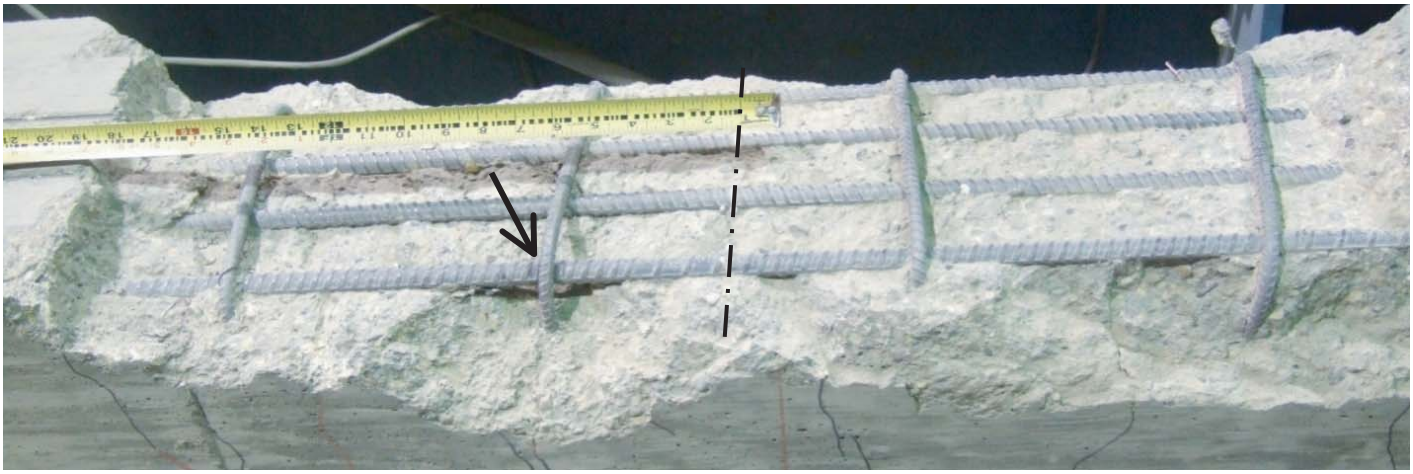

(a) Location of Bar Fracture (Beam is Inverted, Cover Has Been Removed)

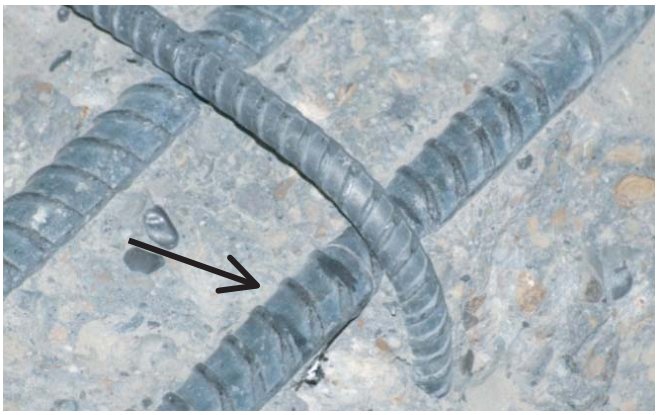

(b) Fatigue Fracture of Bar 1

(c) Fracture Surface

Figure 15. Fatigue failure of single bar in Fatigue Test 2.

curve, it may be said that the specimen performance exceeded that predicted by the curve (i.e., for a given stress range, *S*, the fatigue life, *N*, was greater than predicted), although not by a significant degree. Both tests serve as proof tests of the AASHTO LRFD recommendations (Equation 9) and the proposed revision (Equation 10) that both limit the fatigue stress range to 24 ksi for the case of tension-tension fatigue (i.e., $f_{min} > 0$). The adoption of Equation 10 is recommended to address the unwarranted reduction in fatigue stress range that results from the use of the present AASHTO recommendation (Equation 9) in conjunction with high-strength reinforcing steel.

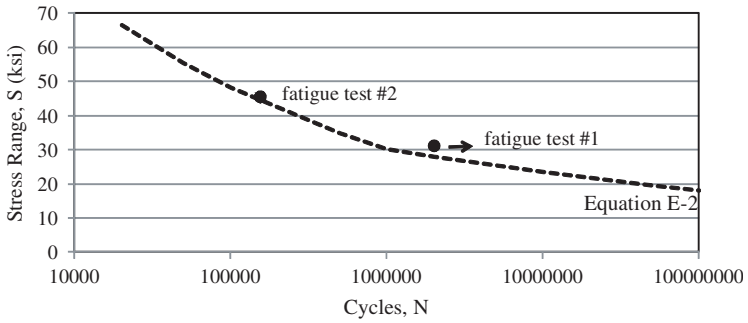

Figure 16. Predicted and experimental S-N data.

2.5 Shear Reinforcement

The use of A1035 steel as transverse reinforcement for flexural members was examined experimentally. The experimental data from full-scale testing of reinforced and prestressed beams were augmented by the results from analytical studies. The performance of high-strength steel as shear reinforcement is evaluated in this section.

2.5.1 Shear Resistance

Under current AASHTO *LRFD Bridge Design Specifications,* the Sectional Design Model, which was derived from the Modified Compression-Field Theory (Vecchio and Collins, 1986), is prescribed for determining the required amount of shear reinforcement. The Sectional Design Model provides strain-based relationships to account for contributions from the concrete and the transverse reinforcement to overall shear capacity. A value for the yield strength of the transverse steel is needed in order to apply the design equations in AASHTO LRFD (2007) §5.8.3. For design of the test specimens, a value of 100-ksi was selected as the "yield strength" of the A1035 steel. A complete synopsis of the design steps and equations is provided in Appendix F.

2.5.2 Experimental Evaluation

A total of nine shear specimens were designed, fabricated, tested, and analyzed. The specimens consisted of five rectangular reinforced-concrete beams and four AASHTO Type I prestressed girders. Of the nine specimens, all but one contained both high-strength (A1035) and A615 shear reinforcement. The primary goal was to evaluate the performance of high-strength steel as shear reinforcement in comparison to that of the commonly used A615 steel. Appendix F provides detailed information regarding the experimental program as well as a complete record of the test data.

2.5.2.1 Test Specimens and Experimental Program

Specimen Details. The five reinforced-concrete test beams (designated by SR_) were all 12 in. wide by 24 in. deep. The first four of these specimens (SR1 through SR4) were designed based on a nominal concrete strength of 10 ksi and included #3 A1035 stirrups along with #4 A615 stirrups, placed in either half of the beam. Specimen SR5, however, was designed based on a 15 ksi nominal concrete strength and contained only #3 A1035 stirrups throughout the entire length of the beam. The spacing of stirrups in specimens SR1, SR4, and SR5 was governed by the amount required to resist a prescribed value of ultimate shear force. On the other hand, the maximum stirrup spacing currently allowed by AASHTO *LRFD Bridge Design Specifications* was used as the basis of design for specimens SR2 and SR3. For the specimens containing both types of transverse steel, the spacing and size of stirrups were selected such that the stirrup force as computed by $V_s = \frac{A_v f_y d_v}{S}$ would be nearly equal for the A615 and A1035 stirrups reinforcing in either half of the beam. The value of f_y was taken as 100 ksi and 60 ksi for A1035 and A615 stirrups, respectively. All of the specimens were reinforced with #8 A1035 longitudinal bars to induce shear failure prior to reaching their flexural capacities. Table 16 summarizes specimen details for the reinforced-concrete beams.

The four prestressed AASHTO Type I girders (designated by SP_) had 7 in. deep by 48 in. wide composite slabs. All of the Type I girders were designed based on a nominal concrete strength of 10 ksi in the girder and 5 ksi in the slab. Each of these specimens had both #3 A1035 and #4 A615 stirrups along with 0.6-inch low-relaxation strands. The design of SP1 and SP3 was controlled by the amount of transverse reinforcement required to resist an ultimate shear force. The shear capacities of these specimens were expected to be near their flexural capacities given the nature of the loading arrangement. Specimen SP2 used the maximum stirrup spacing currently allowed by AASHTO *LRFD Bridge Design Spec-*

Table 16. Shear specimens (reinforced-concrete beams).

Specimen ID	Transverse Reinforcement	f'_c (ksi)		Design Criterion
		Design	Measured	
SR1	#4 A615 @ 9.5 in. #3 A1035 @ 8.5 in.	10	12.2	As Needed to Resist V_u
SR2	#4 A615 @ 13 in. #3 A1035 @ 13 in.	10	12.9	Max. Allowed Spacing
SR3	#4 A615 @ 13 in. #3 A1035 @ 13 in.	10	13.0	Max. Allowed Spacing
SR4	#4 A615 @ 8.5 in. #3 A1035 @ 8 in.	10	13.1	As Needed to Resist V_u
SR5	#3 A1035 @ 8.5 in.	15	16.9	As Needed to Resist V_u

Table 17. Shear specimens (AASHTO Type I girders).

Specimen ID	Transverse Reinforcement	Girder f'_c (ksi)		Slab f'_c (ksi)		Design Criterion
		Design	Measured	Design	Measured	
SP1	#4 A615 @ 8 in. #3 A1035 @ 7.5 in.	10	11.9	5	7.2	As Needed to Resist V_u
SP2	#4 A615 @ 24 in. #3 A1035 @ 22 in.	10	12.4	5	9.9	Max. Allowed Spacing
SP3	#4 A615 @ 11 in. #3 A1035 @ 10 in.	10	13.1	5	10.1	As Needed to Resist V_u
SP4	#4 A615 @ 16 in. #3 A1035 @ 18 in.	10	10.5	5	6.3	Under-Designed A1035

ifications, and was expected to fail in shear. By selecting different bar sizes and spacing in these three specimens, the amount of shear force provided by A615 and A1035 stirrups was kept nearly identical. Specimen SP4, on the other hand, was designed such that the A615 shear capacity exceeded the A1035 shear capacity in order to induce shear failure on the A1035 side. Table 17 summarizes specimen details. The material properties of transverse reinforcement are summarized in Table 18. Appendix A provides an in-depth discussion of material properties.

Testing Program. Three different loading arrangements were selected to test the specimens. Specimens SR1, SR2, and SR5 were all 13.5 ft long and were tested over an 11-ft simple span in three-point bending. Specimens SR3 and SR4 were both 26 ft long and tested as a simply supported beam with a 6-ft overhang where the load was applied 1 ft from the tip of the overhang. Specimens SR3 and SR4 were tested in two phases such that one test isolated the loading to just one type of stirrup. The side of specimen SR3 reinforced with A1035 stirrups was tested first. For specimen SR4, the side using A615 stirrups was tested first. The side tested first was not loaded to failure in order to be able to reposition the specimen and load the other side. The prestressed specimens (SP1 to SP4) were all 30 ft long and tested over a 26.5-ft simple span in four-point bending with a constant moment region of 11 ft. For each test, specimens were instrumented to measure load, deflection, and both steel and concrete strains in given locations.

2.5.2.2 Results and Discussions

The measured and observed responses are used to assess the performance of various specimens as described in the following sections.

2.5.2.2.1 Observed Failure Modes. Both specimens SR1 and SR2 failed in shear on the side reinforced with #4 A615 stirrups. Figure 17 displays specimen SR2 after failure. In terms of strength, the failure on the portion of the beam using A615 transverse reinforcement suggests satisfactory performance of the A1035 stirrups. The side of specimen SR3 with A1035 stirrups was loaded first before testing the A615 side to failure. The failure load was higher than what was applied to the A1035 side; hence, no conclusion regarding performance of A1035 stirrups versus A615 stirrups can be drawn from specimen SR3. The order of testing of specimen SR4 was reversed from SR3; therefore, the A615 side was loaded short of failure. The failure on the A1035 side could be characterized as flexural. The observed failure mode was unexpected according to the computed capacities. Loading of specimen SR5 had to be stopped prior to failure after reaching the loading apparatus' capacity, which was 20% larger than the best-predicted capacity (based on compression field theory) and

Table 18. Measured properties of transverse reinforcement.

Stirrup	Specimens	Rupture Strain	Calculated Modulus of Elasticity (ksi)	Ultimate Strength (ksi)	Yield Strength (ksi)		
					@ Strain = 0.0035	@ Strain = 0.0050	0.2% Offset
#4 A615	SR1-SR4	n.r.	26934	100.7	62.6	64.2	63.5
#4 A615	SP1-SP3	n.r.	27596	105.4	86.3	88.2	88.2
#4 A615	SP4	n.r.	23945	105.0	83.4	92.9	90.2
#3 A1035	SR1-SR5	0.111	29800	156.0	95.0	112.0	130.0
#3 A1035	SP4	0.070	27740	164.1	93.0	117.2	131.9

Notes:
There are no sample data for #3 A1035 stirrups used in SP1-SP3; n.r. = not reported.

Figure 17. Failure mode of SR2 (A615 side).

67% larger than the capacity computed based on AASHTO equations. The behavior of specimens SR4 and SR5 suggests that the shear strength of members reinforced with A1035 appears to be appreciably larger than what is computed.

Specimen SP1 was designed with the highest shear capacity and failed in a flexural manner with no signs of excessive shear cracking. Specimen SP2, which had the least amount of shear reinforcement, failed in shear. The failure, which occurred on the A615 side, was quite brittle. Specimen SP3 had slightly larger stirrup spacing than SP1, and the computed capacities indicated a failure mode bordering flexural and shear failure. Loading of this specimen was stopped after excessive flexural cracks began to open at midspan. Specimen SP4 was designed after all the other shear specimens had been tested. In order to examine shear failure due to A1035 stirrups, specimen SP4 was designed such that the capacity provided by #4 A615 stirrups would be approximately 15% higher than that from #3 A1035 stirrups. This specimen experienced shear failure on the side of the specimen with A1035 stirrups. Similar to specimen SR2, the failure was brittle—see Figure 18. It should be noted that the failure load was 40% higher than the expected capacity based on a detailed analysis using compression-field theory, and 75% larger than the capacity computed according to AASHTO provisions. The failure load was also 51% and 25% larger than the capacity of #4 A615 stirrups depending on whether AASHTO capacity or compression-field theory is used.

Figure 18. Failure mode of SP4 (A1035 side).

Capacity. Capacities were computed according to the Sectional Design Model in the AASHTO LRFD Specifications using as-built material properties. A program called Response 2000 (Bentz 2000), abbreviated as R2K in Table 19, also was used to compute the capacities. This program is a non-linear sectional analysis program for the analysis of reinforced-concrete elements subjected to shear based on the modified compression-field theory. As shown in Appendix F, load-deflection responses from Response 2000 are reasonably close to the experimental results. A summary of the measured and computed capacities for the shear specimens is given in Table 19. This table also provides the ratios of measured capacities to the computed capacities. All of the specimens far exceeded the predicted capacities based on AASHTO. Even Response 2000 underestimates the shear capacities in most cases. The only specimen for which Response 2000 was found to be slightly unconservative was specimen SP1, which failed in a decidedly flexural manner. The large ratios of measured to computed capacities have also been observed by others (Kuchma et al. 2005) and indicate the challenges of capturing shear behavior. The measured and computed capacities suggest adequate shear strength of A1035 stirrups designed based on current design equations in which stirrup yield strength is taken as 100 ksi.

Shear Crack Patterns and Widths. One concern for using high-strength steel for stirrups is whether the high stress levels induced in the reinforcement may cause excessive cracking in the concrete resulting in degradation of the concrete component of shear resistance. Figure 19 displays the crack patterns for specimen SR4 corresponding to when the stress in A1035 stirrups was approximately 100 ksi. Crack patterns for the regions with A615 and A1035 stirrups were quite similar in terms of the load at which they formed and how they propagated. None of the test specimens exhibited an unusual behavior of A1035 stirrups in terms of crack formation and crack patterns.

In addition to marking the diagonal cracks, their widths were measured at various load increments using a crack comparometer. Those increments correspond to approximately 60% to 100% of the "yield strength" of the stirrups (f_y=100 ksi for A1035). Below those increments, diagonal cracking was minimal or nonexistent. The loads at which diagonal cracks (i.e., shear cracks) could be measured are appreciably larger than service loads. The largest measured crack widths in the regions reinforced with #4 A615 and #3 A1035 stirrups are summarized in Table 20. In this table, the load increments are

Table 19. Measured and computed capacities.

Specimen ID	Stirrup Type	Failure Mode	Measured Capacity (kips)	AASHTO Capacity		R2K Capacity	
				Computed (kips)	Measured/ Computed	Computed (kips)	Measured/ Computed
SR1	A615	Shear, A615 side	26	175	1.51	233	1.14
	A1035			175	1.51	233	1.14
SR2	A615	Shear, A615 side	228	147	1.55	190	1.20
	A1035			141	1.62	165	1.38
SR3	A615	Shear, A615 side	121	76	1.59	N/A (R2K cannot model these specimens that have overhangs.)	
	A1035		114*	73	1.56		
SR4	A615	Flexure, A1035 side	117*	85	1.38		
	A1035		147	85	1.73		
SR5	A1035	N/A	300**	181	1.66	251	1.20
SP1	A615	Flexure	242	199	1.22	244	0.99
	A1035			170	1.42	244	0.99
SP2	A615	Shear, A615 side	238	139	1.71	157	1.52
	A1035			130	1.83	149	1.60
SP3	A615	Flexure	250	175	1.43	243	1.03
	A1035			154	1.62	239	1.05
SP4	A615	Shear, A1035 side	231	153	1.51	188	1.23
	A1035			132	1.75	164	1.41

Notes:
* Loading was stopped prior to failure so the other side could be tested.
** Loading was stopped after reaching the actuator's capacity, which was 300 kips.

(a) A615 Side

(b) A0135 Side

Figure 19. Crack patterns of SR4.

presented in terms of shear stress. The information in Table 20 is presented graphically in Figure 20. As expected, the shear crack widths exhibit a large scatter; however, the trends of the data indicate differences between A615 and A1035 stirrups. At lower levels of shear stress, the crack widths for the regions with A1035 stirrups are comparable in size to the crack widths for the regions using A615 stirrups. With an increase in shear stress, the cracks on the side reinforced with A1035 stirrups widened at a faster rate than the side with A615 stirrups. This trend should be anticipated because the A1035 stirrups were smaller than the A615 stirrups (#3 vs. #4).

Despite these differences, it should be noted that the diagonal cracks became measurable at shear stresses exceeding $2\sqrt{f_c'}$ which is commonly used as concrete shear strength. At such stress levels, the magnitude of crack width is less of a concern because ensuing adequate load-carrying capacity is the main design objective. Moreover, the differences between the crack widths for regions with A615 and A1035 are relatively small.

Strain Levels and Stirrup Forces. Even though the longitudinal bars are all A1035 steel, the strains recorded on the two sides with A615 and A1035 stirrups should be equivalent if the stirrups are performing equally according to compression-field theory. A representative load-longitudinal strain relationship is shown in Figure 21; this figure is for specimen SR1. The longitudinal strains (measured by strain gages SG6 and

Table 20. Maximum shear crack width.

Specimen ID	Shear Stress ($\sqrt{f'_c}$)	Maximum Crack Width in a Given Region (in.)	
		A615 Side	A1035 Side
SR1	3.21	0.0098	0.0098
	3.56	0.0118	0.0138
	3.93	0.0157	0.0157
	4.37	0.0217	0.0236
SR2	2.45	0.0157	0.0118
	2.88	0.0256	0.0157
	3.09	0.0276	0.0177
SR3	2.53	0.0118	0.0236
	2.99	0.0157	0.0295
	3.42	0.0236	0.0335
SR4	2.57	0.0138	0.0098
	2.99	0.0197	0.0157
	3.45	0.0217	0.0197
	3.87	0.0236	0.0276
	4.30	0.0315	0.0354
SR5	2.26	N/A (This specimen only had A1035 stirrups.)	0.0098
	2.69		0.0118
	3.00		0.0157
	3.28		0.0177
SP1	**Cracks were too small to measure.		
SP2	6.38	0.0118	0.0157
	7.27	0.0157	0.0177
	7.95	0.0256	0.0276
SP3	6.93	0.0079	0.0079
	7.88	0.0098	0.0118
	8.79	0.0118	0.0138
SP4	7.01	0.0059	0.0138
	8.03	0.0098	0.0177
	8.99	0.0118	0.0276

Shear stress = Shear force divided by $b_v d_v$.

SG7) near the mid-span are exceptionally similar, and those measured near the quarter points are also good with a difference of only a few hundred microstrain. The sudden jump in the strain readings around 145 kips on the A1035 side is attributed to formation of a crack near the strain gage, which led to continued differences between the strain values. All things considered, the longitudinal strain data again point toward similar behavior between the two types of steel used for the stirrups.

In addition to placing strain gages on the longitudinal bars, strain gages also were bonded to the stirrups at the mid-depth. Using the measured stress-strain relationships of the #4 A615 and #3 A1035 steel (Appendix A), the strain readings can be converted into stirrup forces using $V_s = \frac{A_v f_s d_v}{S}$ which can then be used to analyze the performance of the stirrups. Figure 22 illustrates the variation of stirrup force as a function of applied shear for specimen SR2. The two mirrored strain gage locations (refer to the inset) show nearly identical results. The similarities of the stirrup forces suggest that the stirrups performed in accordance with the design objective of developing nearly equal forces in #4 A615 and #3 A1035 stirrups. Yielding of A615 stirrups is evident from SG1 that was outside of the region influenced by the concentrated load applied at the midspan and reactions. Between approximately 70 and 85 kips, the stirrup force remained essentially unchanged even though the applied shear force was increased by nearly 15 kips. In contrast, A1035 stirrups could continue to provide shear resistance after A615 stirrups had yielded. The trend of data was generally similar for the other specimens, although formation of cracks near the strain gages occasionally affected the computed stirrup forces.

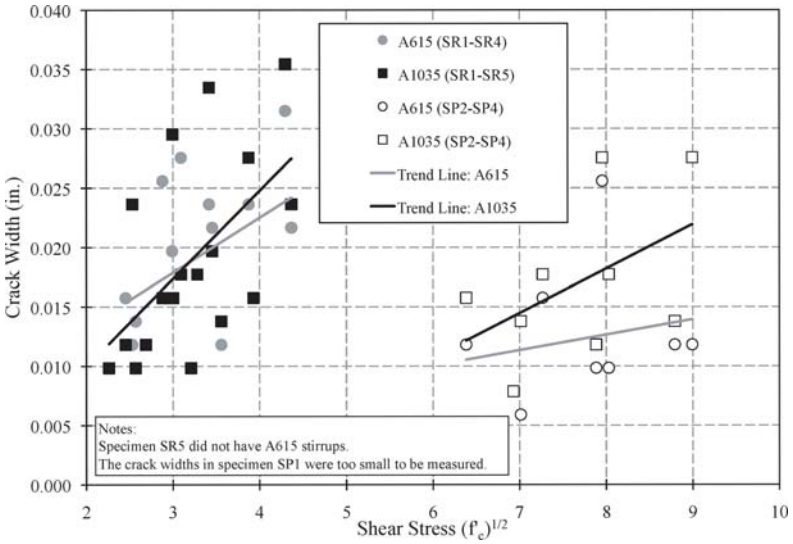

Figure 20. Maximum shear crack width—shear stress.

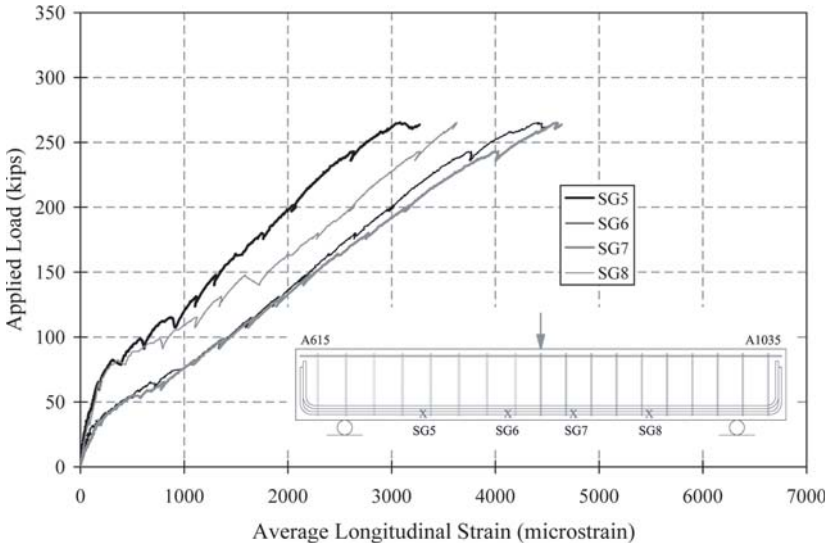

Figure 21. Comparison of longitudinal strains.

2.5.2.3. Summary

The current provisions, in which the yield strength of A1035 stirrups is taken as 100 ksi, were used to design reinforced-concrete and prestressed beams. These specimens performed well in terms of crack patterns, crack widths, and capacity. The experimental data do not suggest any unusual attributes insofar as using A1035 as shear reinforcement.

2.6 Shear Friction

The shear-carrying mechanism present when shear is transferred across a concrete interface subject to Mode II (sliding mode) displacement is commonly known as aggregate interlock, interface shear transfer, or shear friction. The last of these terms will be used here. The interface on which shear acts is referred to as the shear or slip plane. A schematic representation of the shear friction mechanism is shown in Figure 23. The shear friction mechanism arises by virtue of the roughness of concrete crack interfaces. As a rough interface displaces in a shear mode (slipping, resulting in a deformation Δ as shown in Figure 23), a "wedging action" develops forcing the crack to open in a direction perpendicular to the interface (crack width, w). This crack opening or "dilation of the shear crack" engages the reinforcement (having area A_{vf}) crossing the crack resulting in a "clamping" force, $A_{vf}f_s$ being generated. The clamping force attributed to the interface reinforcing steel, $A_{vf}f_s$, is engaged as the crack opens. Thus,

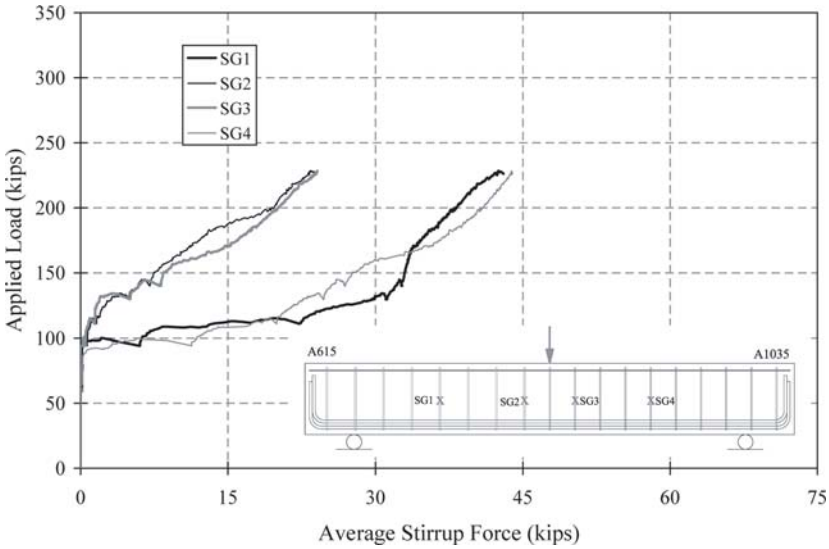

Figure 22. Load—average stirrup forces (Specimen SR2).

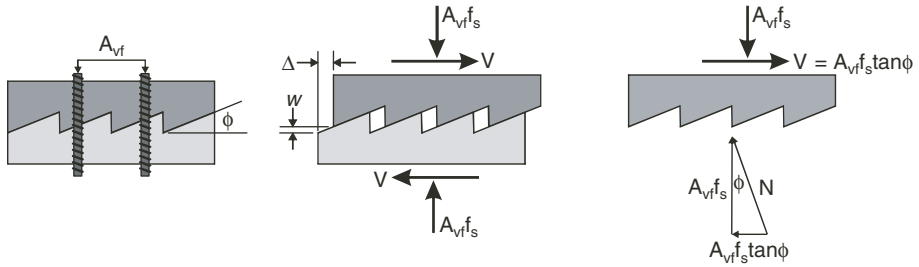

Figure 23. Shear friction analogy proposed by Birkeland and Birkeland (1966) (redrawn).

the clamping force is passive in nature. The crack must open sufficiently to develop the "design" clamping force, $A_{vf}f_s$. Loov and Patnaik (1994) conclude that a slip of $\Delta = 0.02$ in. is required to result in yield of conventional reinforcing steel having $f_y = 60$ ksi. They additionally point out the inconsistency of limiting slip (a previous proposal by Hanson [1960], for instance, suggested limited slip to $\Delta = 0.005$ in.) to a lower value since this may be insufficient to generate f_y in the interface reinforcement. Most critical to this discussion is the fact that only limited data are available for steel interface reinforcement having a nominal yield capacity greater than 60 ksi. Kahn and Mitchell (2002) report a study where the actual yield stress of the interface reinforcing steel was either 70 or 83 ksi. In this study, they report significantly increased scatter in shear friction prediction reliability when using the measured values of f_y and conclude that f_y should not be taken to exceed 60 ksi for design. Additionally, when normalized by concrete strength, the experimental results show no effect resulting from the different values of f_y. The understanding of the shear friction resisting mechanism has evolved to recognize the complex nature of the crack interface behavior and to include the effects of aggregate and cement matrix properties, dowel action of the interface reinforcement, and the localized effects of interface reinforcement within the interfacial area (Walraven and Reinhardt 1981). Nonetheless, code approaches remain based on simple formulations derived from the work of Birkeland and Birkeland (1966).

Considering only normal weight concrete and interface reinforcement oriented perpendicular to the interface, the provisions from AASHTO (2007) §5.8.4 to calculate the nominal shear friction capacity, V_{ni}, are as follows:

$$V_{ni} = cA_{cv} + \mu\left(A_{vf} f_y + P_c\right)$$
$$V_{ni} \le K_1 f_c' A_{cv}$$
$$V_{ni} \le K_2 A_{cv} \qquad \text{(Eq. 11)}$$

Where:

A_{cv} = area of concrete shear interface;
A_{vf} = area of interface shear reinforcement;
P_c = permanent net compressive force across interface;
f_y = yield strength of interface shear reinforcement; $f_y \le 60$ ksi;
f_c' = concrete compressive strength;
μ = "friction factor" (see below);
c = "cohesion factor" (see below);
K_1 = fraction of concrete strength available to resist interface shear (see below); and
K_2 = limiting interface shear resistance (see below).

The factors μ, c, K_1 and K_2 are given based on the interface condition as follows:

Interface condition	c (ksi)	μ	K_1	K_2 (ksi)
Monolithically cast	0.400	1.4	0.25	1.50
Slabs on ¼ in. amplitude roughened surface	0.280	1.0	0.30	1.80
Other on ¼ in. amplitude roughened surface	0.240	1.0	0.25	1.50
Cast against surface with no roughening	0.075	0.6	0.20	0.80

The inclusion of the cA_{cv} term in Equation 11 (which is reported to account for the effects of cohesion and aggregate interlock) requires that minimum interface reinforcement also be provided ($A_{vf} \ge 0.05A_{cv}/f_y$) since the design shear, V_u, could be less than cA_{cv}, technically requiring no reinforcement across the interface. The parameters of Equation 11 are highly empirical and have been calibrated over a relatively narrow band of parameters; most significantly, limited data exist for $f_y > 60$ ksi.

2.6.1 Experimental Program

An experimental study, intended as a series of proof tests of Equation 11 for shear interfaces having high-strength A1035 reinforcement was carried out. This test program is the only known study of shear friction behavior to include high-strength steel.

Typical push-off specimens, having dimensions and details shown in Figure 24, were used in this study. This specimen geometry is commonly used for such tests. The applied load is concentric with the test interface, which is therefore effec-

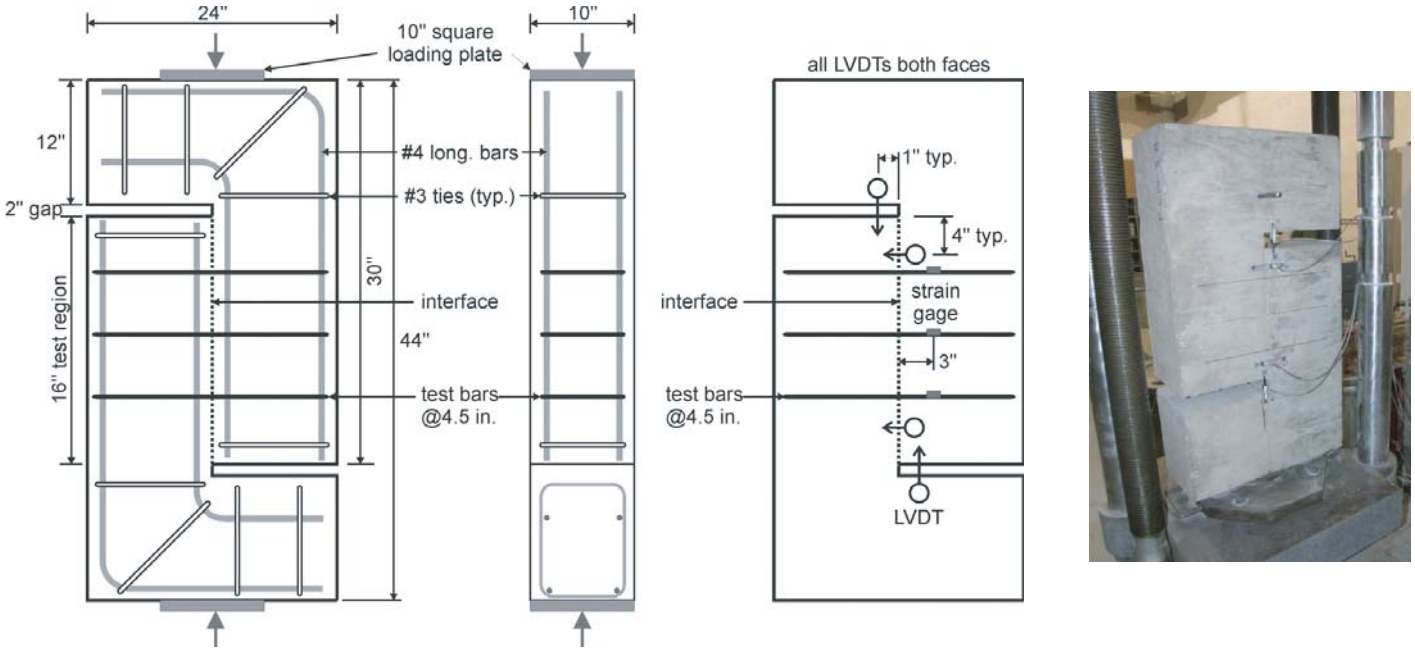

(a) Test Specimen

(b) Instrumentation

(c) Specimen Prior to Testing

Figure 24. Test specimen details and instrumentation.

tively subjected to only shear stress. The shear is resisted by the concrete along the test interface and the steel ties crossing the interface. For these tests, the interface was placed as a "cold joint" with the concrete on one side placed and allowed to cure for 14 days prior to the placement of the other side of the interface. Prior to placing the second side of the interface, it was cleaned of laitance and roughened to create a surface condition with *at least* ¼-in. amplitude. The interface was horizontal during concrete placement; thus, the interface may be thought of as representing the interface between a precast concrete girder and cast-in-place concrete deck. The interface steel reinforcement, therefore, represents the stirrup extensions or interface shear reinforcement along such a cold joint. The parameters measured during the experiments were magnitude of the shear load, displacement parallel to the shear interface, crack width perpendicular to the shear interface, and strain in the steel reinforcement across the test interface.

The specimen designations and measured material properties of the eight push-off specimens tested are shown in Table 21. Four types of duplicated specimens were tested. Specimen labels are preceded with "P" (push-off); the numbers "615" or "1035" indicate the type of steel reinforcement used (ASTM A615 and A1035, respectively); the numbers "3" or "4" indicate the size of the interface steel reinforcement (#3 and #4, respectively); and the letters "A" and "B" are used to identify the duplicated specimens.

All measured concrete and steel reinforcing bar material properties are reported in Table 21. Detailed material data are provided in Appendix A. The concrete used was a conventional 4000 psi mix having a w/c ratio of 0.44 and 1-in. maximum aggregate size. As noted in Table 21, the concrete strength on either side of the interface was 4220 psi and 6020 psi. For subsequent shear capacity calculations, the lower value is used. Two types of interface steel reinforcement were tested: ASTM A615 and A1035 with nominal yield strengths of 60 and 100 ksi, respectively. Two bar sizes of each steel type were tested: #3 and #4. All specimens had three double-legged ties crossing the interface; thus, the interface reinforcing ratios were 0.0041 and 0.0075 for the specimens having #3 and #4 ties, respectively.

The instrumentation used in the experiments consisted of three strain gauges, one located on each of the interface ties approximately 3 in. from the interface, and eight linear variable displacement transducers (LVDTs) as shown in Figure 24. The strain gages were located away from the interface in order to improve their reliability and ensure that they were not damaged. Thus, the actual bar strain at the interface is expected to be greater than that measured by the gages since some of the bar stress is transmitted back into the concrete over this short development length. As the concrete is damaged during testing, the difference in strain between the interface and measurement location becomes less significant.

Testing consisted of the application of a monotonically increasing load to the top and bottom surfaces of the specimens until the ultimate shear capacity of the test interface was reached. The load was applied through a 10-in. diameter plate

Table 21. Shear friction specimen details and experimental results.

Specimen ID	P615-3		P615-4		P1035-3		P1035-4	
	A	B	A	B	A	B	A	B
Interface Steel	6 #3 A615		6 #4 A615		6 #3 A1035		6 #4 A1035	
	Material Properties							
f_c' (psi)	Cast #1: 6020 psi @ 28 days; 7120 psi @ 104 days (age at testing) Cast #2: 4220 psi @ 28 days; 5800 psi @ 90 days (age at testing)							
A_{vf} (in^2)	0.66		1.20		0.66		1.20	
A_{cv} (in^2)	160.4	163.2	165.0	162.5	157.5	160.7	162.5	160.7
$\rho = A_{vf}/A_{cv}$	0.0041	0.0040	0.0073	0.0074	0.0042	0.0041	0.0074	0.0075
f_y (ksi)	67.3		61.5		130.0	126.0	140.0	131.3
f_u (ksi)	103.0		102.3		156.0	157.6	174.0	172.3
ε_u	0.153		0.206		-	0.111	-	0.071
	Experimental Results at Cracking Shear Load							
V_{cr} (kips)	66.2	66.8	50.0	58.2	57.2	72.5	58.4	60.0
$\tau_{cr} = V_{cr}/A_{cv}$ (ksi)	0.41	0.41	0.30	0.36	0.36	0.45	0.36	0.37
Δ_{cr} (in.)	0.008	0.010	0.006	0.007	0.009	0.011	0.007	0.009
w_{cr} (in.)	<0.001	<0.001	<0.001	<0.001	<0.001	<0.001	<0.001	<0.001
ε_{scr} (με)	23	30	27	28	38	42	24	61
$f_{scr} = E_s \varepsilon_{scr}$ (ksi)	0.68	0.87	0.78	0.81	1.11	1.21	0.70	1.78
	Experimental Results at Ultimate Shear Load							
V_u (kips)	112.5	96.5	114.5	129.0	90.0	105.0	135.7	113.5
$\tau_u = V_u/A_{cv}$ (ksi)	0.70	0.59	0.69	0.79	0.57	0.65	0.84	0.71
Δ_u (in.)	0.025	0.027	0.037	0.038	0.027	0.031	0.032	0.041
w_u (in.)	0.008	0.007	0.009	0.008	0.007	0.008	0.008	0.010
ε_{su} (με)	238	405	515	410	222	527	529	579
$\sigma_{su} = E_s \varepsilon_{su}$ (ksi)	6.92	11.74	14.93	11.90	6.44	15.29	15.35	16.79
	Comparison with Equation 11							
V_{ni} (f_y = 60 ksi)	78.1	78.8	111.3	111.0	77.4	78.2	110.8	110.6
V_u/V_{ni}	1.44	1.23	1.03	1.16	1.16	1.35	1.25	1.03
V_{ni} (measured f_y)	82.9	83.6	113.1	112.8	122.7	121.7	201.6	196.1
V_u/V_{ni}	1.36	1.15	1.01	1.14	0.73	0.87	0.69	0.58

Note: Shaded entries indicate that if the measured values of f_y are used, Equation 11 becomes significantly unconservative when the higher strength A1035 bars are used.

at both the top and bottom of the specimens; a ball joint was used at the top to address small alignment discrepancies (none were observed in any test). A view of the test set-up is shown in Figure 24. The load was applied at a rate of approximately 5,000 lbs/min. Once the ultimate shear capacity was reached, loading was continued in displacement control until the specimen failed due to spalling or excessive deformation. Complete details of the experimental program are provided in Zeno (2009).

2.6.2 Experimental Results

A summary of results for applied shear (V), shear displacement parallel to the interface (Δ), crack width perpendicular to the interface (w), and interface steel reinforcement strain (ε_s) for each specimen is given in Table 21. For clarity, the gross section shear stress ($\tau = V/A_{cv}$) and the apparent stress in the reinforcing steel ($f_s = E_s\varepsilon_s$) also are reported. The shear-displacement (V-Δ), shear-crack width (V-w), and shear-interface steel reinforcement strain (V-ε_s) plots of all specimens are shown in Figure 25. In general, duplicate instruments tracked each other very well; therefore, average values of Δ, w, and ε_s are reported. Figure 26 shows examples of observed test behavior taken well after the ultimate load was achieved (displacements at ultimate load were too small to be seen in photographs).

Two important shear load values were monitored during the push-off experiments: the load to cause the initial shear crack, referred to as the "cracking shear load" (V_{cr}); and the highest shear capacity obtained, referred to as the "ultimate shear load" (V_u). After V_{cr} is attained, shear friction dominates the behavior of the loaded specimen until V_u is achieved. As described above, the shear friction mechanism arises from the roughness of the concrete interface and the clamping force by the interface reinforcement. After V_u is achieved, the specimen continues to deform with no further increase in capacity. The crack width increases, reducing the friction component, although theoretically increasing the clamping force. Additionally, the roughness of the shear interface is reduced due to shearing off of the local asperities.

2.6.2.1 Shear Friction Behavior

The experimental behavior illustrates that the shear friction mechanism can be divided into three stages as follows:

Stage 1: Pre-Cracked Behavior. Behavior at loads below the cracking shear load (V_{cr}) is very similar for all specimens.

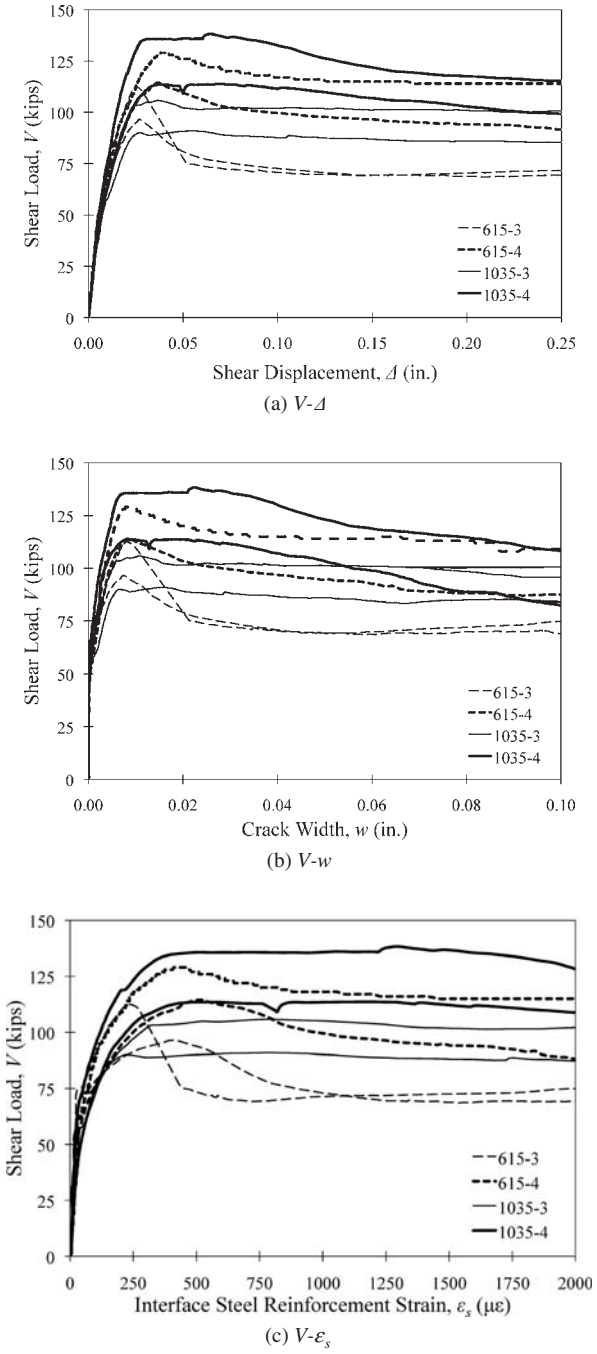

Figure 25. Test results.

It is characterized by a relatively linear relationship between the applied load (V) and shear displacement (Δ), and negligible interface crack widths (w) and interface steel reinforcement strains (ε_s). Prior to cracking, applied load is resisted by concrete shear associated with the strength of the bond between the two surfaces that form the shear interface. The average value of cracking stress (τ_{cr}) for the cold-jointed specimens tested was found to be 380 psi and have a coefficient of variation (COV) of 12%. This stress corresponds to a value of $5\sqrt{f_c'}$ (psi), based on the lower concrete strength at the interface at the time of testing: $f_c' = 5800$ psi. As should be expected, this value is largely unaffected by the steel reinforcement. The strain, and therefore stress, in the reinforcing steel at V_{cr} is negligible—varying only up to 61 με in the present study. Hence, shear friction reinforcement does not significantly contribute to the shear capacity of the interface up to the instant of cracking. The shear displacement at V_{cr} was less than 0.01 in. in all specimens.

Stage 2: Post-Cracked Behavior. The post-cracked behavior from loads ranging from V_{cr} to V_u is characterized by a softening behavior, larger and visible interface crack widths, and higher interface steel reinforcement strains than in the pre-cracked stage. During the second stage, both Δ and w exhibit a relatively linear relationship with the applied shear load. The shear friction mechanism is engaged in the second stage. The capacity of the now cracked interface to resist shear is primarily attributed to the friction that originates from the roughness of the two concrete surfaces that form the interface. The interface surfaces are tied together by the interface steel reinforcement. The ultimate shear capacity of those specimens having #4 bars was 760 psi, which is approximately 20% greater than those having #3 bars (630 psi). These values correspond to $10\sqrt{f_c'}$ (psi) and $8\sqrt{f_c'}$ (psi), respectively. Significantly, the ultimate capacity is unaffected by the grade of reinforcing steel, demonstrating the same average value (690 psi) for specimens having A615 and A1035 bars.

Significant variability of shear displacement (Δ) values was observed ranging from 0.025 to 0.041 in. at V_u. Values of the crack width (w) at V_u show less variability, ranging from 0.007 to 0.010 in. In both cases, this variability appears to be related to the size of the interface steel reinforcement provided: the specimens with #3 bars have somewhat smaller values of Δ and w than those with #4 bars. This observation is expected due to the greater capacity of the specimens having #4 bars and indicates that the apparent stiffness of the cracked specimens is unaffected by the bar size; thus, the greater the capacity, the greater the displacement.

Average interface steel reinforcement strain values (ε_s) at V_u range between 222 and 579 με. Associated with the greater capacity of the specimens having #4 bars, these specimens also exhibited greater bar strains at V_u. In general, the strains measured in the A1035 bars were marginally greater than those measured in the A615 bars. This observation is believed to be associated with the different bond characteristics of the bars used and is discussed further below. Because of the still low interface steel reinforcing strains, there is little active clamping force across the interface in this stage.

Stage 3: Post-Ultimate Behavior. The behavior following achieving V_u is characterized by an increase in Δ, w, and ε_s without any additional increase in applied loading. However,

(a) P615-3B at a slip exceeding 1in. (Δ can be seen as displaced horizontal lines representing interface reinforcement locations)

(b) Distortion of the interface steel reinforcement of specimen P1035-3A following large slip and cover spalling

Figure 26. Specimens following testing.

as seen in Figure 25, the behavior of the specimens with A615 interface steel reinforcement in this stage is different from that of the specimens with A1035 steel reinforcement. The specimens with A1035 steel reinforcement exhibit continued load carrying capacity after the ultimate shear load is achieved, which can be seen as a plateau in the plots shown in Figure 25. The specimens with A615 steel reinforcement, on the other hand, demonstrate a more rapid degradation in post-ultimate load carrying capacity. Although this study is unable to determine the reasons for the different Stage 3 behavior, it is proposed that it may be attributed to the different bond characteristics of the bars used and is discussed further below.

2.6.2.2 Development of Clamping Force in Interface Steel

In general, it can be seen that, as expected, the shear friction capacity of the specimens increased as the area of interface steel reinforcement increased. This increase is because the area of interface steel reinforcement is proportional to the clamping force (i.e., $f_s = f_s A_s$, where $f_s = \varepsilon_s E_s$) and thus, the shear friction capacity. On the other hand, it can be seen that the use of A1035 high-strength steel instead of A615 steel as interface reinforcement did not increase the shear friction capacity of the specimens significantly. This trend is because, in all of the specimens, V_u was reached well before steel yielding occurred. In fact, as seen in Table 21, the stress in the interface steel reinforcement is significantly lower than its yield strength when the ultimate shear load is achieved. The slight increase in capacity of the specimens with A1035 interface reinforcement may be attributed to the enhanced bond characteristics of this steel (Sumpter 2007), because a better bond results in higher steel strains and increases the shear friction capacity of the interface. Although this study was not intended to investigate bond characteristics of the bars used and there was no discernable difference in rib configuration between the A615 and A1035 bars, the data do suggest marginally better bond characteristics of the A1035 bars in this instance (Zeno 2009).

Based on the AASHTO design equation (Equation 11), it would be expected that the use of high-strength interface reinforcement would increase the shear friction capacity of the specimens. In fact, if the interface reinforcement had reached its yield strength during the experiments, it would be expected that specimens P615-4 and P1035-3, having similar nominal values of $A_{vf} f_y$, would have achieved similar shear friction capacities. However, the interface reinforcement did not yield. In fact, the P615-4 specimens had significantly greater capacity than the P1035-3 specimens, even though the latter had high-strength interface reinforcement. These results illustrate that because the ultimate shear capacity is dominated by concrete behavior and is reached well before steel yielding occurs, the clamping force is a function of the steel modulus rather than the yield strength.

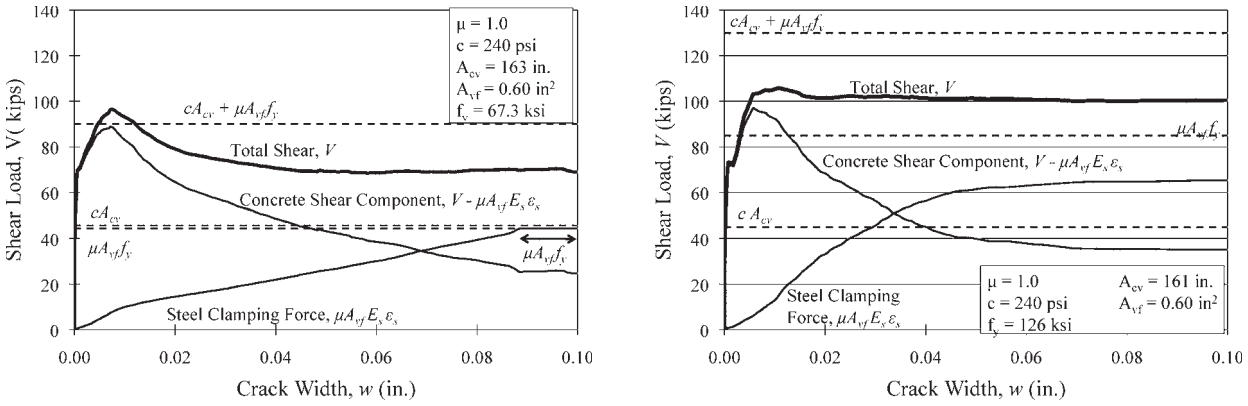

(a) Specimen P615-3B

(b) Specimen P1035-3B

Figure 27. Components of shear friction behavior.

2.6.2.3 Components of Shear Friction

The behavior described in the previous section is illustrated in Figure 27, which shows the load-crack width (V-w) plots decomposed into their steel and concrete components for Specimens P615-3B and P1035-3B. Similar plots were developed for all specimens (Zeno 2009). In Figure 27, the steel clamping component of shear friction was calculated using the measured interface reinforcement strain (ε_s) to calculate the actual steel stress and assumes a friction factor, μ, equal to 1.0 (consistent with AASHTO provisions); thus, the steel clamping force component of the total shear friction is $\mu A_{vf} \varepsilon_s E_s$. The concrete component was calculated by subtracting the steel component from the applied shear load: $V - \mu A_{vf} \varepsilon_s E_s$. Figure 27 also shows the calculated capacity for the specimens obtained using Equation 11 and measured values of f_y. From Figure 27 it can be seen that at its peak, the apparent concrete component greatly exceeds the nominal concrete component (cA_{cv}) and contributes to the majority of the shear friction capacity of the specimens. The corollary of this observation is that the steel component is significantly lower than the assumed design value ($\mu A_{vf} f_y$) and reaches its peak value well after the shear friction capacity of the specimens is exceeded. As can be seen in Figure 27, steel yielding was observed in P615-3B but only after a crack opening of 0.09 in. while the steel in P1035-3B did not yield. The behavior of P1035-3B appears to achieve a "steady state" (i.e., balance between the steel and concrete components after a crack opening of about 0.08 in.). Similar behavior was exhibited by all specimens having A1035 reinforcing (Zeno 2009). In all cases shown, the prescribed limits on shear friction capacity ($K_1 f'_c A_{cv}$ and $K_2 A_{cv}$) are greater than the values of $cA_{cv} + \mu A_{vf} f_y$ shown. Furthermore, it is acknowledged that the use of the empirical value μ = 1 is arbitrary although supported by current codes and much previous research. The assumption of a μ value is necessary to resolve the concrete component from an otherwise indeterminate equation. Different assumptions of μ will shift the curves in a linear manner.

These findings demonstrate that Equation 11 does not represent the shear friction mechanism since it implies that the maximum concrete and steel components of the shear friction occur simultaneously. In fact, as seen in Figure 27, the concrete component contributes to the majority of the shear friction capacity before the ultimate shear load is reached and then falls to a residual value while the steel component increases. However, the steel component never reaches its peak value, $\mu A_{vf} f_y$, before the ultimate shear load is reached. Nonetheless, empirically limiting the yield strength, f_y, to 60 ksi in Equation 11 does provide safe design values.

Values of the nominal design shear friction capacity (V_{ni}) calculated from Equation 11 are given in Table 21. Provided the limitation $f_y < 60$ ksi is imposed, Equation 11 gives conservative estimates of capacity. However, if the measured values of f_y are used, Equation 11 becomes significantly unconservative when the higher strength A1035 bars are used (shaded entries).

2.6.3 Conclusions with Regard to Shear Friction

The present AASHTO requirement for shear friction capacity (Equation 11) may be safely adopted for use with high-strength steel reinforcement and other steel not experiencing a well-defined yield plateau provided the value of f_y used in the formulation is not taken greater than 60 ksi. This recommendation is the present requirement and no change to AASHTO LRFD §5.8.4 is required to accommodate high-strength steel.

2.7 Compression Members

Analytical parametric studies were performed to examine behavior of columns reinforced with A1035 longitudinal and transverse reinforcement. The current AASHTO requirements

for spacing of A1035 spirals were also examined and revisions have been recommended.

2.7.1 Column Capacity

Parametric studies were conducted to determine whether columns reinforced with A1035 longitudinal and transverse reinforcement will reveal any unexpected results compared to columns reinforced with commonly used A615 steel. Other steel types (A706, A496, A82, and A955) were not initially included in the parametric studies in order to first evaluate the results for A1035 reinforcement.

2.7.1.1 Details

The parametric studies were performed by analyzing 270 cases with the variables shown in Table 22. For all cases, the amount of longitudinal steel for columns reinforced with ASTM A615 and ASTM A1035 bars was determined by using a target reinforcement ratio of 4% and 2%, respectively. Spacing for the transverse reinforcement was determined using AASHTO §5.10.6 and §5.10.11.4.1e. The column overall dimensions were arbitrarily selected to cover a wide range of practical column dimensions. The complete details of all 270 cases are provided in Appendix G.

2.7.1.2 Modeling

A fiber analysis program called XTRACT (Imbsen 2007) was used to perform detailed cross-sectional fiber analyses. The stress-strain relationship for ASTM A615 reinforcement was based on an available model that replicates typical behavior of such bars. A user-defined material model, in which discrete strain and stress data points were input, was used to represent the stress-strain relationship of ASTM A1035. The strain and stress values for each data point were established from an appropriate Ramberg-Osgood function (Appendix A). The material behaviors of the unconfined concrete shell and confined concrete core were based on the Razvi and Saatcioglu (1999) model that has been calibrated for concrete strengths up to 15 ksi.

2.7.1.3 Results

Representative moment-curvature relationships and axial load-moment (P-M) interaction diagrams are shown in Figures 28a and 28b, respectively, for a 24-inch diameter non-seismic, spirally reinforced column using #3, #4, and #5 spirals and 10-ksi concrete. The moment-curvature responses were generated for an axial load corresponding to $0.1f'_cA_g$ where A_g is the column gross section area. The complete set of results is provided in Ward (2009). The variation in the moment-curvature diagrams is due to the differences in reinforcement ratios. The columns reinforced with A615 have more longitudinal bars and hence a greater stiffness. The reduced stiffness of columns with A1035 bars needs to be taken into account for design of bridges subjected to seismic loads. The different sizes of transverse steel do not significantly influence the moment-curvature relationships. This trend should be expected because the properties of concrete (confined and unconfined cores) do not appreciably influence the response of members with small axial loads. Moreover, as discussed previously, the confined concrete properties are not affected by the size of transverse bars. The axial load-moment interaction diagrams (see Figure 28b) for columns with A615 and A1035 reinforcement vary primarily because of the larger amount of A615 longitudinal reinforcement. For a given type of steel (A615 or A1035), the size of transverse reinforcement does not affect the interaction diagrams.

The aforementioned results and discussions do not suggest any unexpected responses when A1035 steel is used. In comparison to A1035, the strengths and properties of other steel types (A706, A496, A82, and A955) are closer to the characteristics of A615. Since the responses of columns with A1035 steel do not suggest any unusual or unexpected trends, it was deemed unnecessary to perform similar parametric studies for A706, A496, A82, and A955.

Table 22. Variables for column parametric studies.

Variable	Value/Description
Column Type	Square tied columns designed and detailed for seismic loads; Circular spirally reinforced columns used in non-seismic regions; and Circular spirally reinforced columns for bridges subjected to seismic loads.
Type of Reinforcement	ASTM A615 with f_y = 60 ksi and ASTM A1035 with f_y = 120 ksi (for longitudinal and transverse bars)
Column Size	Square column dimension or diameter = 18, 24, 36, 48, 60 in.
Transverse Reinforcement	#3, #4, and #5
Concrete Strength	f'_c = 5, 10, 15 ksi

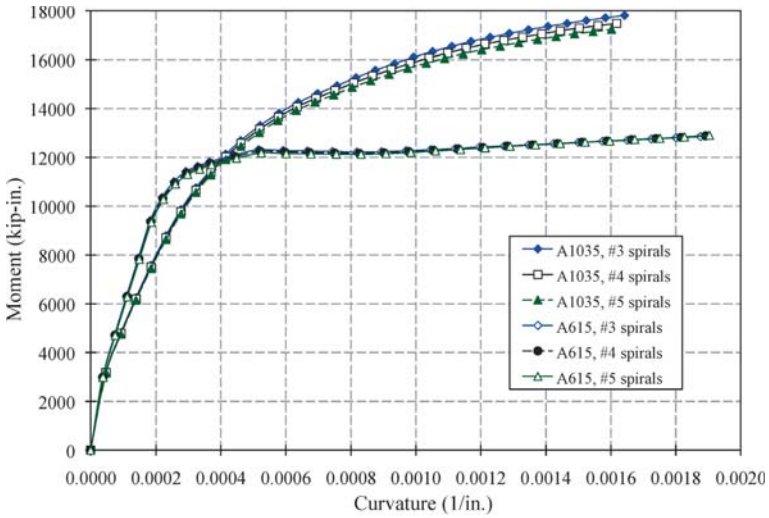

(a) Moment-Curvature Response

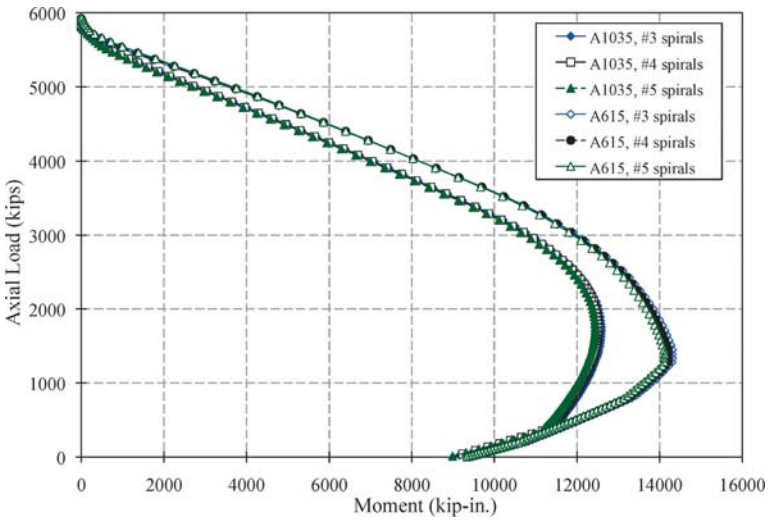

(b) Axial Load-Moment Interaction

Figure 28. Representative responses.

2.7.2 Spacing of Spiral Reinforcement

For cases that are not controlled by seismic requirements, the volumetric ratio of spiral reinforcement must satisfy AASHTO Equation 5.7.4.6-1, that is

$$\rho_s \geq 0.45\left(\frac{A_g}{A_c}-1\right)\frac{f_c'}{f_{yh}}$$

Additionally, according to §5.10.6.2, the center-to-center spacing shall not exceed six times the diameter of the longitudinal bar or 6 in. From a practical point of view, the clear spacing of spirals cannot be less than 1 in. or 1.33 times the maximum size of the aggregate (AASHTO §5.10.6.2). The basis of AASHTO Equation 5.7.4.6-1 is to ensure that the axial load capacity of columns after spalling of the concrete cover is at least equal to the capacity before spalling. This provision was reviewed to determine whether it accurately describes the confining ability of high-strength transverse steel.

2.7.2.1 Formulation

The axial load before spalling of cover (P_o) and the capacity after spalling of cover (P') can be computed from the following equations:

$$P_o = f_c'\left(A_g - A_s\right) + A_s f_y$$
$$P' = f_{cc}'\left(A_c - A_s\right) + A_s f_y$$

Where:

A_g = gross column area;
A_s = area of longitudinal bar;
f_y = yield strength of longitudinal bars;

f'_c = unconfined concrete strength; and
f'_{cc} = confined concrete strength, which is a function of spacing of spiral(s).

The provided spiral should be sufficient such that P_o and P' are equal to each other, as follows:

$$f'_c(A_g - A_s) = f'_{cc}(A_c - A_s)$$

For a given concrete compressive strength, column size, cover, longitudinal reinforcement ratio, longitudinal bar size, spiral size, yield strength of spiral, and modulus of elasticity, iterate the value of the spiral spacing such that this equality is satisfied. The Razvi and Saatcioglu (1999) model was used to compute f'_{cc}. Additional details, including the use of another confined concrete model, are provided in Appendix G.

2.7.2.2 Parametric Study

Using the AASHTO provision and the aforementioned formulation, the required spiral spacing was computed for a number of columns with the parameters listed in Table 23. All of the columns were reinforced with #9 longitudinal bars, and the longitudinal reinforcement ratio was set equal to 1.5%. The cover to the spiral was taken as 1.5 in. The aim of this study was to evaluate the spacing of high-strength spiral reinforcement.

2.7.2.3 Results and Discussions

The calculated required spacings for a representative case are summarized in Table 24. The results for the other cases are provided in Appendix G. For a given concrete strength, the calculated spacing using any of the methods increases as the yield strength of the spiral increases. In terms of reducing the spiral spacing in columns cast with high-strength concrete, the use of larger, high-strength spirals is more efficient. For a number of cases (shaded in Table 24), the calculated spacings exceed the maximum limit of 6 in. These cases involve columns using 5-ksi concrete. The calculated spacings in columns with a concrete strength of 15 ksi are below the maximum limit for all steel strengths.

The trend of the computed spacings is expected. That is, as the column diameter becomes larger, the difference between the core and gross areas diminishes; hence, the ratio of axial load capacity before and after spalling of cover approaches unity and spirals can be placed at larger spacings. From a confinement point of view, for an "infinitely" large column, the spiral spacing is expected to become "infinitely large." The formulation presented in Section 2.7.2.1 accurately replicates this trend. The difference between the spacings based on current AASHTO requirements (Equation 5.7.4.6-1) and more rational methodology presented in Section 2.7.2.1 becomes more pronounced as the column diameter increases. Unfortunately, the available test data do not include test results for columns larger than 24 in. because of the large amount of axial force required to test such large columns.

The level of axial load in most bridge columns is relatively small (on the order of $0.05f'_cA_g$) and is appreciably less than the axial load capacity. Therefore, the capacity after the loss of cover will be above the normal loads that typical bridge columns are expected to experience. This point is evident from Figure 29 in which the ratio of the axial load capacity (taken as $0.85f'_cA_c$, where f'_c = unconfined concrete strength,

Table 23. Parameters for transverse spacing study.

Variable	Value/Description
Concrete Compressive Strength*	5, 10, 15 ksi
Spiral Yield Strength	60 ksi, 100 ksi, 120 ksi
Column Diameter	18-80 in. (2-in. increments)
Spiral Bar Size	#3, #4, #5

Note: *The strain at peak stress (ε_{co}) was taken as 0.0025.

Table 24a. Spacing of spiral (#4 Spiral, f_{yh} = 60 ksi).

D (in.)	f'_{co} =5 ksi		f'_{co} =10 ksi		f'_{co} =15 ksi	
	AASHTO	Model R-S	AASHTO	Model R-S	AASHTO	Model R-S
18	3.12	2.24	1.56	1.29	1.04	0.93
20	3.17	2.4	1.59	1.38	1.06	0.99
22	3.21	2.55	1.6	1.46	1.07	1.06
24	3.24	2.83	1.62	1.62	1.08	1.17
26	3.27	3.09	1.63	1.77	1.09	1.22
28	3.29	3.35	1.64	1.92	1.1	1.25
30	3.31	3.72	1.65	2.07	1.1	1.27
32	3.32	3.97	1.66	2.11	1.11	1.3
34	3.34	4.32	1.67	2.15	1.11	1.32
36	3.35	4.56	1.67	2.19	1.12	1.34
38	3.36	4.89	1.68	2.22	1.12	1.36
40	3.37	5.19	1.69	2.25	1.12	1.38
42	3.38	5.26	1.69	2.28	1.13	1.4
44	3.39	5.33	1.69	2.31	1.13	1.42
46	3.4	5.39	1.7	2.34	1.13	1.43
48	3.4	5.45	1.7	2.37	1.13	1.45
50	3.41	5.51	1.7	2.39	1.14	1.47
52	3.41	5.57	1.71	2.41	1.14	1.48
54	3.42	5.62	1.71	2.44	1.14	1.5
56	3.43	5.67	1.71	2.46	1.14	1.51
58	3.43	5.72	1.71	2.48	1.14	1.52
60	3.43	5.77	1.72	2.5	1.14	1.54
62	3.44	5.82	1.72	2.53	1.15	1.55
64	3.44	5.87	1.72	2.54	1.15	1.56
66	3.45	5.91	1.72	2.56	1.15	1.57
68	3.45	5.95	1.72	2.58	1.15	1.58
70	3.45	6	1.73	2.6	1.15	1.6
72	3.45	6.04	1.73	2.62	1.15	1.61
74	3.46	6.08	1.73	2.64	1.15	1.62
76	3.46	6.12	1.73	2.65	1.15	1.63
78	3.46	6.15	1.73	2.67	1.15	1.64
80	3.46	6.19	1.73	2.69	1.15	1.65

Notes:
Shaded cells indicate where calculated spacings exceed the maximum limit of 6 in. The tabulated values of spacings are in inches. Method R-S is based on the confined model proposed by Razvi and Saatcioglu (1999 and 2002).

Table 24b. Spacing of spiral (#4 Spiral, f_{yh} = 100 ksi).

D (in.)	f'_{co} =5 ksi		f'_{co}=10 ksi		f'_{co} =15 ksi	
	AASHTO	Model R-S	AASHTO	Model R-S	AASHTO	Model R-S
18	5.21	3.15	2.6	1.81	1.74	1.31
20	5.29	3.38	2.64	1.94	1.76	1.4
22	5.35	3.59	2.67	2.06	1.78	1.48
24	5.4	3.97	2.7	2.28	1.8	1.64
26	5.44	4.35	2.72	2.49	1.81	1.8
28	5.48	4.72	2.74	2.7	1.83	1.95
30	5.51	5.23	2.76	3	1.84	2.12
32	5.54	5.58	2.77	3.2	1.85	2.16
34	5.56	6.07	2.78	3.48	1.85	2.2
36	5.58	6.41	2.79	3.65	1.86	2.24
38	5.6	6.88	2.8	3.7	1.87	2.27
40	5.62	7.33	2.81	3.75	1.87	2.3
42	5.63	7.78	2.82	3.8	1.88	2.33
44	5.65	8.21	2.82	3.85	1.88	2.36
46	5.66	8.64	2.83	3.9	1.89	2.39
48	5.67	9.07	2.84	3.94	1.89	2.42
50	5.68	9.19	2.84	3.99	1.89	2.45
52	5.69	9.28	2.85	4.02	1.9	2.47
54	5.7	9.37	2.85	4.06	1.9	2.49
56	5.71	9.45	2.85	4.1	1.9	2.52
58	5.72	9.54	2.86	4.14	1.91	2.54
60	5.72	9.62	2.86	4.17	1.91	2.56
62	5.73	9.7	2.87	4.21	1.91	2.58
64	5.74	9.78	2.87	4.24	1.91	2.6
66	5.74	9.85	2.87	4.27	1.91	2.62
68	5.75	9.92	2.87	4.31	1.92	2.64
70	5.75	9.99	2.88	4.33	1.92	2.66
72	5.76	10.06	2.88	4.37	1.92	2.68
74	5.76	10.13	2.88	4.39	1.92	2.7
76	5.77	10.19	2.88	4.42	1.92	2.71
78	5.77	10.26	2.89	4.45	1.92	2.73
80	5.77	10.32	2.89	4.48	1.92	2.75

Notes:
Shaded cells indicate where calculated spacings exceed the maximum limit of 6 in. The tabulated values of spacings are in inches. Method R-S is based on the confined model proposed by Razvi and Saatcioglu (1999 and 2002).

Table 24c. Spacing of spiral (#4 Spiral, f_{yh} = 120 ksi).

D (in.)	f'_{co} = 5 ksi		f'_{co}=10 ksi		f'_{co}=15 ksi	
	AASHTO	Model R-S	AASHTO	Model R-S	AASHTO	Model R-S
18	6.25	3.56	3.12	2.04	2.08	1.47
20	6.34	3.82	3.17	2.19	2.11	1.58
22	6.42	4.05	3.21	2.32	2.14	1.68
24	6.48	4.45	3.24	2.57	2.16	1.86
26	6.53	4.83	3.27	2.8	2.18	2.03
28	6.57	5.2	3.29	3.01	2.19	2.19
30	6.61	5.72	3.31	3.31	2.2	2.41
32	6.64	6.07	3.32	3.51	2.21	2.51
34	6.67	6.56	3.34	3.8	2.22	2.53
36	6.7	6.89	3.35	3.99	2.23	2.55
38	6.72	7.35	3.36	4.15	2.24	2.57
40	6.74	7.8	3.37	4.18	2.25	2.59
42	6.76	8.24	3.38	4.2	2.25	2.6
44	6.78	8.66	3.39	4.23	2.26	2.62
46	6.79	9.08	3.4	4.26	2.26	2.63
48	6.81	9.49	3.4	4.28	2.27	2.65
50	6.82	9.79	3.41	4.3	2.27	2.66
52	6.83	9.83	3.41	4.32	2.28	2.68
54	6.84	9.88	3.42	4.35	2.28	2.69
56	6.85	9.93	3.43	4.37	2.28	2.7
58	6.86	9.97	3.43	4.39	2.29	2.71
60	6.87	10.02	3.43	4.41	2.29	2.72
62	6.88	10.06	3.44	4.42	2.29	2.74
64	6.88	10.11	3.44	4.44	2.29	2.75
66	6.89	10.15	3.45	4.46	2.3	2.76
68	6.9	10.19	3.45	4.48	2.3	2.77
70	6.9	10.22	3.45	4.49	2.3	2.78
72	6.91	10.26	3.45	4.51	2.3	2.79
74	6.91	10.29	3.46	4.52	2.3	2.8
76	6.92	10.33	3.46	4.54	2.31	2.81
78	6.93	10.37	3.46	4.55	2.31	2.81
80	6.93	10.4	3.46	4.57	2.31	2.82

Notes:
Shaded cells indicate where calculated spacings exceed the maximum limit of 6 in. The tabulated values of spacings are in inches. Method R-S is based on the confined model proposed by Razvi and Saatcioglu (1999 and 2002).

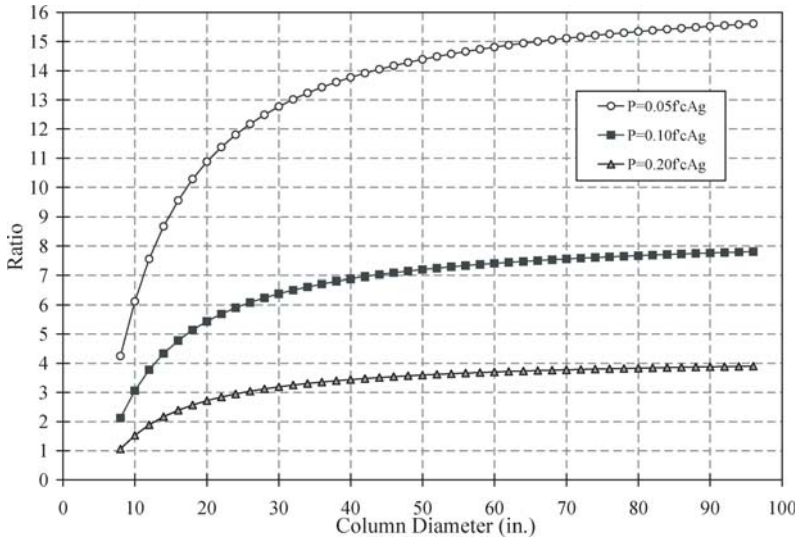

Figure 29. Ratio of core axial load capacity to axial load demands.

A_c = core area) to the expected axial load demand (taken as $0.05f'_cA_g$, $0.10f'_cA_g$, or $0.20f'_cA_g$) is plotted for columns with diameters ranging from 8 in. to 96 in. with 2 in. of cover. For an 8-in. diameter, the loss of a 2-in. cover will significantly reduce the available area (the core area is only 25% of the gross area for this rather small column). However, even for this small column, the axial load capacity of the core (taken simply as $0.85f'_cA_c$) is about 6% larger than an unrealistic axial load demand of $0.20f'_cA_g$. For more typical load demands and more realistic column sizes, the remaining capacity after the loss of cover will be sufficient.

2.7.3 Summary and Conclusions

ACI 318-08 allows the use of an equation identical to AASHTO Equation 5.7.4.6-1 for f_{yh} up to 100 ksi. The references cited as the basis of allowing f_{yh} = 100,000 ksi are those used as the basis of formulation presented in Section 2.7.2.1. In view of ACI 318-08 provisions, the results of the aforementioned parametric study (Table 24), and the axial load capacity of the core relative to the expected axial load demands (Figure 29), it appears that the use of current AASHTO Equation 5.7.4.6-1 for f_{yh} up to 100 ksi can be justified for Seismic Zone 1. The extension of this equation beyond 100 ksi is questionable at this time.

2.8 Bond and Anchorage

2.8.1 Splice Development

AASHTO LRFD (2007) §5.11.2.1.1 prescribes the basic tension development length of #11 bars and smaller, l_{db}, as follows:

$$\ell_{db} = \frac{1.25A_b f_y}{\sqrt{f'_c}} > 0.4d_b f_y \qquad \text{(ksi units)} \qquad \text{(Eq. 12)}$$

Where:

- A_b and d_b are the area and diameter of the bar being developed;
- f'_c is the concrete strength; and
- f_y is the bar yield stress (i.e., the stress to be developed by the splice).

Recent recommendations of NCHRP Project 12-60 (Ramirez and Russell 2008) are based on the ACI 318 (2008) requirements for basic tension development length with an additional factor, $\Psi_c = 1.2$, applied when f'_c exceeds 10 ksi as follows:

$$\ell_{db} = \left(\frac{3f_y \Psi_c \Psi_t \Psi_e \lambda}{40\sqrt{f'_c}\left((c_b + K_{tr})/d_b\right)} \right) d_b \qquad \text{(psi units)} \qquad \text{(Eq. 13)}$$

Where Ψ_t and Ψ_e are factors to account for "top cast" bars and the use of epoxy-coated reinforcing steel (in this study both are taken as unity); λ is a factor accounting for the use of lightweight concrete (also unity for this study). The term $(c_b + K_{tr})/d_b$ accounts for the beneficial effects of transverse confinement and has an upper limit of 2.5. For values of $(c_b + K_{tr})/d_b$ less than 2.5, splitting failures are likely; for values greater than 2.5, pullout failures are likely. The latter cannot be affected by the addition of more confining reinforcement. The NCHRP 12-60 recommendations also differ from the ACI 318 formulation by removing the Ψ_s factor, which reduces the development length ($\Psi_s = 0.8$) for #6 bars and smaller.

A comparison of development length calculations made using Equations 12 and 13 is presented in Figure 30. In this figure, calculated values for #8 bars are shown although all bar sizes exhibit similar trends. For the NCHRP 12-60 calculation (Equation 13), the value of $(c_b + K_{tr})/d_b = 2.5$ since this limit is typically obtained when confinement is present. It is clear that the present AASHTO requirements are more conservative than those proposed by NCHRP 12-60. The latter is used in the present study and thus the experimental "proof test" is conservative when compared to present AASHTO requirements.

Although the current AASHTO requirement (Equation 12) does not address confinement, it can be shown to result in development lengths comparable to those resulting from the ACI 408 (2003) requirements and to be more conservative than those resulting from the use of ACI 318 when typical levels of confinement are used. The AASHTO requirement may underestimate the development required in cases where no confining reinforcement is provided. However, as discussed in Chapter 1, confining reinforcement should always be used when developing or splicing ASTM A1035 or other high-strength reinforcing steel.

2.8.1.1 Splice Development Tests

Eight spliced bar flexural specimens, shown in Figure 31, were tested in four-point flexure. Specimen labels begin with "D" (for development) and indicate the bar size, followed by the specimen number. Each specimen had two tension bar

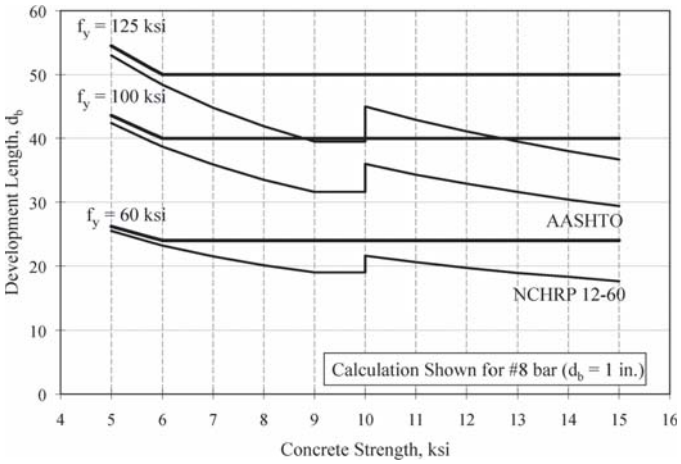

Figure 30. Comparison of development length calculations.

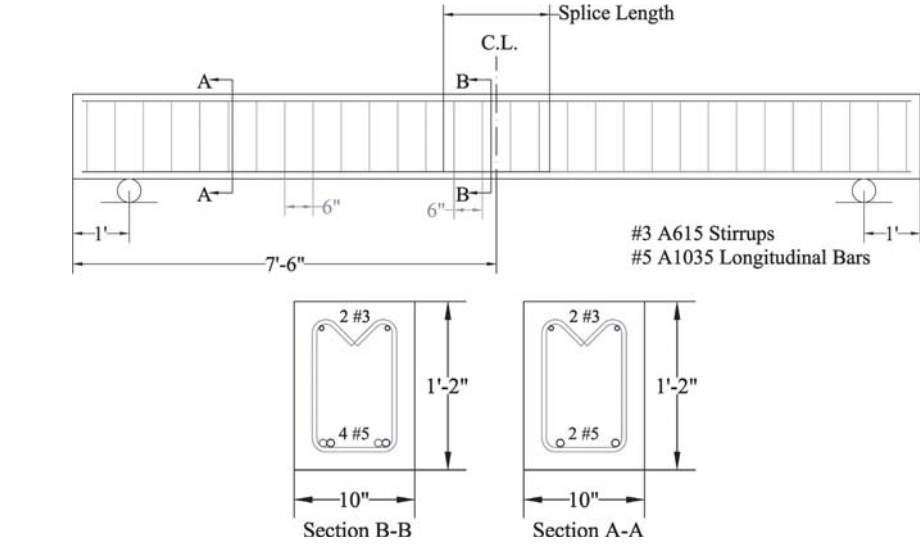

(a) #5 Specimens (D5-1, D5-2, D5-3, D5-4)

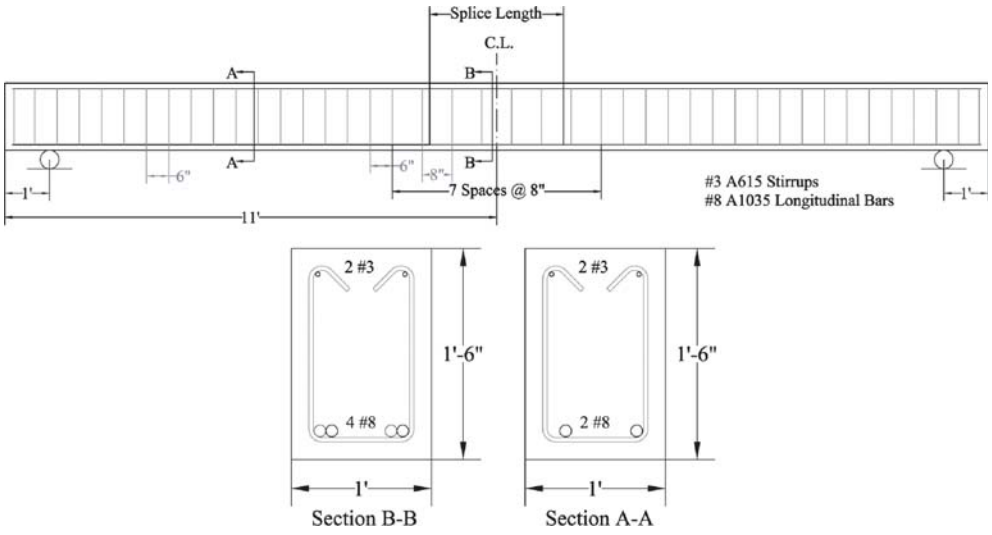

(b) #8 Specimens (D8-1, D8-2, D8-3, D8-4)

Figure 31. Splice development test specimen details.

splices located entirely within the constant moment region of the test span. Two bar sizes were tested: #5 and #8. Nominal concrete strengths used for design were 10 and 15 ksi. The actual 28-day concrete strength was determined to be 12.9 and 15.4 ksi (see Appendix A). Measured steel reinforcing properties are given in Table 25 and details are provided in Appendix A. The splice lengths provided, summarized in Table 26, were obtained from Equation 13 to be sufficient to develop bar stresses (f_y in Equation 13) of 100 and 125 ksi, respectively. The use of Equation 13 results in shorter development lengths than Equation 12 and is therefore less conservative than Equation 12; thus, it was used in this study.

Table 25. Reinforcing steel properties.

		#3*	#3†	#4	#5	#8
ASTM grade		A615	A615	A1035	A1035	A1035
f_y‡	ksi	65.0	68.0	140.0	130.2	118.6
f_u	ksi	101	108.8	174.0	164.1	154.6
ε_u		0.159	0.154	not reported	0.103	0.115

* Confining stirrups used in splice tests.

† Confining ties used in hook anchorage tests labeled "D" in Figure 33b and Table 27.

‡ Calculated using 0.2% offset method.

Table 26. Splice development test results.

Specimen	Design f'_c (ksi)	Spliced Bars	Splice Length		Design Bar Stress to be Developed; f_y in Equation 13		Experimentally Observed Bar Stress Developed	
				(in.)	Stress (ksi)	Strain	Stress (ksi)	Strain
D5-1	10	2 #5	$36d_b$	22.5	100	0.0041	161	0.0261
D5-2	10	2 #5	$45d_b$	28.2	125	0.0063	160	0.0232
D5-3	15	2 #5	$29d_b$	18.4	100	0.0039	152	0.0135
D5-4	15	2 #5	$37d_b$	23.0	125	0.0060	163	0.0254
D8-1	10	2 #8	$36d_b$	36.0	100	0.0042	140	0.0126
D8-2	10	2 #8	$45d_b$	45.0	125	0.0074	152	0.0306
D8-3	15	2 #8	$29d_b$	29.0	100	0.0043	133	0.0096
D8-4	15	2 #8	$37d_b$	37.0	125	0.0070	139	0.0122

Strain gages were bonded on the bars immediately beyond their splice length from which the stress developed by each splice was determined using experimentally obtained stress-strain relationships (Appendix A). Confinement reinforcement in the splice region (and along the entire span) consisted of #3 stirrups having a nominal yield capacity of 60 ksi spaced at 6 in. Based on the confinement provided, a value of $(c_b + K_{tr})/d_b$ greater than 2.5 is calculated; thus, $(c_b+K_{tr})/d_b = 2.5$ for all specimens.

2.8.1.2 Splice Development Results

All eight specimens developed their design bar stresses of 100 or 125 ksi exhibiting significant reserve capacity (Table 26). Nonetheless, all specimens except for specimen D5-4 eventually exhibited a failure of the splice rather than rupture of the spliced bars. The bars in specimen D5-4 ruptured. Figure 32 shows the measured load-deflection behavior of all specimens, and the predicted beam behaviors determined based on a Response 2000 (Bentz 2000) section analysis (see Appendix H) that assumes no splice is present. Since the splices did eventually slip, the full ductility of the sections was not achieved. Also shown on Figure 32 are the displacements at which the primary reinforcing steel achieved the design stresses of 100 and 125 ksi. Reasonable reserve capacity beyond these design values is achieved in all cases, particularly for the smaller #5 bars. The improved capacity of the smaller bars is accounted for in the ACI 318 version of Equation 13 by the $\Psi_s = 0.8$. This factor has been removed from the NCHRP 12-60 version of Equation 13 and was not applied in the present work. Spliced beams exhibited good deflection capacity, achieving midspan deflections on the order of L/55 at splice failure. Splice details focus on developing reinforcing bar strength; member ductility is achieved in practice through detailing such as staggering splice locations.

The splice test series is intended as proof tests of the NCHRP 12-60 straight bar tension development length recommendation given by Equation 13. These tests have clearly shown that this recommendation is adequate to develop up to 125 ksi in 15 ksi concrete. The present AASHTO requirements, given in Equation 12, are more conservative than those given by Equation 13 (Figure 30). The AASHTO requirements would have resulted in development lengths 11% and 36% longer for 10 and 15 ksi concrete, respectively. In all cases, the $0.4d_bf_y$ limit to Equation 12 controls the development length. Thus, the present AASHTO requirements also have been demonstrated to be conservative through this test program.

2.8.2 Hook Anchorage

AASHTO LRFD (2007) §5.11.2.4 provides geometric requirements for standard 90° or 180° hooked anchorages of deformed reinforcing bars in tension. The basic development length (l_{hb}) of such standard hooked anchorages for bars having $f_y \leq 60$ ksi is as follows:

$$\ell_{hb} = \frac{38\, d_b}{\sqrt{f'_c}} \geq 8d_b \geq 6.0 \text{ in.} \qquad (\text{ksi units}) \qquad \text{(Eq. 14)}$$

Where:

d_b = bar diameter in inches and
f'_c = concrete strength in ksi.

For bars having a yield strength greater than 60 ksi, Equation 14 is modified by the factor $f_y/60$, effectively scaling the development length in an inverse manner with the bar capacity to be developed. Factors that increase the basic development length are prescribed for cases where lightweight aggregate (adjustment factor = 1.3) or epoxy-coated reinforcing steel (1.2) are used. These factors were not relevant in the present work and were taken as unity. For #11 bars and smaller, provided with sufficient concrete cover, the basic development length may be reduced as follows:

1. For side cover normal to the plane of the hook exceeding 2.5 in. and back cover to the 90° hook extension exceeding 2 in., the basic development length may be factored by 0.7.
2. For hooked bars enclosed by vertical or horizontal ties or stirrups having a spacing not exceeding $3d_b$, the basic development length may be factored by 0.8.

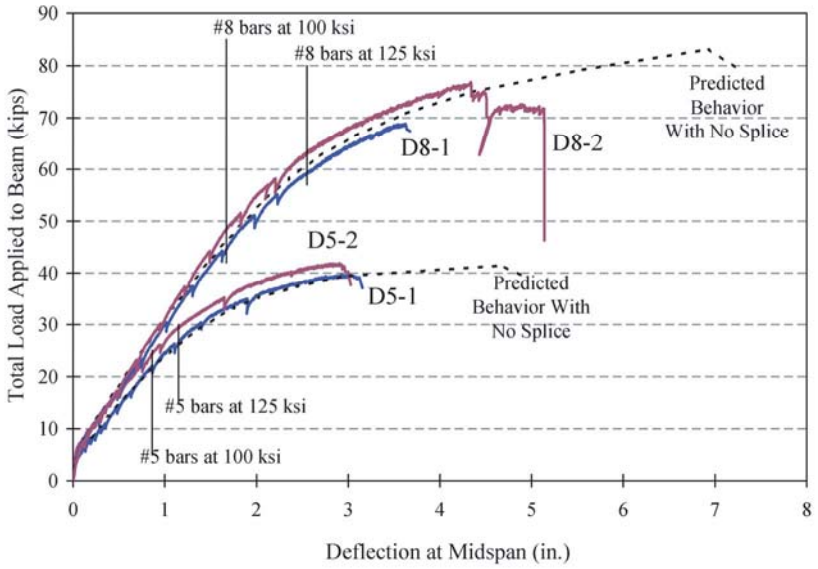

(a) Splice Specimens Having Nominal Concrete Strength, f_c' = 10 ksi

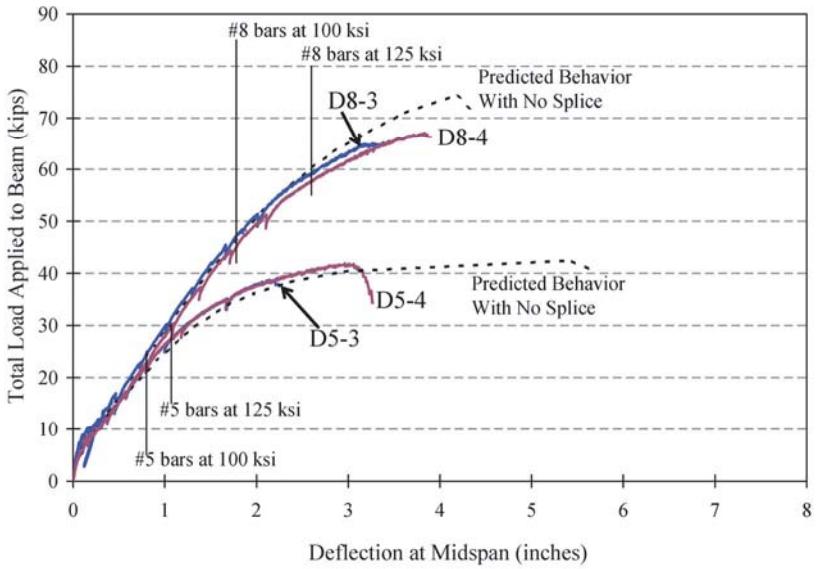

(b) Splice Specimens Having Nominal Concrete Strength, f_c' = 15 ksi

Figure 32. Load-deflection behavior of splice test beams. Deflection at which the stress in the primary reinforcing achieves the intended design value is noted in each case.

Both factors may be applied simultaneously, resulting in a reduction factor of 0.56 for well-confined hook regions with sufficient concrete cover.

2.8.2.1 Hook Anchorage Tests

Eighteen ASTM A1035 hook anchorage specimens were tested. The specimen details shown in Figure 33b and Table 27 include two concrete strengths, nominally 5 and 10 ksi, and three bar sizes: #4, #5, and #8. The #4 bars were provided with standard 180° hooks and are intended to represent (1) the anchorage of stirrups in girder sections where the stirrups are also called upon to serve as interface reinforcement for a cast-in-place deck; or (2) the anchorage of primary reinforcing in cantilever slabs. The #5 and #8 bars were provided with standard 90° hooks and are intended to represent anchorage of these bars where insufficient length is provided to develop a straight bar. This condition may occur in starter bars for piers or abutments, wall piers, or in short flexural members such as pier caps. Specimen labels begin with "H" (for hook) and indicate the bar size followed by the specimen number; a trailing "N" indicates that no confining reinforcement was provided.

All hook development lengths were designed using Equation 14 with all appropriate modifications. In all specimens,

the calculated value of l_{hb} was modified by the selected nominal values of f_y, 100 or 125 ksi (see Table 27), using the factor $f_y/60$. All specimens were provided with sufficient cover to permit the 0.7 reduction factor to be applied. For all specimens having confining reinforcement (all but specimens in Table 27 ending in N), the confinement was adequate to permit the 0.8 reduction factor to be applied. The objective of this limited test series was to serve as a series of proof tests: applying the existing AASHTO hooked bar development length requirements to the higher strength A1035 reinforcing steel. The measured material properties of the hooks and confining steel are given in Table 25. The measured 28-day concrete strength for the specimens having nominal strengths of $f_c' = 5$ and 10 ksi were 6.02 and 9.71 ksi, respectively. Strain gages were applied over the length of hooked embedment (see inset in Figure 35) to determine bar stresses.

The test setup, shown in Figure 33a, was designed to replicate as closely as possible (without a full-scale element test) the stresses in the vicinity of a hook anchorage in tension. The hydraulic ram places the bar in tension and the lever arm reaction to the right of the bar provides the equilibrating compression. In the setup used, the compression reaction is 1.2 times the bar tension, more than sufficient to provide the appropriate reaction force necessary to develop the hook. A short region of the hook was left unbonded as it entered the concrete block (achieved by wrapping the bar in foam pipe insulation) resulting in the development length beginning 3 in. below the concrete surface. The debonded region was provided to (1) mitigate the pullout of a cone of concrete at the concrete surface, which affects the development behavior and slip results; and (2) to provide additional concrete depth (h in Table 27) to mitigate the shear failure of a "cone" of concrete anchored by the hook itself (this was nonetheless observed in Specimens H4-2 and H8-2, as discussed below).

Each bar was anchored using a bolted, in-line mechanical splice anchor with both sides of the splice anchor engaged. All bolts were fully torqued except for the lower two that were provided with only ⅓ and ⅔ of their recommended torque values, respectively. The reduced torque levels were intended (following the test of H5-1, see below) to mitigate failure associated with the stress raisers that this anchorage produces. Although the anchorage performed flawlessly in this arrangement, it is not the subject of this study, nor can any conclusions with respect to its performance be drawn.

2.8.2.2 Hook Anchorage Results

The results in terms of bar stress achieved and the failure mode observed for all 18 specimens are shown in Table 27. All test specimens exceeded their design stresses of 100 or 125 ksi (f_y in Table 27). Indeed, most specimens achieved their ultimate

Table 27. Hook specimen details and test results.

ID	A*	f_c'	f_y†	ℓ_{hd}‡	h*	D*	s_1*	B*	C*	Ultimate	Failure**
	bar size – hook angle	ksi	ksi	in.	in.	in.	in.	bars	in.	ksi	
H4-1N	#4 – 180°	5	100	10	16	none	n.a.	4 #4	#3 @ 6	179	R
H4-4N	#4 – 180°	5	125	12	18	none	n.a.	4 #4	#3 @ 6	177	R
H4-1	#4 – 180°	5	100	8	14	5 #3 @ 1.5	1	4 #4	#3 @ 6	177	R
H4-4	#4 – 180°	5	125	10	16	6 #3 @ 1.5	1	4 #4	#3 @ 6	177	R
H4-2	#4 – 180°	10	100	6††	12	3 #3 @ 1.5	1	4 #4	#3 @ 6	173	C/R
H4-5	#4 – 180°	10	125	8	14	5 #3 @ 1.5	1	4 #4	#3 @ 6	176	R
H5-1N	#5– 90°	5	100	13	19	none	n.a.	4 #5	#3 @ 6	168	R
H5-4N	#5 – 90°	5	125	16	22	none	n.a.	4 #5	#3 @ 6	168	R
H5-1	#5 – 90°	5	100	10	16	5 #3 @ 1.88	1.25	4 #5	#3 @ 6	160	RA
H5-4	#5 – 90°	5	125	13	19	6 #3 @ 1.88	1.25	4 #5	#3 @ 6	168	R
H5-2	#5 – 90°	10	100	8	14	4 #3 @ 1.88	1.25	4 #5	#3 @ 6	167	R
H5-5	#5 – 90°	10	125	9	15	4 #3 @ 1.88	1.25	4 #5	#3 @ 6	168	R
H8-1N	#8 – 90°	5	100	20	26	none	n.a.	4 #8	#3 @ 6	140	TS
H8-4N	#8 – 90°	5	125	25	31	none	n.a.	4 #8	#3 @ 6	140	TS
H8-1	#8 – 90°	5	100	16	22	5 #3 @ 3	2	4 #8	#3 @ 6	153	TS
H8-4	#8 – 90°	5	125	20	26	6#3 @ 3	2	4 #8	#3 @ 6	138	TS
H8-2	#8 – 90°	10	100	12	18	3 #3 @ 3	2	4 #8	#3 @ 6	162	C (no R)
H8-5	#8 – 90°	10	125	15	21	4#3 @ 3	2	4 #8	#3 @ 6	166	R

Notes:
*See Figure 33b.
†Design yield stress to be developed in Equation 14.
‡See Equation 14.
**Failure mechanisms: R = bar rupture; RA = bar rupture affected by bar anchor; C = concrete shear failure; n.a. = not applicable; TS = test stopped prior to failure for safety considerations—in this case, the maximum obtained bar stress is reported.
††Minimum development length.

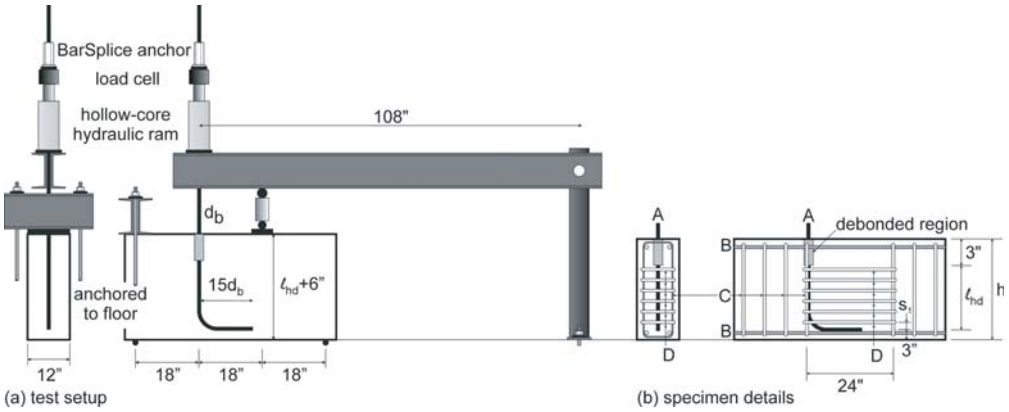

Figure 33. Hook test setup and specimen details.

capacity (f_u in Table 25) as evident by a bar rupture failure in the exposed region of the bar—denoted by "R" in Table 27. All ruptured bars exhibited significant necking and elongation and were unaffected (except H5-1) by the bar anchorage or loading mechanism. Observed rupture stresses agree well with the previously tested material properties (Table 25).

Specimen H5-1 (the first tested) exhibited a bar rupture affected by the installation of the splice anchor used to react the applied load (not actually part of the test). Nonetheless, this specimen still achieved a stress of 160 ksi. A change was made to the splice installation and this failure mode was mitigated for all subsequent tests. Only two of the #8 specimens were tested to bar rupture; the remaining tests were stopped prior to failure at a stress of 140 ksi, which was still greater than the required proof load. The stoppage was done in the interest of laboratory safety (a rupturing #8 A1035 is a significant projectile). In two specimens having very short development lengths, the ultimate failure was a shear "cone" in the concrete (denoted by "C" in Table 27). This failure mode (1) took place at loads that significantly exceeded the required proof loads; (2) occurred at loads very close to those expected to cause bar rupture; and (3) is an artifact of the test specimen and would not be expected in real-world applications. Figure 34 shows an example of such a "C" failure.

Strain profiles demonstrate that the hooks are well developed and transfer stress to the concrete through bond. Figure 35 plots the bar strains with length along the #8 hooks (reported in units of bar diameters (d_b) for the sake of normalization). The uppermost data point on each curve ($d_b = 0$) is obtained from the clip gage mounted a few inches above the concrete specimen. The next data point ($d_b = 3$) is obtained from the strain gage located $3d_b$ into the concrete (see the right-hand inset in Figure 35). As would be expected, these first two strains are similar since little development has yet been engaged. The next data point down is obtained from the strain gage located $5d_b$ from the hook bend and the final data point is $5d_b$ around the bend on the hook itself. The strains at this final location are all very small indicating that the hooked region is not being engaged in tension. The strain gages used were very small (0.25 in. overall length); their installation does not affect the bond stress development in any significant manner. The data in Figure 35 are given at stresses of 60 ksi (yield of mild steel), 100 ksi and 125 ksi (design values for this test), and 140 ksi (maximum value at which data are available for all specimens).

The "slip" of the hook also was measured using displacement transducers that measured the relative movement of the bar as it is "pulled out" of the concrete. Since the slip measurement is obtained over a distance of exposed bar (about 5 in. in most tests), the reported slip is greater than the actual slip due to the elastic, and eventually inelastic, strain present over this unbonded length. Figure 36a shows the slip recorded at stress levels of 60, 100, 125, and 140 ksi. The "ultimate" stress is the slip reported at the maximum stress obtained as given in Table 27.

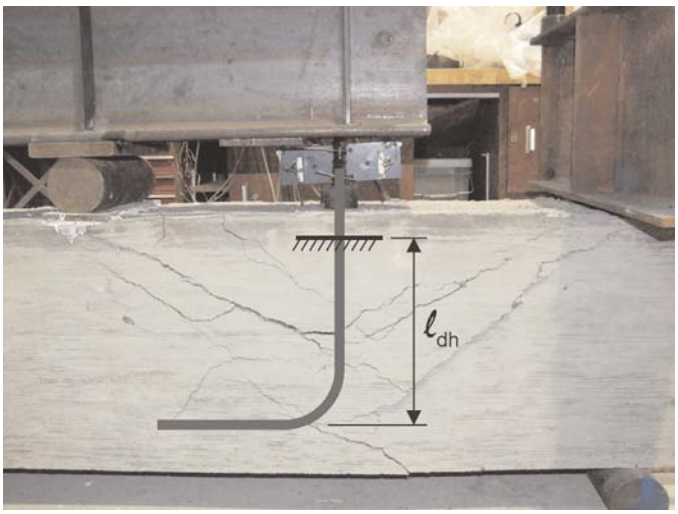

Figure 34. Typical concrete shear failure (Specimen H8-2).

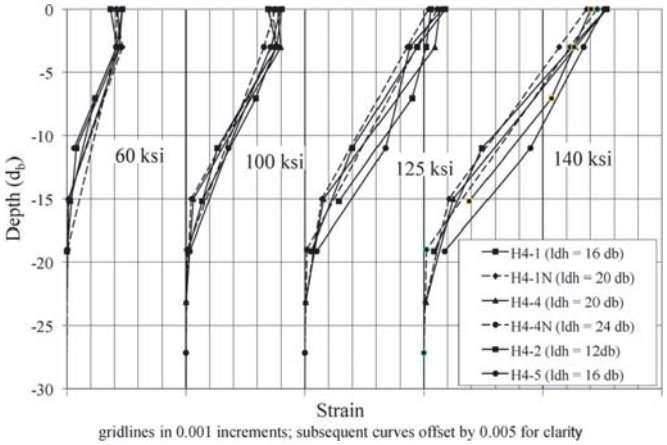

(a) #8 90° hook specimens

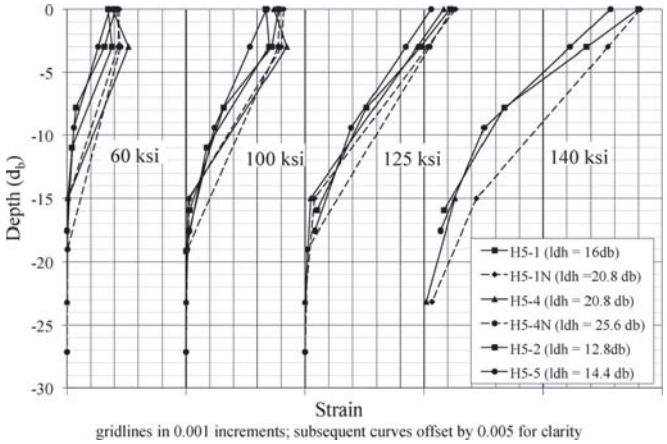

(b) #5 90° hook specimens

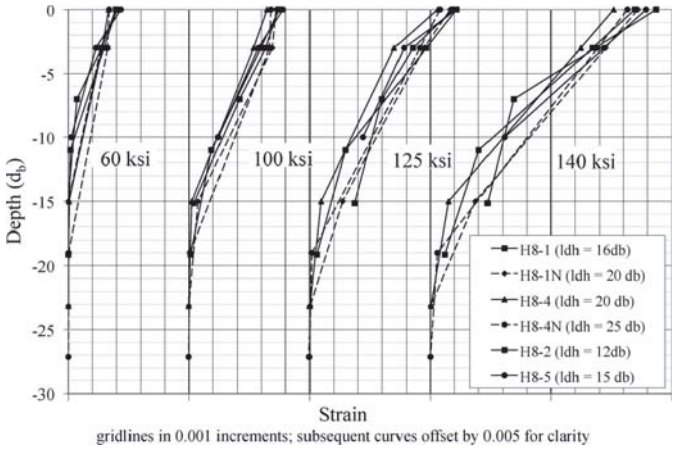

(c) #4 180° hook specimens

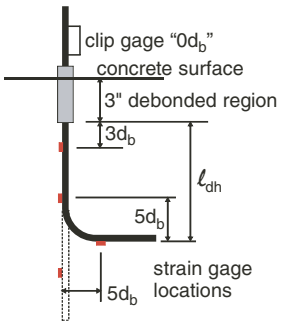

Figure 35. Strains along hook embedment at selected bar stresses.

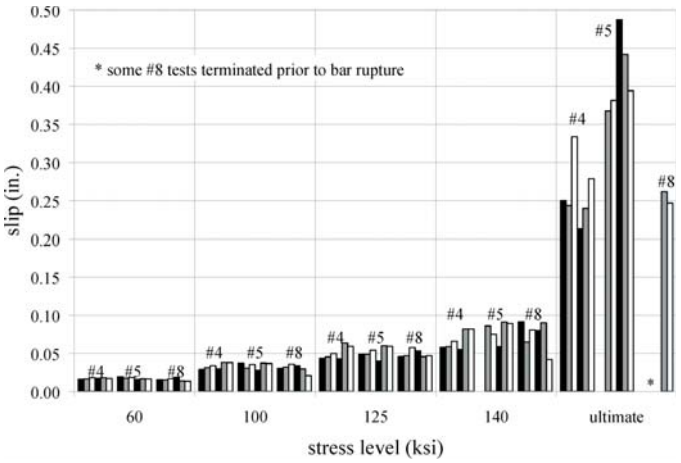

(a) Slip at Different Stress Levels

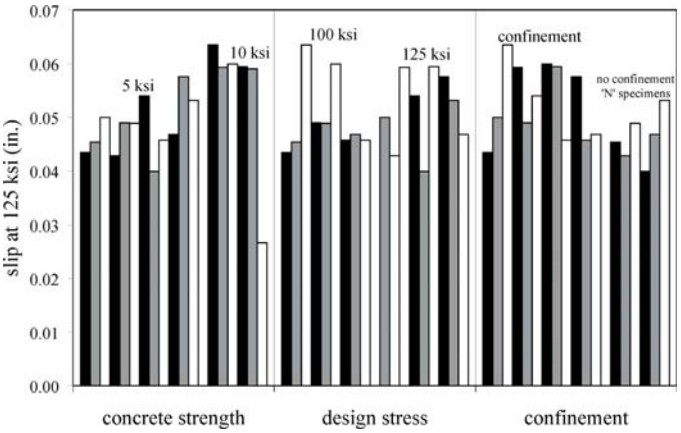

(b) Slip at 125 ksi

Figure 36. Slip of embedded hooks.

Figure 36b shows only the slip values reported at 125 ksi sorted against (1) concrete strength (5 or 10 ksi); (2) design bar stress (100 or 125 ksi); and (3) the presence of confining reinforcement (N specimens had no confining reinforcement).

Conclusions drawn from Figures 35 and 36 include the following:

1. Through the proof loads (100 and 125 ksi), slip is limited and rarely exceeds 0.06 in. Indeed, through stresses of 140 ksi, slip rarely exceeds 0.09 in. and is not affected by bar size, concrete strength, development length, or the presence of confining reinforcement.
2. Slip is not significant until near the ultimate load (greater than 140 ksi). It is noted that in some cases, the large values of slip include the plastic deformation of the reinforcing bar in the gage length over which slip is measured.
3. Slip at 125 ksi is marginally (<0.01 in.) more pronounced for the 10 ksi concrete. This slight increase is attributed to the use of smaller aggregate (see Appendix A) and its effect on mechanical bond.
4. Slip at 125 ksi is unaffected by the development length provided. Hence, there is reserve bond capacity beyond that implicitly assumed by the development length calculation.
5. The specimens having confining steel exhibited marginally (<0.02 in.) greater slip at 125 ksi than those that did not. This observation is counterintuitive although the difference is small and may be attributed to experimental scatter.

The hook test series was intended as proof tests of the present AASHTO hook development requirements given by Equation 14. These tests have shown that the present requirement is adequate to develop up to 125 ksi in 10 ksi concrete in cases where adequate cover and confinement—based on current design requirements—are provided.

2.8.3 Summary and Conclusions

The objective of this portion of the study was to evaluate existing AASHTO requirements in reference to the use of high-strength reinforcement (represented by ASTM A1035) with respect to issues of bar splice development and hooked bar anchorages. Spliced beam straight bar development tests and hooked anchorage pullout tests were performed as proof tests of the current AASHTO requirements as expressed by Equations 12 and 14. The small number of splice beam tests conducted augmented the extensive study by Seliem et al. (2009) and extended the available database to higher strength concrete.

The results demonstrate that the present AASHTO requirements for both straight bar tension development and hooked anchorage tension development may be extended to develop bar stresses of at least 125 ksi for concrete strengths up to 10 ksi provided adequate cover and confinement are provided.

In using higher strength steel, greater bar strain and slip will occur prior to development of the bar. The associated displacement of the bar lugs drives a longitudinal splitting failure beyond that where yield of conventional bars would occur; thus, confining reinforcement is critical in developing higher strength bars. The results of this study and previous work clearly indicate that confining reinforcement, designed in a manner consistent with current practice, should always be used when developing, splicing, or anchoring ASTM A1035 or other high-strength reinforcing steel.

2.9 Serviceability Considerations

A fundamental issue in using A1035 or any other high-strength reinforcing steel is that the stress at service load (f_s; assumed to be on the order of $0.6f_y$) is expected to be greater

than with conventional Grade 60 steel. Consequently, the service load reinforcing strains are greater (i.e., $\varepsilon_s = f_s/E_s$). This larger strain affects deflection and crack widths at service loads. In the following sections, discussion focuses on the behavior at loads corresponding to longitudinal reinforcing bar stresses of 36, 60, and 72 ksi, representing service load levels (i.e., $0.6f_y$) for steel having $f_y = 60$, 100, and 120 ksi, respectively. At these service load stresses, the use of $E_s = 29000$ ksi for all steel grades is acceptable (see Section 1.3.2.1) although experimentally determined R-O curves have nevertheless been used in all cases to calculate stress from measured reinforcing bar strains.

2.9.1 Deflections of Flexural Members

Table 28 summarizes the midspan deflections of all flexural beam specimens (F1 through F6) corresponding to longitudinal bar stresses of 36, 60, and 72 ksi. The experimentally measured deflections include any support settlement but do not include deflection due to self-weight. Also shown in Table 28 are the deflections calculated using both the Branson (Equation 1) and Bischoff (Equation 2) formulations (see Chapter 1) for effective moment of inertia (I_e). In calculating the applied moment (M_a in Equations 1 and 2), the self-weight of the beam is accounted for; thus, the effective moment of inertia is based on the appropriate cracked section for the load level considered.

$$M_a = \frac{Pa}{2} + \frac{wL^2}{8} \qquad \text{(Eq. 15)}$$

Where:

P = total applied load in four-point bending (sum of two point loads);
w = self weight of beam;
L = length of simple span, 240 in. in all cases;
a = length of shear span, 102 in. in all cases.

In the formulations of effective moment of inertia (Equations 1 and 2), the moment to cause cracking is calculated as 80% of the moment corresponding to modulus of rupture.

$$M_{cr} = 0.80\left(\frac{7.5\sqrt{f_c'}I_g}{y}\right) = \frac{6\sqrt{f_c'}I_g}{y}(\text{psi}) \qquad \text{(Eq. 16)}$$

Where:

I_g = moment of inertia of gross concrete section, nominally 4096 in.^{4};
y = neutral axis distance from the tensile face for gross concrete section, nominally 8 in.

The use of the reduced value of M_{cr} accounts for cases where the applied moment (M_a) is only slightly less than the unrestrained M_{cr} (based on $7.5\sqrt{f_c'}$) since factors such as shrinkage and temperature may still cause a section to crack over time (Scanlon and Bischoff 2008).

Table 28. Comparison of experimental and calculated deflections at service load levels.

Beam and Bar Stress	$\rho = A_s/bd$	M_a	Deflection		
			Experimental	Branson	Bischoff
		(kip-in.)	(in.)	(in.)	(in.)
F1 @ 36 ksi	0.012	898	0.582	0.372	0.365
F1 @ 60 ksi	0.012	1318	1.145	0.600	0.590
F1 @ 72 ksi	0.012	1553	1.400	0.723	0.713
F2 @ 36 ksi	0.016	1038	0.527	0.318	0.312
F2 @ 60 ksi	0.016	1726	1.145	0.567	0.561
F2 @ 72 ksi	0.016	2084	1.450	0.695	0.690
F3 @ 36 ksi	0.007	645	0.527	0.269	0.288
F3 @ 60 ksi	0.007	900	0.855	0.478	0.482
F3 @ 72 ksi	0.007	1099	1.182	0.633	0.629
F4 @ 36 ksi	0.016	895	0.625	0.286	0.280
F4 @ 60 ksi	0.016	1405	1.146	0.501	0.492
F4 @ 72 ksi	0.016	1650	1.354	0.601	0.592
F5 @ 36 ksi	0.023	1313	0.688	0.330	0.326
F5 @ 60 ksi	0.023	2096	1.271	0.551	0.547
F5 @ 72 ksi	0.023	2517	1.583	0.669	0.666
F6 @ 36 ksi	0.012	569	0.458	0.156	0.166
F6 @ 60 ksi	0.012	1012	0.938	0.429	0.424
F6 @ 72 ksi	0.012	1242	1.229	0.561	0.552

In the calculation of deflection, the self-weight is neglected since this component of the deflection is also not included in the experimentally determined deflections, against which comparisons are made. For the beams considered, the deflection associated with beam self-weight is approximately 19%, 11%, and 9% of the deflections corresponding to applied load at bar stress levels of 36, 60, and 72 ksi, respectively. The midspan deflections associated with the applied four-point bending are calculated as follows:

$$\Delta = \frac{PL^3}{48E_cI_e}\left(3\left(\frac{a}{L}\right) - 4\left(\frac{a}{L}\right)^3\right) \qquad \text{(Eq. 17)}$$

The Branson and Bischoff formulations yield very similar results for the specimens tested. The correlation between the formulations is not as good for the lower reinforcing ratio of 0.007 (F3). This difference is consistent with the observation that Branson's Equation underestimates short-term deflection for concrete members when the reinforcing ratio is less than approximately 1% (Bischoff 2005). Although both equations are suitable for calculating deflections, the Bischoff approach is based on fundamental mechanics and may therefore be applied for any type of elastic reinforcing material. The Branson formulation is empirical and calibrated for mild steel.

2.9.2 Crack Widths

Extensive crack width data were collected in the flexural test series (F1 to F6). To assess the effects of using higher strength steel, the crack widths corresponding to a variety of stresses in the reinforcing steel were determined and are plotted in Figure 37. Figure 37a provides the average crack width measured at the height of the extreme tension steel from all cracks in the constant moment region. Figure 37b provides the maximum crack width measured in this region. The ratio of maximum to average measured crack widths for all specimens at all stress levels is 1.8, consistent with available guidance for this ratio, which tends to range between 1.5 and 2.0 (CEB-FIP 1993). In all cases, the ratio of maximum to average crack width falls with increasing bar stress. At approximately 36 ksi, this ratio is 1.7, falling to 1.6 at 60 ksi and 1.5 at 72 ksi.

The data shown in Figure 37 clearly show that at all considered service load levels ($f_s < 72$ ksi), average crack widths are all below the present AASHTO de facto limits for Class 1 and Class 2 exposure (0.017 in. and 0.01275 in., respectively; see Section 1.3.7.2). Indeed, with the exception of beam F2, maximum crack widths also fall below the Class 1 threshold through bar stresses of 72 ksi. Crack width is largely unaffected by the reinforcing ratio within the range given. It is noted that all 12-in. wide beams had four bars (#5 or #6) in the lowermost layer; thus, crack control reinforcing would be considered excellent for these beams. Considering the measured crack widths in this experimental study, it appears that the inherent conservativeness in existing equations allows present specifications to be extended to the anticipated higher service level stresses associated with the use of high-strength reinforcing steel.

Using Equation 6 (as discussed in Chapter 1, this equation was derived from the present AASHTO LRFD provisions for crack control given in Equation 5), the expected crack width (w) for a given reinforcing bar strain (ε_s) is calculated. Figures 38a and 38b show the calculated crack width for both Class 1 and 2 exposure conditions, respectively, compared with measured average crack width from specimens F1 to F6. The generally

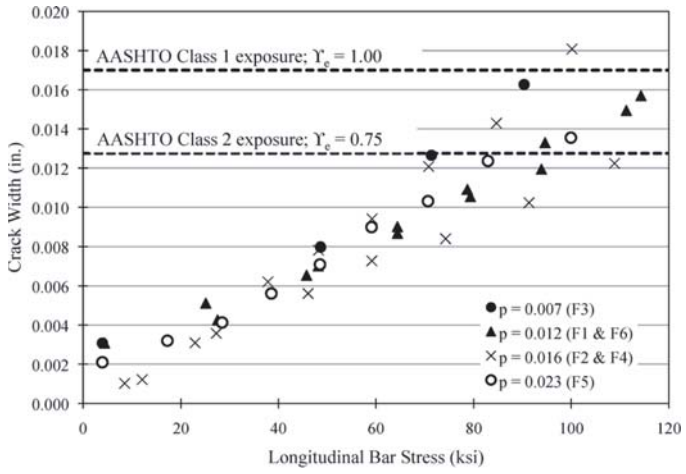

(a) Average Crack Widths

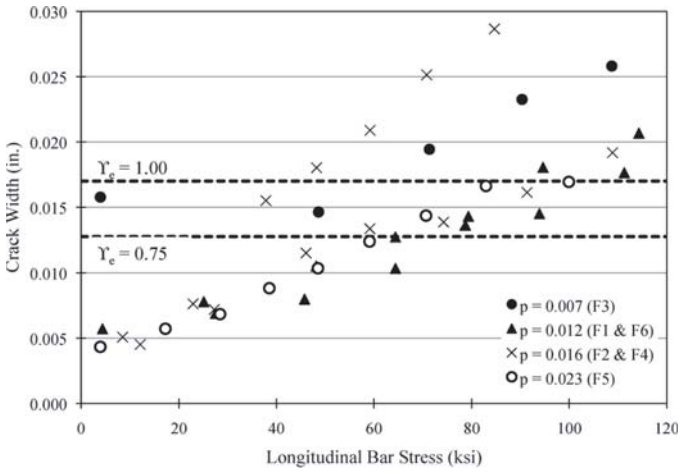

(b) Maximum Crack Widths

Figure 37. Measured crack widths with longitudinal bar reinforcing bar stress for flexural beams.

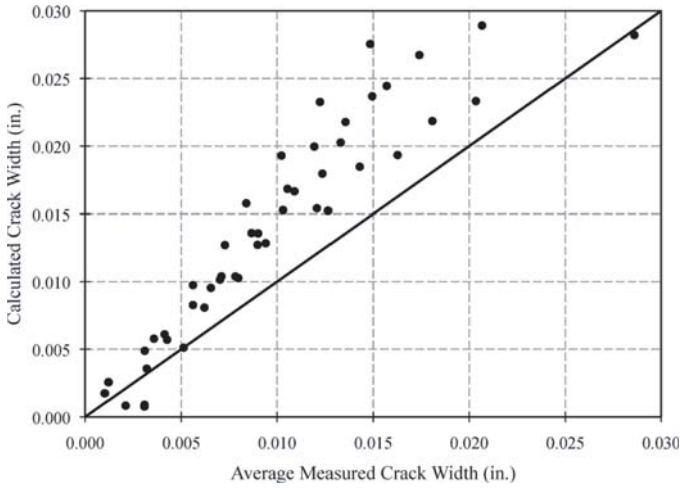

(a) Class 1 Exposure; $\gamma_d = 1.00$

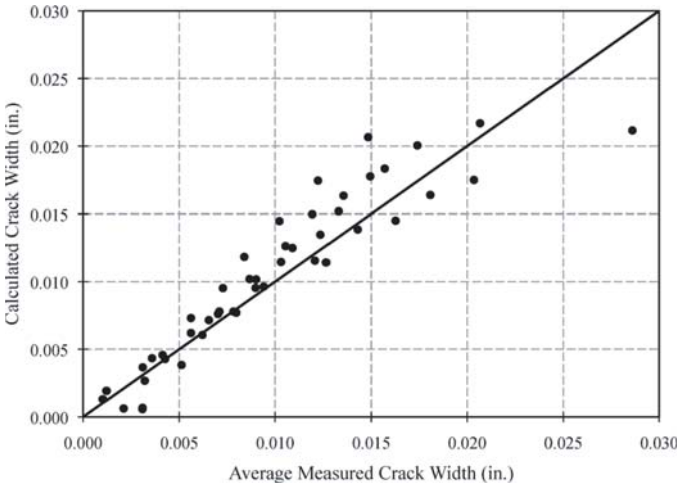

(b) Class 2 Exposure; $\gamma_d = 0.75$

Figure 38. Measured versus calculated crack widths.

conservative nature of existing AASHTO crack control requirements (Equation 5) is evident in Figure 38, supporting the discussion in Section 1.3.7.2.

2.9.3 Summary and Conclusions

The AASHTO LRFD specifications use the Branson formulation for computing an effective moment of inertia used to compute deflection. An alternative approach developed by Bischoff has been demonstrated to yield similar results and is based on fundamental mechanics, rather than being empirically calibrated as is Branson's Equation. Bischoff's approach is also appropriate for any type of elastic reinforcing material.

The average measured crack widths are below the present AASHTO de facto limits for Class 1 and Class 2 exposure. The inherent conservativeness in existing equations allows present specifications to be extended to the anticipated higher service level stresses associated with the use of high-strength reinforcing steel.

CHAPTER 3

Recommendations, Conclusions, and Suggested Research

3.1 Summary of AASHTO LRFD Clauses Having Recommended Changes

The objective of this work was to evaluate existing AASHTO *LRFD Bridge Design Specifications* relevant to the use of high-strength reinforcing steel and grades of reinforcing steel having no discernable yield plateau. The primary deliverable is recommended changes to the AASHTO specifications. The recommended changes were submitted to the project panel in the form of a redline copy of the specifications; this document is not included here. The following provides a summary of the nature of the proposed changes. Specific language is not provided in this report, as this may conflict with eventual AASHTO-adopted language.

In all cases, language was proposed that specifically permits the use of high-strength reinforcing steel with specified yield strengths not greater than 100 ksi when the specific article permits it. This methodology is consistent with the manner by which the AASHTO specifications handle high-strength concrete, allowing its use only when a specific article permits it. LRFD specifications Sections 3, 5, and 9 were identified as having clauses potentially requiring changes. Although considered in its entirety, no potential changes were identified in the AASHTO *LRFD Bridge Construction Specifications.* It is noted that 2009 revisions to §9.2 of the construction specifications permit the use of A1035 reinforcing steel.

3.1.1 Proposed Changes to Section 3 of the LRFD Specifications

Appendix B3 of the specifications was identified as possibly requiring changes. This appendix deals with plastic hinging of columns and references §3.10.9.4.3a, which deals with earthquake forces and design procedures in Seismic Zones 3 and 4. In Section 5, the proposed use of reinforcing steels with specified strengths up to 100 ksi is restricted to Seismic Zone 1 due to lack of research (NCHRP 12-77 did not conduct seismic testing). For this reason, no changes are proposed to the 75-ksi limit for Seismic Zones 3 and 4, and, therefore, no changes are required in Section 3.

3.1.2 Proposed Changes to Section 5 of the LRFD Specifications

Section 5 has the most proposed changes; these are summarized in Table 29. Corresponding changes also are proposed for the commentaries.

3.1.3 Proposed Changes to Section 9 of the LRFD Specifications

Article 9.5.3, Fatigue and Fracture Limit State, states that the fatigue limit state does not need to be investigated for bridge decks in multi-girder applications. Although reinforcing steel having yield not exceeding 100 ksi is proposed to be permitted in bridge decks, no changes to this requirement are recommended for the following reasons: (1) Although the stress levels in higher strength reinforcing bars will be higher, data indicate that the fatigue limit is also higher (proposed changes to §5.5.3.2 address this); (2) in multi-girder applications, research shows that the concrete decks carry load primarily through arching action rather than flexure (see C9.7.2.1, Empirical Design); and (3) bridge deck design tends to be driven by stiffness concerns and, therefore, the increase in reinforcing bar stress associated with the use of high-strength bars will be marginal.

Article 9.5.2, Empirical Design, specifies bar area and maximum spacing, independent of yield strength. Using higher strength reinforcing steel results in a one-for-one bar substitution, which is permitted now regardless of steel strength. Thus, no changes are needed.

The use of higher strength reinforcing steel affects §9.7.3.2, Distribution Reinforcement, as far as the use of such reinforcement in the primary direction will result in a lower required

Table 29. Summary of proposed changes to Section 5 of AASHTO LRFD specifications.

Article	Brief Summary of Changes
5.2 DEFINITIONS	Modified the definition of tension-controlled section by changing "0.005" to "tension-controlled strain limit." Added definition of tension-controlled strain limit.
5.3 NOTATION	Modified the definition of f_y to allow higher yield strengths. Added definitions of ε_{cl} and ε_{tl}; compression- and tension-controlled strain limits, respectively.
5.4.3.1 and C5.4.3.1 Reinforcing Steel, General	Permits the use of reinforcing steel with specified yield strengths up to 100.0 ksi when allowed by specific articles.
5.4.3.2 Reinforcing Steel, Modulus of Elasticity	E_s=29,000 may be used for specified yield strengths up to 100.0 ksi.
5.4.3.3 and C5.4.3.3 Reinforcing Steel, Special Applications	Permits the use of reinforcing steel with specified yield strengths up to 100.0 ksi in Seismic Zone 1.
5.5.3.2 and C5.5.3.2 Fatigue Limit State, Reinforcing Bars	Modifies the fatigue equation for reinforcing bars to allow the equation to be used for specified yield strengths up to 100.0 ksi.
5.5.4.2.1 and C5.5.4.2.1 Resistance Factors, Conventional Construction	Allows the use of reinforcing steel with specified yield strengths up to 100.0 ksi in Seismic Zone 1. Modifies the equation, figure, and commentary. These now use ε_{cl} and ε_{tl}, (compression- and tension-controlled strain limits) in place of 0.002 and 0.005.
5.7 and adds C5.7 DESIGN FOR FLEXURAL AND AXIAL FORCE EFFECTS	Allows the use of reinforcing steel with specified yield strengths up to 100.0 ksi in Seismic Zone 1.
5.7.2.1 and C5.7.2.1 Assumptions for Strength and Extreme Event Limit States	Keeps compression- and tension-controlled strain limits of 0.002 and 0.005 for reinforcing steels with specified yield strengths up to 60.0 and 75.0 ksi, respectively. Provides compression- and tension-controlled strain limits of 0.004 and 0.008 for reinforcing steel with a specified yield strength equal to 100.0 ksi. Linear interpolation is used for reinforcing steels with specified yield strengths between 60.0 or 75.0 ksi and 100.0 ksi. Equations are provided for when f_y may replace f_s or f_s' in 5.7.3.1 and 5.7.3.2.
5.7.3.2.5 Strain Compatibility Approach	Limits the steel stress in a strain compatibility calculation to the specified yield strength.
C5.7.3.3.1 Maximum Reinforcement	Replaces 0.005 with "tension-controlled strain limit."
5.7.3.5 and C5.7.3.5 Moment Redistribution	Adjusts strain limit to allow moment redistribution in structures using reinforcing steel with specified yield strengths up to 100.0 ksi.
C5.7.4.2 and C5.7.4.4. Limits for Reinforcement	Warns that designs should consider that columns using higher strength reinforcing steel may be smaller and have lower axial stiffness.
5.7.4.6 Spirals and Ties	Permits spirals and ties made of reinforcing steel with specified yield strengths up to 100.0 ksi in Seismic Zone 1.
5.8.2.4 and C5.8.2.4 Regions Requiring Transverse Reinforcement 5.8.2.5 and C5.8.2.5 Minimum Transverse Reinforcement	Permits transverse reinforcement with specified yield strengths up to 100.0 ksi in applications with flexural shear without torsion.
C5.8.2.7 Maximum Spacing of Transverse Reinforcement	Indicates that spacing requirements have been verified for transverse reinforcement with specified yield strengths up to 100.0 ksi in applications of shear without torsion.
5.8.2.8 and C5.8.2.8 Design and Detailing Requirements.	Permits transverse reinforcement with specified yield strengths up to 100.0 ksi in applications with flexural shear without torsion.

Table 29. (Continued).

Article	Brief Summary of Changes
C5.8.3.3 Nominal Shear Resistance	Identifies that transverse reinforcement with specified yield strengths up to 100.0 ksi may be used in applications with flexural shear without torsion.
5.8.3.5 Longitudinal Reinforcement	Permits longitudinal reinforcing steel with specified yield strengths up to 100.0 ksi.
5.8.4.1 Interface Shear Transfer, General	Clarifies that f_y is limited to 60.0 ksi in Equation 5.8.4.1.3.
5.10.2 and C5.10.2 Hooks and Bends	Permits hooks with specified yield strengths up to 100.0 ksi with transverse confining steel in Seismic Zone 1.
5.10.6.1 and C5.10.6.1 Transverse Reinforcement for Compression Members, General	Permits spirals with specified yield strengths up to 100.0 ksi in Seismic Zone 1.
5.10.11.1 Provisions for Seismic Design, General	Permits the use of reinforcing steel with specified yield strengths up to 100.0 ksi in Seismic Zone 1.
5.11.1.1 and C5.11.1.1 DEVELOPMENT AND SPLICES OF REINFORCEMENT, Basic Requirements 5.11.2 and C5.11.2 Development of Reinforcement	Permits the development length equations to be used for reinforcing steel with specified yield strengths up to 100.0 ksi.
5.11.2.1 Deformed Bar and Wire in Tension	Requires transverse confining steel for development of reinforcing steel with specified yield strengths greater than 75.0 ksi.
5.11.5 and adds C5.11.5 Splices of Bar Reinforcement 5.11.5.3 and C5.11.5.3 Splices of Reinforcement in Tension	Permits splices in reinforcing steel with specified yield strengths up to 100.0 ksi and requires transverse confining steel.
Table 5.11.5.3.1-1 Classes of Tension Lap Splices	Requires transverse confining steel in splices of reinforcing steel with specified yield strengths exceeding 75.0 ksi.

area of reinforcement in the secondary direction. However, spacing requirements of §5.7.3.4 will limit how much the area of the primary reinforcement can be reduced, and thus, also limits the permitted reduction in the secondary reinforcement. No change is proposed.

3.2 Conclusions

Based on the presented experimental and analytical studies, the following conclusions are drawn. The conclusions are grouped based on the main tasks of this work.

3.2.1 Yield Strength

A critical objective of the present work was to identify an appropriate steel strength and/or behavior model to adequately capture the behavior of high-strength reinforcing steel while respecting the tenets of design and the needs of the designer. A value of yield strength, f_y, not exceeding 100 ksi was found to be permissible without requiring significant changes to the specifications.

3.2.2 Flexure

The current specifications design methodology for flexure, that is, a simple plane sections analysis using stress block factors to model concrete behavior and an elastic-perfectly plastic steel behavior (having $E_s = 29{,}000$ ksi), is shown to be appropriate for values of $f_y \leq 100$ ksi. To ensure ductility, steel strains corresponding to tension- and compression-controlled limits (defined in §5.7.2.1 of specifications) are recommended as follows:

	Current §5.7.2.1; No Recommended Changes	Recommended Limits for High-Strength Reinforcement
	$f_y \leq 60$ ksi	$f_y = 100$ ksi
Tension-Controlled Section	$\varepsilon_t \geq 0.005$	$\varepsilon_t \geq 0.008$
Compression-Controlled Section	$\varepsilon_t \leq 0.002$	$\varepsilon_t \leq 0.004$
	Values may be interpolated between limits.	

These strain limits were developed through a rigorous analytical study of 286 cases, which included seven different grades of reinforcing steel, three concrete strengths, and multiple section geometries. Six large-scale beam specimens reinforced with A1035 reinforcing steel confirmed the appropriateness of the proposed tension- and compression-controlled limits. All beam specimens met and exceeded their designed-for strength and ductility criteria and exhibited predictable behavior and performance similar to beams having conventional reinforcing steel.

3.2.3 Fatigue

Two large-scale proof tests conducted as part of this study and a review of available published data demonstrate that presently accepted values for the fatigue or "endurance" limit for reinforcing steel are applicable, and likely conservative, when applied to higher strength bars. Additionally, it is shown that fatigue considerations will rarely affect the design of typical reinforced-concrete members having $f_y \leq 100$ ksi.

3.2.4 Shear

Five large–scale, reinforced-concrete beams and four AASHTO Type I prestressed girders were tested to evaluate the performance of high-strength A1035 steel as shear reinforcement in comparison to that of the commonly used A615 steel. Test specimens were designed using the specifications' approach of summing concrete and steel contributions to shear resistance (i.e., $V_c + V_s$). All beams exhibited good performance with little difference noted between the behavior of spans reinforced with A1035 or A615 transverse steel. The use of current specifications procedures for calculating shear capacity were found to be acceptable for values of shear reinforcement yield $f_y \leq 100$ ksi.

3.2.5 Shear Friction

A series of eight direct push-off (shear proof) tests of "cold construction joint" interfaces reinforced with either A1035 or A615 bars demonstrated that current specifications requirements for such joints are adequate. Significantly, the restriction that f_y be limited to 60 ksi when calculating shear friction capacity must be maintained regardless of the reinforcing steel used. This limit is, in fact, calibrated to limit strain (and, therefore, interface crack opening) to ensure adequate aggregate interlock capacity across the interface and is, hence, a function of steel modulus rather than strength. As noted, steel modulus does not vary with reinforcing bar grade.

3.2.6 Compression

Analytical parametric studies were performed to examine behavior of columns reinforced with A1035 longitudinal and transverse reinforcement. Results indicate the current specifications requirements for both longitudinal and transverse reinforcement design in compression members are applicable for $f_y \leq 100$ ksi.

3.2.7 Bond and Development

The applicability of current specification requirements for straight bar and hooked bar development lengths was confirmed through a series of spliced-bar beam tests and pull-out tests, respectively. "Proof test" spliced-bar beam specimens, having development lengths that were shorter than those required by the present specifications equations (with all appropriate reduction factors applied), were tested. All developed bar stresses exceeding f_y and approaching the ultimate bar capacity, f_u, prior to the splice slipping and in one case bar fracture. Tests of hooked bar anchorage resulted in bar rupture outside of the anchorage region with very little slip clearly indicating the efficacy of the hooked bar development requirements in the specifications. Significantly, it is recommended that development, splice, and anchorage regions be provided with cover and confining reinforcement—based on current design requirements—when high-strength bars are used. Existing equations for development where no confinement is present are demonstrated to be unconservative. The presence of confining reinforcement effectively mitigates potential splitting failures and results in suitably conservative development, splice, and anchorage capacities.

3.2.8 Serviceability—Deflections and Crack Widths

A fundamental issue in using A1035 or any other high-strength reinforcing steel is that the stress at service load (f_s; assumed to be on the order of $0.6f_y$) is expected to be greater than when conventional Grade 60 steel is used. Consequently, the service-load reinforcing strains (i.e., $\varepsilon_s = f_s/E_s$) are greater than those for conventional Grade 60 steel. The large strains affect deflection and crack widths at service loads. Based on the results of the flexural tests conducted in this study, deflections and crack widths at service load levels were evaluated. Both metrics of serviceability were found to be within presently accepted limits and were predictable using current specifications provisions. A limitation on service-level stresses of $f_s \leq 60$ ksi is recommended; this is consistent with the recommendation that $f_y \leq 100$ ksi.

3.3 Recommended Research

The following topics associated with the adoption of high-strength reinforcing steel and steel grades having no discernable yield plateau have been identified as requiring further study.

3.3.1 Application in Seismic Zones 2, 3, and 4

The present study did not address seismic applications and is, therefore, limited in its application to Seismic Zone 1. In bridge structures, the seismic effects on single- and multiple-column piers are most significant. The design of these elements would potentially benefit from the use of higher strength re-

inforcing by both reducing element size and congestion of reinforcement.

3.3.2 Fatigue

Limited available data indicate that the fatigue limit of higher strength, and particularly micro-composite alloy steel, may be markedly improved over that of conventional black steel. A study to establish reliable S-N relationships for different grades of reinforcing steel is recommended. Such a study must consider full-section bars (not coupons) and include a range of bar sizes.

3.3.3 Shear Friction

As discussed in Section 2.6 and in Zeno (2009), the basis for current shear friction design methodology is entirely empirical and does not represent the actual observed behavior. While the current design approach is calibrated for the use of steel having yield strength less than 60 ksi, it is shown to be inadequate for other cases (both higher and lower yield strengths). It is recommended that an extensive study be undertaken to establish a more rational design basis for establishing shear friction capacity. Such a study will also support the understanding of shear capacity in general.

3.3.4 Moment Redistribution

Analytical formulations were used to establish the strain limit for which negative moments at the internal supports of continuous beams can be redistributed. This strain limit needs to be verified experimentally by testing continuous beams.

3.3.5 Control of Flexural Cracking and Corrosion

The current provisions in the AASHTO specifications for maximum spacing of reinforcement for Class 1 exposure are based on an assumed crack width of 0.017 in. A Class 2 exposure corresponds with a crack width of 0.013 in. At the same time, there appears to be little or no correlation between crack width and corrosion. The current equation for maximum spacing requires that the tensile stress in steel reinforcement at the service limit state be calculated. For a beam, this is relatively simple. However, for a bridge deck, it is more complicated because of arching action and two-dimensional load distribution. Research is needed to address the issue of control of cracking by distribution of reinforcement and its impact on corrosion of reinforcement. The research should include all types and grades of corrosion-resistant reinforcement.

References

AASHTO, 2009. *MP 18M/MP18-09 Standard Specification for Uncoated, Corrosion-Resistant, Deformed and Plain Alloy, Billet-Steel Bars for Concrete Reinforcement and Dowels,* American Association of State Highway and Transportation Officials, Washington, D.C.

AASHTO, 2007. *LRFD Bridge Design Specifications,* 4th edition and 2008–2009 interims, American Association of State Highway and Transportation Officials, Washington, D.C.

AASHTO, 2004. *LRFD Construction Specifications,* 2nd edition and 2006–2008 revisions, American Association of State Highway and Transportation Officials, Washington, D.C.

ACI Committee 224, 2001. *ACI 224R-01 Control of Cracking in Concrete Structures,* American Concrete Institute, Farmington Hills, MI, 46 pp.

ACI Committee 318, 2008. *ACI 318-08/ACI 318R-08 Building Code Requirements for Reinforced Concrete and Commentary,* American Concrete Institute, Farmington Hills, MI.

ACI Committee 363, 1992. *ACI 363R-92 State of the Art Report on High Strength Concrete,* American Concrete Institute, Farmington Hills, MI, 55 pp.

ACI Committee 408, 2003. *ACI 408R-03 Bond and Development of Straight Reinforcing Bars in Tension,* American Concrete Institute, Farmington Hills, MI, 49 pp.

AMEC Earth and Environmental, 2006. *Comparative Performance of MMFX Microcomposite Reinforcing Steel and Other Types of Steel with Respect to Corrosion Resistance and Service Life Prediction in Reinforced Concrete Structures,* AMEC, Burnaby, BC.

Ahlborn, T. and DenHartigh, T., 2002. "A Comparative Bond Study of MMFX Reinforcing Steel in Concrete," *Michigan Tech Report CSD-2002-03,* July 2002.

Ahmed, S.H. and Shah, S.P., 1982. "Stress-Strain Curves of Concrete Confined by Spiral Reinforcement," *ACI Journal,* Vol. 79, No. 6, pp 484–490.

Al-Shaikh, A.H. and Al-Zaid, R.Z. 1993. "Effect of Reinforcement Ratio on the Effective Moment of Inertia of Reinforced Concrete Beams," *ACI Structural Journal,* Vol. 90, No. 2, pp 144–149.

Al-Zaid, R.Z., Al-Shaikh, A.H. and Abu-Hussein, M.M., 1991. "Effect of Loading Type on the Effective Moment of Inertia of Reinforced Concrete Beams," *ACI Structural Journal,* Vol. 88, No. 2, pp 184–190.

ASTM, 2009. *ASTM A615-09 Standard Specification for Deformed and Plain Carbon-Steel for Concrete Reinforcement,* ASTM International, Conshohocken, PA.

ASTM, 2009. *ASTM A706-09 Standard Specification for Low-Alloy Steel Deformed and Plain Bars for Concrete Reinforcement,* ASTM International, Conshohocken, PA.

ASTM, 2009. *ASTM A955-09 Standard Specification for Deformed and Plain Stainless-Steel Bars for Concrete Reinforcement,* ASTM International, Conshohocken, PA.

ASTM, 2009. *ASTM A1035-09 Standard Specification for Deformed and Plain, Low-Carbon, Chromium, Steel Bars for Concrete Reinforcement,* ASTM International, Conshohocken, PA.

ASTM, 2009. *ASTM E8-09 Standard Test Methods for Tension Testing of Metallic Materials,* ASTM International, Conshohocken, PA.

ASTM, 2007. *ASTM A82-07 Standard Specification for Steel Wire, Plain, for Concrete Reinforcement,* ASTM International, Conshohocken, PA.

ASTM, 2007. *ASTM A496-07 Standard Specification for Steel Wire, Deformed, for Concrete Reinforcement,* ASTM International, Conshohocken, PA.

Barker, R.M. and Puckett, J.A., 2007. *Design of Highway Bridges an LRFD Approach,* 2nd edition, Wiley-Interscience, New York, 1010 pp.

Beeby, A.W., 1983. "Cracking, Cover and Corrosion of Reinforcement," *Concrete International: Design and Construction,* Vol. 5, No. 2, pp 35–40.

Bentz, E.C., 2000. *Response 2000,* http://www.ecf.utoronto.ca/~bentz/home.shtml, accessed April 6, 2010.

Birkeland, P.W., and H.W. Birkeland, 1966. "Connections in Precast Concrete Construction," *Journal of the American Concrete Institute,* Vol. 63, No. 3, pp 345–368.

Bischoff, P.H., 2005. "Reevaluation of Deflection Prediction for Concrete Beams Reinforced with Steel and Fiber Reinforced Polymer Bars," *Journal of Structural Engineering,* ASCE, May 2005, pp 752–767.

Bischoff, P. and Paixao, R., 2004. "Tension Stiffening and Cracking of Concrete Reinforced with GFRP Bars," *Canadian Journal of Civil Engineering,* Vol. 31, No. 4, pp 579–588.

Bjerkeli, L., Tomaszewicz, A., and Jensen, J.J., 1990. "Deformation Properties and Ductility of High-Strength Concrete," *ACI SP-121 - High Strength Concrete,* pp 215–238.

Branson, D.E., 1963. *Instantaneous and Time-Dependent Deflections of Simple and Continuous Reinforced Concrete Beams,* Research Report No. 7, Alabama Highway Department, Montgomery, AL, August 1963, 94 pp.

Brown, V. and Bartholomew, C., 1996. "Long-Term Deflections of GFRP-Reinforced Concrete Beams." *Fiber Composites in Infrastructure, Proc. of the First International Conference on Composites in Infrastructure.* Tucson, AZ.

Carey, S.A. and Harries, K.A., 2005. "Axial Behavior and Modeling of Small-, Medium- and Large-Scale Circular Sections Confined with CFRP Jackets," *ACI Structures Journal,* Vol. 102, No. 4, pp 596–604.

CEB-FIP, 1993. *CEB-FIP Model Code (MC-90),* Comité Euro-International du Béton (CEB), Thomas Telford Service Ltd., London, England.

Ciancone, G.G., Michael, A.P., and Hamilton III, H.R., 2008. "Behavior of Standard Hook Anchorage with Corrosion Resistant Reinforcement," *Technical Report FDOT No. BD 545-40,* June 2008.

Clemena and Virmani, 2004. "Comparing the Chloride Resistances of Reinforcing Bars," *Concrete International,* November 2004, pp 39–49.

Comité Euro-International du Béton (CEB), 1990. *CEB-FIP Model Code 1990: CEB Bulletin d'Information 213–214,* Thomas Telford Service Ltd., London, England.

Corley, W.G., Hanson, J.M., and Helgason, T., 1978. "Design of Reinforced Concrete for Fatigue," *Journal of the Structural Division,* ASCE, Vol. 14, No. ST6, pp 921–932.

Creazza, G. and Russo, S., 2001. "Crack Width Evaluation in FRP Reinforced Concrete Members," *Materials and Structures,* Vol. 34, No. 2, pp 119–125.

Cusson, D. and Paultre, P., 1994. "High-Strength Concrete Columns Confined with Rectangular Ties," *Journal of Structural Engineering,* Vol. 120, No. 3, pp 783–804.

Darwin, Browning, Nguyen, and Locke, 2002. "Mechanical and Corrosion Properties Testing of a High-Strength, High-Chromium Reinforcing Steel for Concrete," Report SD2001-05-F, South Dakota DOT.

DeJong, S.J., and MacDougall, C., 2006. "Fatigue Behaviour of MMFX Corrosion-Resistant Reinforcing Steel," *Proceedings of the 7th International Conference on Short and Medium Span Bridges,* Montreal, Canada.

DeJong, S.J., 2005. "Fatigue of Corrosion Resistant Reinforcing Steels," MS thesis, Queen's University.

de V Batchelor, B., Hewitt, B.E., and Csagoly, P.F., 1978. "Investigation of the Fatigue Strength of Deck Slabs of Composite Steel/Concrete Bridges," *Transportation Research Record 644,* Transportation Research Board, Washington, D.C.

Dolan, C.W., 1989. "Prestressed Concrete Using Kevlar Reinforced Tendons," PhD thesis, Cornell University.

El-Hacha, R., El-Agroudy, H., and Rizkalla, S., 2006. "Bond Characteristics of High-Strength Steel Reinforcement," *ACI Structural Journal,* Vol. 103, No. 6, Nov-Dec 2006, pp 771–782.

El-Hacha, R. and Rizkalla, S., 2002. "Fundamental Material Properties of MMFX Steel Rebars," Research Report: RD-02/04, North Carolina State University, July 2002, 62 pp.

Fang, K.I., 1985. "Behavior of Ontario-Type Bridge Decks on Steel Girders," PhD dissertation, University of Texas at Austin.

Fikry, A.M. and Thomas, C., 1998. "Development of a Model for the Effective Moment of Inertia of One-Way Reinforced Concrete Elements," *ACI Structural Journal,* Vol. 95, No. 4, pp 444–455.

Florida DOT, 2002. *Investigation into the Structural Performance of MMFX Reinforcing Bars.*

Frosch, R.J., 1999. "Another Look at Cracking and Crack Control in Reinforced Concrete," *ACI Structural Journal,* Vol. 96, No. 3, pp 437–442.

Frosch, R.J., 2001. "Flexural Crack Control in Reinforced Concrete," *ACI SP204: Design and Construction Practices to Mitigate Cracking,* American Concrete Institute, pp 135–154.

Gao, D., Benmokrane, B., and Masmoudi, R., 1998. *A Calculating Method of Flexural Properties of FRP-Reinforced Concrete Beam: Part 1: Crack Width and Deflection,* University of Sherbrooke, Quebec, Canada.

Gergely, P. and Lutz, L.A., 1968. "Maximum Crack Width in Reinforced Concrete Flexural Members," *ACI SP20: Causes, Mechanism, and Control of Cracking in Concrete,* American Concrete Institute, pp 87–117.

Ghali, A., 1993. "Deflection of Reinforced Concrete Members: A Critical Review," *ACI Structural Journal,* Vol. 90, No. 4, pp 364–373.

Gilbert, R.I., 1999. "Flexural Crack Control for Concrete Beams and Slabs: An Evaluation of Design Procedures," *Proceedings of the 16th Australasian Conference on the Mechanics of Structures and Materials,* Sydney, Australia, pp 175–180.

Gilbert, R.I., 2006. "Discussion of 'Re-Evaluation of Deflection Prediction for Concrete Beams Reinforced with Steel and FRP Bars' by Peter H. Bischoff," *Journal of Structural Engineering,* ASCE, Vol. 132, No. 8, pp 1328–1330.

Grossman, J.S., 1981. "Simplified Computations for Effective Moment of Inertia Ie and Minimum Thickness to Avoid Deflection Computations," *ACI Journal*, Vol. 78, No. 6, pp 423–439.

Halvorsen, G.T., 1987. "Code Requirements for Crack Control," *ACI SP-104: Concrete and Concrete Construction,* Farmington Hills, MI, pp 275–322.

Hanson, N.W., 1960. "Precast-Prestressed Concrete Bridges: Horizontal Shear Connections," *Journal PCA Research and Development Laboratories,* Vol. 2, No. 2, pp 38–58.

Harries, K.A., Zorn, A., Aidoo, J., and Quattlebaum, J., 2006. "Deterioration of FRP-to-Concrete Bond Under Fatigue Loading," *Advances in Structural Engineering,* Special Issue on Bond Behaviour of FRP in Structures, Vol. 9, No. 6, pp 779–789.

Hartt, Powers, Leroux, and Lysogorski, 2004. "A Critical Literature Review of High-Performance Corrosion Reinforcements in Concrete Bridge Applications," FHWA-HRT Report 04-093.

Hassan, T.K., Seliem, H.M., Dwairi, H., Rizkalla, S.H., and Zia, P., 2008. "Shear Behavior of Large Concrete Beams Reinforced with High-Strength Steel," *ACI Structural Journal,* Vol. 105, No. 2, pp 173–179.

Helgason, T., Hanson, J.M., Somes, N.F., Corley, W.G., and Hognestad, E., 1976. *NCHRP Report 164: Fatigue Strength of High-Yield Reinforcing Bars,* Transportation Research Board, Washington, D.C.

Hill, C., Chiaw, C.C., and Harik, I.E., 2003. "Reinforcement Alternatives for Concrete Bridge Decks," Report KTC-03-19/SPR-215-00-1F, July 2003.

Holowka, M., Dorton, R.A., and Csagoly, P.F., 1980. *Punching Shear Strength of Restrained Circular Slabs,* Ontario Ministry of Transportation.

Imbsen Software Systems, 2007. *XTRACT V3.0.8,* http://www.imbsen.com/xtract.htm, accessed November 11, 2007.

Kahn, L.F. and Mitchell, A.D., 2002. "Shear Friction Tests with High Strength Concrete," *ACI Structural Journal,* Vol. 99, No. 1, pp 98–103.

Khader, A., 2002. "Evaluation of MMFX Corrosion-Resistant Steel Dowel Bars in Concrete Pavements," Report WI-07-03, Wisconsin DOT.

Kokubu, M. and Okamura, H., 1965. *Fundamental Study on Fatigue Behavior of Reinforced Concrete Beams Using High Strength Deformed Bars,* Japan Society of Civil Engineers (Tokyo), No. 122, Oct 1965, pp l–28.

Kuchma, D.A., Kim, K.S., Kim, S.H., Sun, S., and Hawkins, N.M., 2005. "NCHRP Project 12-61: Simplified Shear Design of Structural Concrete Members," *Proceedings of the 6th International Bridge Engineering Conference,* July 17–20, 2005. Transportation Research Record CD 11-S, Washington, D.C., pp 129–142.

Lash, S.D., 1969. "Can High-Strength Reinforcement be Used for Highway Bridges?" *ACI SP23: First International Symposium on Concrete Bridge Design,* American Concrete Institute, pp 283–299.

Loov, R.E. and Patnaik, A.K., 1994. "Horizontal Shear Strength of Composite Concrete Beams with a Rough Interface," *PCI Journal,* Vol. 39, No. 1, pp 48–69.

MacGregor, J.G., Jhamb, I.C., and Nuttall, N., 1971. "Fatigue Strength of Hot-Rolled Reinforcing Bars," *ACI Journal Proceedings,* American Concrete Institute, Vol. 68, No. 3, pp 169–179.

Mander, J.B., Priestley, M.J.N., and Park, R., 1988. "Observed Stress-Strain Behavior of Confined Concrete," *Journal of Structural Engineering,* ASCE, Vol. 114, No. 8, pp 1827–1849.

Malhas, F.A., 2002. *Preliminary Experimental Investigation of the Flexural Behavior of Reinforced Concrete Beams Using MMFX Steel,* University of North Florida, July 2002.

Mallet, O., 1991. *Fatigue of Reinforced Concrete,* HMSO, London.

Mancio, Carlos, Zhang, Harvey, and Monteiro, 2007. *Laboratory Evaluation of Corrosion Resistance of Steel Dowels in Concrete Pavements,* report to Caltrans.

Martinez, S., Nilson, A.H., and Slate, F.O., 1982. *Spirally Reinforced High Strength Concrete Columns,* Cornell University Department of Structural Engineering Research Report No. 82-10, 255 pp.

Masmoudi, R., Thériault, M., and Benmokrane, B., 1998. "Flexural Behavior of Concrete Beams Reinforced with Deformed Fiber Reinforced Plastic Reinforcing Rods," *ACI Structural Journal,* Vol. 95, No. 6, pp 665–676.

Mast, R.F., 1992. "Unified Design Provisions for Reinforced and Prestressed Concrete Flexural and Compression Members," *ACI Structural Journal,* Vol. 89, No. 2, March-April 1992, pp 185–199.

Mast, R.F., 2006. Personal Correspondence.

Mast, R.F., Dawood, M., Rizkalla, S.M. and Zia, P., 2008. "Flexural Strength Design of Concrete Beams Reinforced with High-Strength Steel Bars," *ACI Structural Journal,* Vol. 105, No. 4, pp 570–577.

McNally, M.M., 2003. "MMFX Rebar Evaluation for I-95 Service Road Bridge 1-712-B," MS thesis, University of Delaware.

Michael, A., 2004. *Tensile Testing of Mechanical Bar Splices for MMFX Steel,* Florida DOT, February 2004.

Moss, D.S., 1980. "Axial Fatigue of High Yield Reinforcing Bars in Air," Transport and Road Research Laboratory Report SR622.

Moss, D.S., 1982. "Bending Fatigue of High-Yield Reinforcing Bars in Concrete," *TRRL Supplementary Rep. 748,* Transport and Road Research Laboratory, Crowthome, UK.

Muguruma, H., Nishiyama, M., Watanabe, F., and Tanaka, H., 1991. "Ductile Behavior of High Strength Concrete Columns Confined by High Strength Transverse Reinforcement," *ACI SP-128 - Evaluation and Rehabilitation of Concrete Structures and Innovations in Design,* pp 877–891.

Muguruma, H. and Watanabe, F., 1990. "Ductility Improvement of High Strength Concrete Columns with Lateral Confinement," *ACI SP-121 - High Strength Concrete,* pp 47–60.

Murashev, V.I., 1940. *Theory of Appearance and Opening of Cracks, Computation of Rigidity of Reinforced Concrete Members,* Stroitelnaya Promishlenost, Moscow, Vol. 11.

Nagashima, T., Sugano, S., Kimura, H., and Ichikawa, A., 1992. "Monotonic Axial Compression Test on Ultrahigh Strength Concrete Tied Columns," *Proceedings of the Tenth World Conference on Earthquake Engineering,* Madrid, pp 2983–2988.

Nawy, E.G., 1968. "Crack Control in Reinforced Concrete Structures," *Journal of the American Concrete Institute,* Farmington Hills, MI, Vol. 65, October 1968, pp 825–838.

Nawy, E.G. and Neuwerth, G.E., 1977. "Fiberglass Reinforced Concrete Slabs and Beams," *ASCE Journal of the Structural Division,* Vol. 103, No. 2, pp 421–440.

Neville, A.M., 1975. *Properties of Concrete,* 2nd edition, Pitman.

Nishiyama, M., Fukushima, I., Watanabe, F., and Muguruma, H., 1993. "Axial Loading Tests on High Strength Concrete Prisms Confined by Ordinary and High Strength Steel," *Proceedings of the Symposium on High Strength Concrete,* Norway, pp 322–329.

Ospina, C.E. and Bakis, C.E., 2007. "Indirect Flexural Crack Control of Concrete Beams and One-Way Slabs Reinforced with FRP Bars," *Proceedings of FRPRCS-8,* Patras, Greece, July 2007.

PCI Industry Handbook Committee, 2004. *PCI Design Handbook,* Precast/Prestressed Concrete Institute, Chicago, IL, pp 2–42.

Pessiki, S., Graybeal, B. and Mudlock, M., 2002. "Design of High Strength Spiral Reinforcement in Concrete Compression Members," *Proceedings of the International Conference on Advances in Building Technology,* Hong Kong, December 2002, pp 431–438.

Pessiki, S., Graybeal, B., and Mudlock, M., 2001. "Proposed Design of High Strength Spiral Reinforcement in Compression Members," *ACI Structural Journal,* Vol. 98, No. 6, Nov-Dec 2001, pp 799–810.

Pessiki, S.P. and Graybeal, B.A., 2000. "Axial Load Tests of Concrete Compression Members with High Strength Spiral Reinforcement," *PCI Journal,* Vol. 45, No. 2, pp 64–80.

Peterfreund, P., 2003. "Development Length of MMFX Steel Reinforcing Bars Used in Bridge Deck Applications," MSc thesis, University of Massachusetts-Amherst.

Pfister, J.F. and Hognestad, E., 1964. "High Strength Bars as Concrete Reinforcement: Fatigue Tests," *Journal PCA Research and Development Laboratories,* Vol. 6, No. 1, pp 65–84.

Polat, M.B., 1992. "Behavior of Normal and High Strength Concrete under Axial Compression," MASc thesis, University of Toronto, 175 pp.

Poursaee, A., Geiker, M.R., Hansen, K.K., Peled, A., and Weiss, W.J., 2010. "X-Ray Absorption Measurements of Fluid Ingress in Cracked Concrete Under Load," presentation made at ACI Spring Convention, March 22, 2010, Chicago, IL.

Priestley, N.J.M., Seibel, F., and Calvi, G.M., 1996. *Seismic Design and Retrofit of Bridges,* Wiley, 686 pp.

Ramberg, W. and Osgood, W.R., 1943. *Description of Stress-Strain Curves by Three Parameters,* National Advisory Committee on Aeronautics, TN.

Ramirez, J.A. and Russell, B.W., 2008. *NCHRP Report 603: Transfer, Development, and Splice Length for Strand/Reinforcement in High-Strength Concrete,* Transportation Research Board, Washington, D.C.

Rangan, B.V., 1982. "Control of Beam Deflections by Allowable Span-Depth Ratios," *ACI Journal Proceedings,* Vol. 79, No. 5, pp. 372–377.

Rao, P.S., 1966. *Die Grundlagen zur Berechnung der bei Statisch Unbestimmten Stahlbetonkonstruktionen im Plastischen Bereich Auftretenden Umlagerungen der Schnittkräfte* (Basic laws governing moment redistribution in statically indeterminate reinforced concrete structures) DAfStb, Ernst & Sohn, Berlin, Heft 177.

Rasheed, H.A., Nayal, R., and Melhem, H., 2004. "Response Prediction of Concrete Beams Reinforced with FRP Bars," *Composite Structures,* Vol. 65, No. 2, pp 193–204.

Razaqpur, A.G., Svecova, D., and Cheung, M.S., 2000. "Rational Method for Calculating Deflection of Fiber-Reinforced Polymer Reinforced Beams," *ACI Structural Journal,* Vol. 97, No. 1, pp 175–185.

Razvi, S.R. and Saatcioglu, M., 2002. "Displacement Based Design of Reinforced Concrete Columns for Confinement," *ACI Structural Journal,* Vol. 90, No. 1, pp 3–11.

Razvi, S.R. and Saatcioglu, M., 1999. "Stress-Strain Relationship for Confined High-Strength Concrete," *Journal of Structural Engineering,* ASCE, Vol. 125, No. 3, pp 281–289.

Razvi, S.R. and Saatcioglu, M., 1994. "Strength and Deformability of High Strength Concrete Columns," *ACI Structural Journal,* Vol. 91, No. 6, pp 678–687 and Appendix.

Razvi, S.R. and Saatcioglu, M., 1992. "Strength and Ductility of Confined Concrete," *Journal of Structural Engineering,* ASCE, Vol. 118, No. 6, pp 1590–1607.

Restrepo, J.I., Seible, F., Stephan, B., and Schoettler, M.J., 2006. "Seismic Testing of Bridge Columns Incorporating High-Performance Materials," *ACI Structural Journal,* Vol. 103, No. 4, July-August 2006, pp 496–504.

Richart, F.E. and Brown, R.L., 1934. "An Investigation of Reinforced Concrete Columns," *University of Illinois Bulletin,* Vol. XXXI, No. 40.

Richart, F.E., Brandtzaeg, A., and Brown, R.L., 1928. "A Study of the Failure of Concrete under Combined Compressive Stresses," *University of Illinois Bulletin,* Vol. XXVI, No. 12, 104 pp.

Rizkalla, S., Mirmiran, A., Zia, P., Russell, H., and Mast, R., 2007. *NCHRP Report 595: Application of the LRFD Bridge Design Specification to High-Strength Structural Concrete: Flexure and Compression Provisions,* Transportation Research Board, Washington, D.C.

Rizkalla, S., Zia, P., Seliem, H., and Lucier, G., 2005. "Evaluation of MMFX Steel for NCDOT Concrete Bridges," Report FHWA/NC/2006-31, NCDOT Project 2004-27, December 2005.

Scanlon, A., Cagley Orsak, D.R., and Buettner, D.R., 2001. *ACI Code Requirements for Deflection Control in Concrete Structures.* Edited by E.G. Nawy and A. Scanlon. American Concrete Institute, Farmington Hills, MI, SP-203, pp 1–14.

Scanlon, A. and Bischoff, P.H., 2008. "Shrinkage Restraint and Loading History Effects on Deflection of Flexural Members," *ACI Structural Journal,* Vol. 106, No. 4, pp 498–506.

Seliem, H.M., Hosny, A., Rizkalla, S., Zia, P., Briggs, M., Miller, S., Darwin, D., Browning, J., Glass, G.M., Hoyt, K., Donnelly, K., and Jirsa, J.O., 2009. "Bond Characteristics of ASTM A1035 Steel Reinforcing Bars," *ACI Structural Journal,* Vol. 106, No. 4, pp 530–539.

Seliem, H., Hosny, A., Dwairi, H., and Rizkalla, S., 2006. "Shear Behavior of Concrete Beams Reinforced with MMFX Steel Without Web Reinforcement," NC State Report IS-06-08, April 2006.

Shahrooz, B.M., 2010. *Analysis and Design of Flexural Members,* University of Cincinnati, accessed Jan. 17, 2010.

Smith Emery Laboratories, 2006. *Static Compression Tests on MMFX Coupled Reinforcing Steel Bars.*

Soltani, A., 2010. "Bond and Serviceability Characterization of Concrete Reinforced with High Strength Steel," PhD thesis, University of Pittsburgh.

Springstone, 2004. "Modular Pier for Naval Ports," *Proceedings of the ASCE Ports 2004 Conference.*

Stephan, B., Restrepo, J., and Seible, F., 2003. "Seismic Behavior of Bridge Columns Built Incorporating MMFX Steel," UCSD Report SSRP-2003/09.

Sumpter, M.S., 2007. "Behavior of High Performance Steel as Shear Reinforcement for Concrete Beams," *ACI Structural Journal,* Vol. 106, No. 2, pp 171–177.

Thériault, M. and Benmokrane, B., 1998. "Effects of FRP Reinforcement Ratio and Concrete Strength on Flexural Behavior of Concrete Beams," *ASCE Journal of Composites for Construction,* Vol. 2, No. 1, pp 7–16.

Tilly, G.P. and Moss, D.S., 1982. "Long Endurance Fatigue of Steel Reinforcement," *Proc., ABSE Coll.,* Lausanne, Switzerland.

Toutanji, H.A. and Saafi, M., 2000. "Flexural Behavior of Concrete Beams Reinforced with Glass Fiber-Reinforced Polymer (GFRP) Bars," *ACI Structural Journal,* Vol. 97, No. 5, pp 712–719.

Trejo and Pillai, 2004. "Accelerated Chloride Threshold Testing – Part II: Corrosion Resistant Reinforcement," *ACI Materials Journal,* Vol. 101, No. 1, pp 57–64.

Trinnea, 2006. "Corrosion Resistant Reinforcement, *ASM Handbook,* Volume 13C, Corrosion: Environments and Industries.

Vecchio, F.J. and Collins, M.P., 1986. *The Modified Compression-Field Theory for Reinforced-Concrete Elements Subjected to Shear,* American Concrete Institute, Vol. 83 No. 2, pp 219–231.

Vijay, P.V., GangaRao, H.V.S., and Prachasaree, W., 2002. *Bending Behavior of Concrete Beams Reinforced with MMFX Steel Bars,* West Virginia University, July 2002.

Viwathanatepa, S., Popov, E.P., and Bertero, V.V., 1979. "Effects of Generalized Loadings on Bond of Reinforcing Bars Embedded in Confined Concrete Blocks," UCB/EERC-79/22, University of California–Berkeley, Earthquake Engineering Research Center.

Walraven, J.C. and Reinhardt, H.W., 1981. "Theory and Experiments on the Mechanical Behavior of Cracks in Plain and Reinforced Concrete Subjected to Shear Loading," *Heron,* Vol. 26.

Ward, E.L., 2009. "Analytical Evaluation of Structural Concrete Members with High-Strength Steel Reinforcement," MS thesis, University of Cincinnati.

Wascheidt, H., 1965. "On the Fatigue Strength of Embedded Concrete Reinforcing Steel (Zur Frage der Dauerschwingfestigkeit von Betonstahlen im einbetonierten Zustand)," doctoral thesis, Technical University of Aachen.

Wight, J.K. and MacGregor, J.G., 2009. *Reinforced Concrete: Mechanics and Design,* 5th Edition, Prentice-Hall, pp 52–56.

Wipf, Phares, Fanous, Lee, and Jolley, 2005. *Evaluation of Corrosion Resistance of Different Steel Reinforcement Types,* Iowa State University CTRE report.

Wiss, Janney, Elstner Associates, Inc., 2006. *Corrosion Resistance of Alternative Reinforcing Bars: An Accelerated Test Report Prepared for CRSI.*

Yong, Y.K., Nour, M.G., and Nawy, E.G., 1988. "Behavior of Laterally Confined High-Strength Concrete Axial Loads," *ASCE Journal of Structural Engineering,* Vol. 114, No. 2, pp 332–351.

Yost, J.R., Gross, S.P., and Dinehart, D.W., 2003. "Effective Moment of Inertia for Glass Fiber-Reinforced Polymer-Reinforced Concrete Beams," *ACI Structural Journal,* Vol. 100, No. 6, pp 732–739.

Zeno, G.A., 2009. "Use of High Strength Steel Reinforcement in Shear Friction Applications," MSCE thesis, University of Pittsburgh, 91 pp.

Notation

A, B & C	Ramberg-Osgood parameters
A_b	area of reinforcing bar (in^2)
A_c	area of core of spirally reinforced compression member measured to the outside diameter of spiral (in^2)
A_{cv}	area of concrete at shear interface (in^2)
A_g	gross area of section (in^2)
A_{ps}	area of prestressing steel (in^2)
A_s	area of tension reinforcement (in^2)
A_s'	area of compression reinforcement (in^2)
A_{sp}	area of spiral reinforcement (in^2)
$A_{s,min}$	minimum area of longitudinal steel (in^2)
$A_{s,max}$	maximum area of longitudinal steel (in^2)
A_{sb}	area of longitudinal steel to produce a balanced failure (in^2)
A_{tr}	area of each stirrup or tie crossing the potential plane of splitting adjacent to the reinforcement being developed, spliced, or anchored (in^2)
A_v	area of transverse reinforcement within distance s (in^2)
A_{vf}	area of shear-friction reinforcement (in^2)
ADT	average daily traffic
$ADTT$	average daily truck traffic
a	depth of equivalent rectangular stress block (in.); length of beam shear span (in.)
b	width of compression face of a member (in.)
b_c	diameter of core of spirally reinforced compression member measured to the outside of the spiral (in.)
b_v	width of web (in.)
COV	coefficient of variation
c	distance from the extreme compression fiber to the neutral axis (in.); required concrete cover over the reinforcing steel (in.); cohesion factor (psi)
c_b	smaller of: distance from center of bar to nearest concrete edge or one-half the center-center spacing of bars being developed (in.)
c_c	concrete clear cover (in.)
DL	dead load (*AASHTO LRFD §3.6.1*)
d	distance from compression face to centroid of tension reinforcement (in.)
d'	distance from compression face to centroid of compression reinforcement (in.)

d_b diameter of reinforcing bar (in.)
d_c minimum concrete cover measured to center of reinforcing bar (in.)
d_{sp} diameter of spiral reinforcement (in.)
d_t distance from compression face to extreme tension reinforcement (in.)
d_v effective shear depth (in.)
E_c modulus of elasticity of concrete (ksi)
E_{calc} experimentally determined secant modulus of elasticity of reinforcing steel (ksi)
E_p modulus of elasticity of prestressing tendons (ksi)
E_s modulus of elasticity of reinforcing bars (ksi)
f'_c specified compressive strength of concrete for use in design (ksi)
f'_{cc} confined concrete strength (ksi)
f'_{co} unconfined concrete strength (ksi)
f_{ct} average splitting tensile strength of lightweight aggregate concrete (ksi)
f_f permissible fatigue stress range (ksi)
f_{max} maximum stress in fatigue cycle (ksi)
f_{min} minimum stress in fatigue cycle (ksi)
f_{po} "locked-in" stress in prestressing steel (ksi)
f_{pu} specified tensile strength of prestressing steel (ksi)
f_r permissible reinforcing steel stress range (ksi)
f_s tensile stress in tension reinforcement (ksi); reinforcing steel stress at service load, often taken as $0.60f_y$ (ksi)
f'_s tensile stress in compression reinforcement (ksi)
f_{scr} reinforcing steel stress at cracking load (ksi)
f_{sp} tensile stress in spiral reinforcement (ksi)
f_{ss} tensile stress in steel reinforcement at the service limit state (ksi)
f_u ultimate (tensile) strength of reinforcing steel (ksi)
f_y yield strength of reinforcing steel (ksi)
f_{yh} specified yield strength of transverse reinforcement (ksi)
f_{yt} yield strength of the stirrup reinforcement (ksi)
H height of a column (in.)
h overall thickness or depth of a member (in.)
I_{cr} moment of inertia of fully cracked concrete section (in^4)
I_e effective moment of inertia of cracked concrete section (in^4)
I_g moment of inertia of gross concrete section (in^4)
K_1 fraction of concrete strength available to resist interface shear (psi)
K_2 limiting interface shear resistance (psi)
K_{tr} transverse reinforcement factor
L length of simple span beam (in.)
LL_{truck} vehicular live load (*AASHTO LRFD §3.6.1*)
LL_{lane} lane live load (*AASHTO LRFD §3.6.1*)
$LL_{fatigue}$ fatigue live load (*AASHTO LRFD §3.6.1*)
l_d development length (in.)
l_{db} basic development length for straight reinforcement to which modification factors are applied to determine l_d (in.)
l_{dh} development length of standard hook in tension as measured from critical section to outside end of hook (in.)

l_{hb}	basic development length of standard hook in tension (in.)
l_p	length of plastic hinge at the base of a column (in.)
M	moment applied at the section (kip-in)
M_a	moment at which I_e is calculated (kip-in)
M_{cr}	moment to cause cracking in concrete section (kip-in)
M_n	nominal flexural resistance (kip-in)
M_u	factored moment at the section (kip-in)
m	variable exponent in Branson Equation
N	number of cycles of fatigue loading
n	modular ratio = E_s/E_c or E_p/E_c
P	applied axial load (kips)
P'	axial load capacity after spalling of concrete (kip)
P_c	permanent net compressive force across interface (kips)
P_n	nominal axial resistance of a section (kip)
P_o	axial load capacity before spalling of concrete (kip)
r/h	ratio of base radius to height of rolled-on transverse deformations
S	fatigue stress range (ksi)
s	spacing of transverse shear reinforcing steel (in.); spacing of longitudinal reinforcing steel (in.)
s_{max}	maximum permitted spacing of transverse reinforcement (in.)
t_b	distance from the extreme tension fiber to the center of the closest bar (in.)
V	applied shear (kip)
V_c	nominal shear resistance provided by tensile stresses in the concrete (kip)
V_{cr}	applied shear to cause cracking (kip)
V_n	nominal shear resistance of the section considered (kip)
V_{ni}	shear friction capacity (kip)
V_s	shear resistance provided by shear reinforcement (kip)
V_u	ultimate shear capacity (kip)
v_u	shear stress on the concrete (ksi)
w	crack width (in.); self weight of a beam (kip/in)
w_c	unit weight of concrete (pcf); limiting crack width (in.)
w_{max}	maximum crack width at the extreme tension fiber (in.)
w/c	ratio of water to cementitious materials
y	neutral axis depth (in.)
α	angle of inclination of transverse reinforcement to longitudinal axis (°)
β	factor to account for amplification of strain calculated at the bar level to that at the surface due to strain gradient; factor relating effect of longitudinal strain on the shear capacity of concrete, as indicated by the ability of diagonally cracked concrete to transmit tension
β_1	factor relating depth of equivalent rectangular compressive stress block to neutral axis depth
γ	load factor
γ_d, γ_e	crack control exposure condition factor
Δ	shear displacement parallel to shear friction interface (in.)
Δ_{cr}	shear displacement parallel to shear friction interface at cracking load (in.)
Δ_u	shear displacement parallel to shear friction interface at ultimate load (in.)

δ_p	inelastic portion of lateral deflection of column (in.)
δ_y	elastic portion of lateral deflection of column (in.)
ε	strain (in./in.)
ε_{cc}	peak strain of confined concrete (in./in.)
ε_{co}	peak strain of unconfined concrete (in./in.)
ε_{cu}	ultimate compressive strain of concrete (in./in.)
$\varepsilon_{rupture}$	reinforcing steel strain at rupture (in./in.)
ε_s	strain in tension steel (in./in.); reinforcing steel strain at service load (in./in.)
ε'_s	strain in compression steel (in./in.)
ε_{scr}	reinforcing steel strain at cracking load (in./in.)
ε_{sh}	concrete shrinkage strain (in./in.)
ε_{sp}	strain in spiral reinforcement (in./in.)
ε_{su}	reinforcing steel strain at ultimate load (in./in.)
ε_t	net tensile strain in extreme tension steel at nominal resistance (in./in.)
ε_u	reinforcing steel strain at ultimate strength f_u (in./in.)
ε_y	reinforcing steel strain at yield strength f_y (in./in.)
θ	angle of inclination of diagonal compressive stresses (°)
λ	factor reflecting the reduced mechanical properties of lightweight concrete
μ	friction factor
μ_ϕ	curvature ductility
ν	Poisson's Ratio
ρ	reinforcement ratio = A_s/bd
ρ'	reinforcement ratio = A'_s/bd
ρ_b	balanced reinforcement ratio
ρ_g	reinforcement ratio = A_s/A_g
ρ_s	ratio of spiral reinforcement to total volume of column core
σ_{su}	tensile stress in interface steel reinforcement at ultimate shear load (ksi)
τ	shear capacity of reinforcing steel (ksi)
τ_{cr}	concrete shear stress at cracking (ksi)
τ_u	concrete shear stress at ultimate capacity (ksi)
φ	material resistance factor
φ_u	curvature at ultimate strength
φ_y	curvature at yield strength
Ψ_c	factor modifying ACI development length equation based on concrete strength
Ψ_e	factor modifying ACI development length equation based on reinforcement coating
Ψ_s	factor modifying ACI development length equation based on reinforcement size
Ψ_t	factor modifying ACI development length equation based on reinforcement location

APPENDICES

Structural Concrete Design with High-Strength Steel Reinforcement

Unpublished Material

Appendices A through M as submitted by the researchers are not published herein. They are available on the TRB website (Go to http://trb.org/Publications/Public/PubsNCHRPProjectReports.aspx and look for NCHRP Report 679). Titles of Appendices A through M are as follows:

Appendix A: Material Properties
Appendix B: Flexural Resistance of Members with Reinforcing Bars Lacking Well-Defined Yield Plateau
Appendix C: Strain Limits for Tension-Controlled/Compression-Controlled and Strains to Allow Negative Moment Redistribution
Appendix D: Flexure Beam Tests
Appendix E: Fatigue of High-Strength Reinforcing Steel
Appendix F: Shear Beam Tests
Appendix G: Analytical Studies of Columns
Appendix H: Beam Splice Tests
Appendix I: Crack Control
Appendix J: Survey Results
Appendix K: Design Examples
Appendix L: Proposed Changes to Section 5 of the AASHTO LRFD Specification
Appendix M: 2010 AASHTO Bridge Committee Agenda Item

Abbreviations and acronyms used without definitions in TRB publications:

AAAE	American Association of Airport Executives
AASHO	American Association of State Highway Officials
AASHTO	American Association of State Highway and Transportation Officials
ACI–NA	Airports Council International–North America
ACRP	Airport Cooperative Research Program
ADA	Americans with Disabilities Act
APTA	American Public Transportation Association
ASCE	American Society of Civil Engineers
ASME	American Society of Mechanical Engineers
ASTM	American Society for Testing and Materials
ATA	Air Transport Association
ATA	American Trucking Associations
CTAA	Community Transportation Association of America
CTBSSP	Commercial Truck and Bus Safety Synthesis Program
DHS	Department of Homeland Security
DOE	Department of Energy
EPA	Environmental Protection Agency
FAA	Federal Aviation Administration
FHWA	Federal Highway Administration
FMCSA	Federal Motor Carrier Safety Administration
FRA	Federal Railroad Administration
FTA	Federal Transit Administration
HMCRP	Hazardous Materials Cooperative Research Program
IEEE	Institute of Electrical and Electronics Engineers
ISTEA	Intermodal Surface Transportation Efficiency Act of 1991
ITE	Institute of Transportation Engineers
NASA	National Aeronautics and Space Administration
NASAO	National Association of State Aviation Officials
NCFRP	National Cooperative Freight Research Program
NCHRP	National Cooperative Highway Research Program
NHTSA	National Highway Traffic Safety Administration
NTSB	National Transportation Safety Board
PHMSA	Pipeline and Hazardous Materials Safety Administration
RITA	Research and Innovative Technology Administration
SAE	Society of Automotive Engineers
SAFETEA-LU	Safe, Accountable, Flexible, Efficient Transportation Equity Act: A Legacy for Users (2005)
TCRP	Transit Cooperative Research Program
TEA-21	Transportation Equity Act for the 21st Century (1998)
TRB	Transportation Research Board
TSA	Transportation Security Administration
U.S.DOT	United States Department of Transportation